A black and white photograph showing the lower legs and feet of several people walking up a set of stone stairs. The focus is on the movement and the texture of the stone steps.

STP 1486

Pavement Surface Condition/ Performance Assessment:

**Reliability and Relevancy
of Procedures and Technologies**

Bouzid Choubane
editor

The logo for ASTM International, featuring the letters 'ASTM' in a stylized, bold font with a globe-like graphic behind them. Below the logo, the words 'INTERNATIONAL' and 'Standards Worldwide' are written in a smaller, sans-serif font.

ASTM
INTERNATIONAL
Standards Worldwide

STP 1486

*Pavement Surface
Condition/Performance
Assessment: Reliability and
Relevancy of Procedures and
Technologies*

Bouzid Choubane, editor

ASTM Stock Number: STP1486

ASTM
100 Barr Harbor Drive
PO Box C700
West Conshohocken, PA 19428-2959



Printed in the U.S.A.

Library of Congress Cataloging-in-Publication Data

Pavement surface condition/performance assessment : reliability and relevancy of procedures and technologies / Bouzid Choubane, editor.

p. cm. — (STP ; 1486)

Includes index.

ISBN-13: 978-0-8031-5521-3

ISBN-10: 0-8031-5521-2

1. Pavements—Testing—Congresses. 2. Pavements—Evaluation—Congresses. 3. Surface roughness—Measurement—Congresses. I. Choubane, Bouzid. II. International Symposium on Pavement Condition Assessment (2004 : Washington, D.C.)

TE250.P32 2007

625.8028'7—dc22

2007010741

Copyright © 2007 AMERICAN SOCIETY FOR TESTING AND MATERIALS INTERNATIONAL, West Conshohocken, PA. All rights reserved. This material may not be reproduced or copied, in whole or in part, in any printed, mechanical, electronic, film, or other distribution and storage media, without the written consent of the publisher.

Photocopy Rights

Authorization to photocopy items for internal, personal, or educational classroom use, or the internal, personal, or educational classroom use of specific clients, is granted by the American Society for Testing and Materials International (ASTM) provided that the appropriate fee is paid to the Copyright Clearance Center, 222 Rosewood Drive, Danvers, MA 01923; Tel: 978-750-8400; online: <http://www.copyright.com/>.

Peer Review Policy

Each paper published in this volume was evaluated by two peer reviewers and at least one editor. The authors addressed all of the reviewers' comments to the satisfaction of both the technical editor(s) and the ASTM International Committee on Publications.

The quality of the papers in this publication reflects not only the obvious efforts of the authors and the technical editor(s), but also the work of the peer reviewers. In keeping with long-standing publication practices, ASTM International maintains the anonymity of the peer reviewers. The ASTM International Committee on Publications acknowledges with appreciation their dedication and contribution of time and effort on behalf of ASTM International.

Foreword

This publication, *Pavement Surface Condition/Performance Assessment: Reliability and Relevancy of Procedures and Technologies*, contains papers presented at the Symposium of the same title which was held in Washington, DC, on 7-8 December, 2004.

The Symposium was sponsored by ASTM Committee E17 on Vehicle – Pavement Systems. The chairman was Dr. Bouzid Choubane, Florida Department of Trans, Gainesville, FL.

Contents

Overview	vii
An Automatic Pavement Surface Distress Inspection System—Y. HUANG AND B. XU	1
Analysis of Error in Pavement Ground Truth Indicators for Evaluating the Accuracy of Automated Image Collection and Analysis System—H. LEE AND J. KIM	12
Analysis of Surface Inertial Profiles Measured on Jointed Portland Cement Pavements—N. GAGARIN AND MEKEMSON, JR	27
Development of Pavement Smoothness Index Relationship—J. CHEN AND C. HUANG	39
Harmonization of Macrotexture Measuring Devices—G.W. FLINTSCH, M. HUANG, AND K. MC GHEE	47
Measuring Pavement Friction Characteristics at Variable Speeds for Added Safety—N.M. JACKSON, B. CHOUBANE, C. HOLZSCHUHER, AND S. GOKHALE	59
Realistic Approach for Enhancing Reliability of Pavement Surface Friction Testing—S. LI, S. NOURELDIN, AND K. ZHU	73

Overview

Pavement distress assessment and friction characteristics measurements have become important tools in the performance evaluation and management of roadway systems. They are being used to identify potentially hazardous conditions, monitor the surface characteristics of the various in-service pavements, and assess the need for rehabilitation and maintenance. This need to quantify pavement surface condition has resulted in a number of techniques and equipment. Also, advances in testing, sensor and inertial navigation technologies have enhanced the functionality of pavement evaluation equipment, allowing highway engineers and practitioners to capitalize on the large amount of information offered by the state of the art equipment. However, with the ever evolving technologies and increasing needs for faster, more accurate and harmonized pavement performance monitoring technique/procedures, and data interpretation, more venues for sharing, documenting, and disseminating information are needed.

On December 7, 2004, an ASTM International symposium on pavement condition assessment (in terms of friction, texture, and roughness characteristics) was held in Washington, DC. The presentations at that symposium represented an international effort in both the practical as well as the developmental aspects of pavement surface evaluation procedures and technologies including their reliability and relevancy. They covered a broad range of topics that included the following:

- Pavement surface characteristics measurement procedures and equipment as well as their reliability and appropriateness;
- Approaches to enhance the reliability and accuracy of pavement surface evaluation systems;
- Approaches to harmonization between different measurement devices for specific pavement surface condition indicators;
- Assessment of current pavement condition indicators and their relevancy level for use in asset management;
- Assessment of factors influencing the interaction of tire/pavement surface characteristics;
- Assessment of automated distress survey systems; and
- Evaluation of new/promising technologies for pavement condition surveys.

The symposium provided a forum for participants and attendees to gain insight regarding the needs, methodologies, and trends in pavement performance monitoring, and data collection/interpretation. The presentations and subsequent discussions indicated that, although height sensor-based or non-contact technology for pavement surface condition assessment continues to gain wider acceptance, it still has not fully matured. A considerable amount of research has been conducted to gain further understanding on the factors affecting pavement condition evaluation from both the analytical and experimental points of view. Still some problems have not fully been resolved, particularly in the interpretation of the measured data and selection/design of adequate sensing technology.

The technical papers published here provide additional reference material for those concerned with pavement surface performance evaluation and characterization. They cover topics that will be of interest to practitioners as well as to researchers.

viii OVERVIEW

The editor wish to acknowledge all those who participated in the Symposium, those who contributed to this Special Technical Publication (STP), and the many reviewers who provided important feedback to the authors. The editor also wish to acknowledge the ASTM International Committee E17 on Vehicle-Pavement Systems for sponsoring the symposium and the ASTM International staff for their assistance with the organization of the symposium and publication of this volume. The editor is grateful for their diligent efforts and contributing knowledge.

Bouzid Choubane
Florida Department of Transportation
State Materials Office, Gainesville, Florida
Symposium Chair and Editor

Y. Huang¹ and B. Xu¹

An Automatic Pavement Surface Distress Inspection System

ABSTRACT: This paper presents a customized image-processing algorithm for the high-speed and real-time detection of pavement surface distresses. The algorithm was developed based on the “grid cell” analysis, in which a pavement image is divided into a grid of 8×8 pixel cells, and each cell is classified as a non-crack cell or a crack cell based on the statistics of the grayscales of the cell pixels. A crack cell can be regarded as a seed for crack formation. Adjacent crack seeds or seed clusters are connected to a crack segment. Each segment has its own direction and contrast traced from all seed in the path. A full crack is a connection of nearby segments with similar directions and contrasts. Most importantly, there must be a clear crack path along these segments. Because many operations are performed on the grid cells rather than on the original image, the algorithm can detect the cracks in the current image during the time when the camera is capturing a new image. Therefore, the survey can run at real time at a highway speed. The trial test results showed a good repeatability and accuracy when the system conducts multiple surveys and runs at different speeds and different weather conditions.

KEYWORDS: asphalt pavement, cracking distress, seed cluster, crack detection

Introduction

An automated pavement surface distress inspection (APSDI) system is essential for conducting massive and timely distress data collections and for minimizing disturbance to public traffic and road hazard to human inspectors during the survey. The development of the APSDI technology can be traced back to early 1970s [1,2]. The nature of the pavement inspection requires such an APSDI system to be able to detect cracking distress down to less than 2 mm in width from a variety of background textures. This is equal to a captured image with around 2000 pixels in width by 500 pixels in length for every meter of a full lane pavement surface. If the highway speed of 112 km/h (70 mph) is required to avoid traffic disruption, there is very limited time available to acquire and process the image. Considering the complexity of pavement conditions and textures, implementing such an image acquisition system and processing algorithm are a great challenge. As a result, some alternative procedures like multiple cameras, multiple processors with digital signal processing (DSP) hardware support, speed and coverage redundancy, or even off-line processing can be found in some APSDI systems. Some semi-automatic systems became available in the late 1990s [3–5].

A recent study comparing an automated and manual pavement condition index (PCI) survey was conducted by the Naval Facilities Engineering Service Center [5]. The project concluded that both automated and manual techniques provide consistent measurements for the PCI data. The data collection systems used in the project were all the offline image-processing systems. The major disadvantage of using an offline processing system is that the level of the survey cost

Manuscript received 19 October 2004; accepted for publication 22 April 2005; published November 2005. Presented at ASTM Symposium on Pavement Surface Condition/Performance Assessment: Reliability and Relevancy of Procedures and Technologies on 7 December 2004 in Washington, DC.

¹ Center for Transportation Research, University of Texas at Austin, Austin, Texas 78712.

2 PAVEMENT SURFACE CONDITION

is similar to that of a manual survey because it needs intensive human involvement in the post image processing.

In the past five years, the Texas Department of Transportation (TxDOT) sponsored the University of Texas at Austin to develop an APSDI system that can perform real-time, 100 % distance-coverage survey at a vehicle speed ranging from 5 to 112 km/h (3 to 70 mph). The operations include image acquisitions, distress detections, and data classifications in both PMIS (pavement management information system) and AASHTO (American Association of State Highway Transportation Officials) protocols. The system is equipped mainly with a line scan camera, a frame grabber, and a computer with a Windows XP or NT operating system. The camera with a resolution of 2k pixels covers a full lane of 3.65 m (12 ft) in width and scans up to 44 000 lines or maximum 88 m in distance per second. The computer, which has a 2.8 GHz Pentium IV processor, takes only 20 milliseconds to process one 2048×512 image without the help of any DSP hardware.

System Configuration

Figure 1 shows the diagram of the system configuration. The line scan camera, connected to the frame grabber via the Camlink interface, is synchronized by an encoded vehicle speed signal to ensure every scanned line covers the same gap on the pavement when the travel speed varies. The camera exposure time is adjusted dynamically to maintain the consistency of the brightness of images when the road and lighting conditions change. The camera captures a line image of 2048 pixels in the front of the survey vehicle. A frame of 512 lines covering 0.9-m long pavement is accumulated by the frame grabber, giving a resolution of 1.786 mm per pixel. It takes less than 5 milliseconds to transfer an image from the frame grabber to the system memory for the processing. The image grabbed to the system memory is in the 8-bit grayscale format. A network interface card is installed to receive the GPS data and vehicle speed signal broadcast from the central computer. The GPS data are integrated into the crack report and used to record the time and geographical locations of the collected distress data.

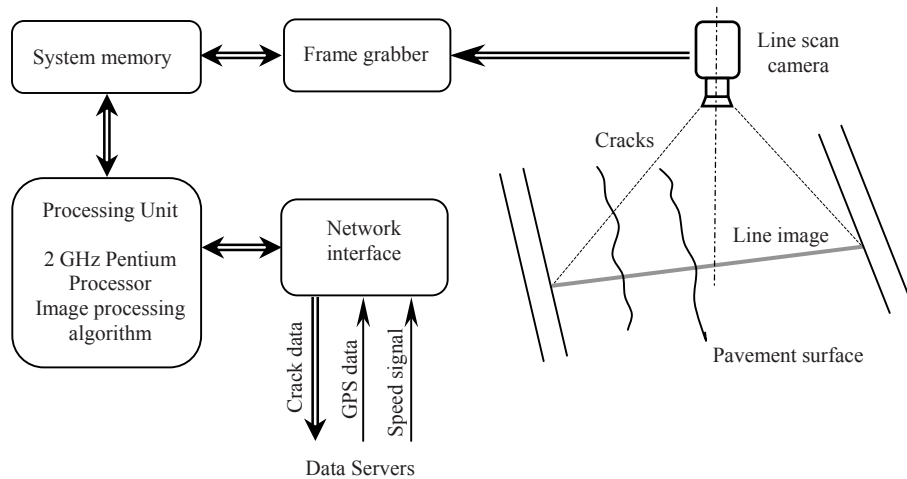


FIG. 1—Pavement image acquisition and processing system.

Crack Detection

The design of the image processing algorithm is crucial in this application. The high speed image acquisition technology, including line scan cameras and image grabbers, has advanced dramatically during the last decade. For the real time system implementation, the hardware is no longer a technical barrier, but the image processing software becomes a bottleneck in the pipeline due to the complexity of pavement surfaces and the large size of images. At a highway speed, the total processing time allowed for each image over one meter of pavement is restricted to 30 milliseconds. It is a great challenge to develop real-time processing algorithms which are able to differentiate a variety of cracking distresses from complicated pavement textures and then to classify them using a standard protocol.

A primary cue for crack identification is that a crack can be distinguished from the background by its darkness. When dark pixels are geometrically connected in the pattern of a thin strip, these pixels may form a crack. Finding dark objects and their length, width, and contrast is the first and most important step of the entire process. An algorithm based on grid cell analysis (GCA) was developed to perform this process. It divides the original image into small cells with a chosen grid. The size of the grid depends on the characteristics of potential objects to be identified. A grid of 8×8 pixels is suitable for locating cracks on asphalt pavements. The information including the average brightness, the minimum brightness, and the presence of a crack strip is firstly determined for each cell. The cells are then categorized either as a non-crack cell or a crack seed by comparing its features to the preset thresholds. Only those crack seeds need further processing to confirm the presence of any cracking distress.

Figure 2a shows three cases of grid cells extracted from a pavement image. A search is conducted around each cell's border as indicated by arrows in Fig. 2b. The average grayscale of the border pixels is used to represent the average brightness of the cell. The minimum grayscale value in a cell and its coordinate are recorded for later crack detection. The coordinate will be used for allocating the axis of a crack, calculating the crack length, and checking the width and contrast of the crack. In the case of a cell containing a crack, border pixels show two valleys as shown in the top plot of Fig. 2c. The coordinate of the minimum grayscale is determined by these two valleys. If there is no crack in the cell or no clear valley in its border pixels, the coordinate is allocated by the darkest pixel in the cell. This cell will be eliminated from further processing. If there is only one valley with high contrast to its neighboring border pixels, the cell may be an edge of a crack. The coordinate is assigned according to the darkness of pixels in the edge area. Further analysis on this cell will be conducted to confirm the existence of a crack. Only this process needs the access to the pixels of the whole image and takes about one-third of the entire processing time. The rest of the analysis will concentrate on the area where cracks may exist.

After all of the cells have been analyzed, a cell map can be drawn using the identified minimum values as shown in Fig. 3b. This cell data structure carries most crack information from the original image while sized in a much smaller scale. It will be used in a seed validation process to classify cells into crack seeds or non-crack cells.

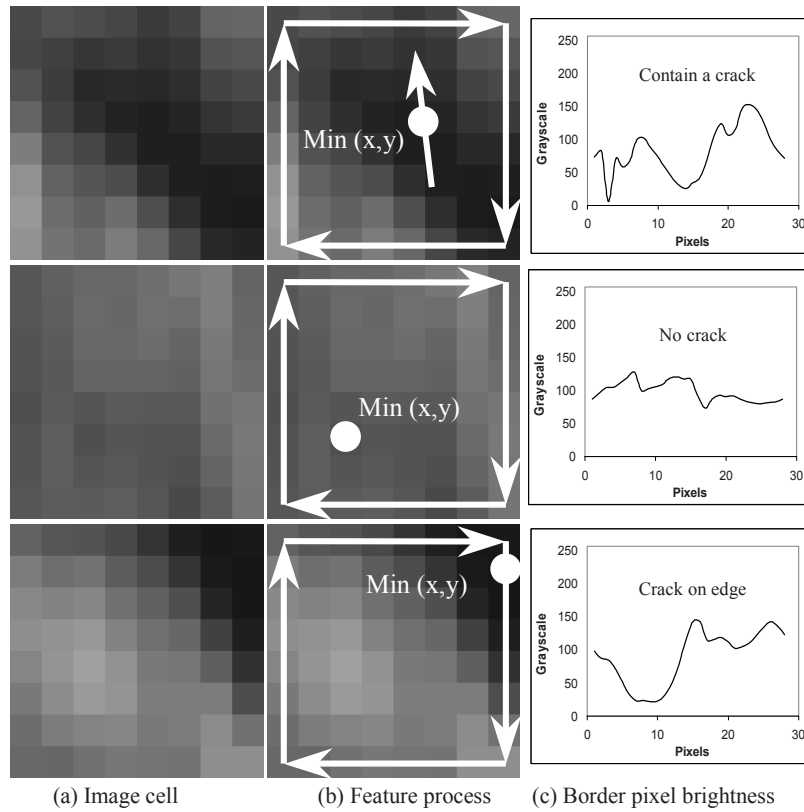


FIG. 2—Cell characteristics in a pavement image.

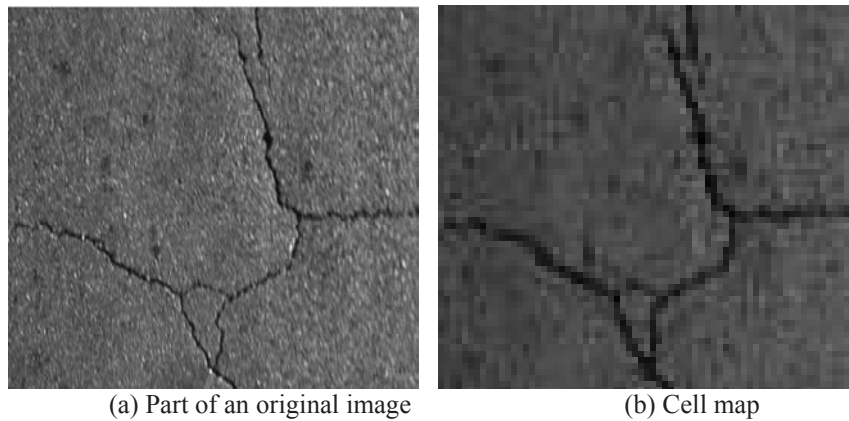


FIG. 3—A part of a pavement image and its cell map.

A crack is a fissure on pavement surface with a large length to width ratio and a significant contrast to its neighboring area. Analyzing brightness changes on neighboring cells can reveal the possible presence of a crack while excluding most non-crack cells from further processing. A group of patterns is designed to find possible crack cells. Each pattern contains six cells as shown in Fig. 4. In the patterns, a black block represents the cell to be evaluated, a gray block is used as a guide cell for the direction, and hollow blocks represent four neighboring cells to be compared and calculated for contrast. The guide cell is used for distinguishing an isolated non-crack cell from a crack cell. A crack cell must have at least one dark neighbor on the same crack. The contrast C_c of a cell is defined by the following equation:

$$C_c = \frac{2 \times \bar{V} - V_b - V_g}{\bar{V}}$$

where \bar{V} is the average value of the six cells, and V_b and V_g are the values of the black and gray cells, respectively.

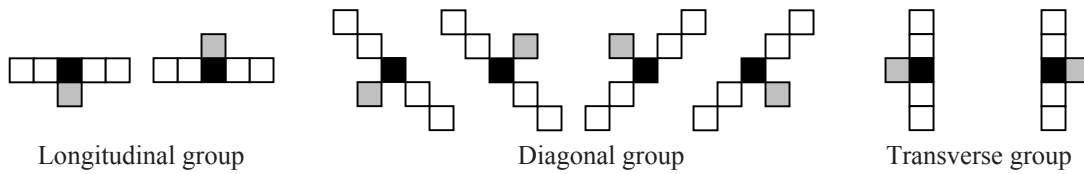


FIG. 4—Patterns for crack seed validation for cells.

For a cell to be classified as a crack seed, it must be the darkest in the pattern group; the contrast C_c must be larger than a given threshold, which is adaptive to each image. The pattern also classifies seeds as longitudinal, transverse, or diagonal. The direction of the cell is assigned to the pattern that gives the maximum C_c to the cell. This is useful to avoid a false connection in the crack tracing. A longitudinal crack could consist of longitudinal and diagonal seeds, while a transverse crack should only have transverse and diagonal seeds.

Figure 5a shows all checked seeds for the image in Fig. 2a. Compared to the original image, the volume of data has been dramatically reduced. The detection and verification of different cracks will be based on the found seeds.

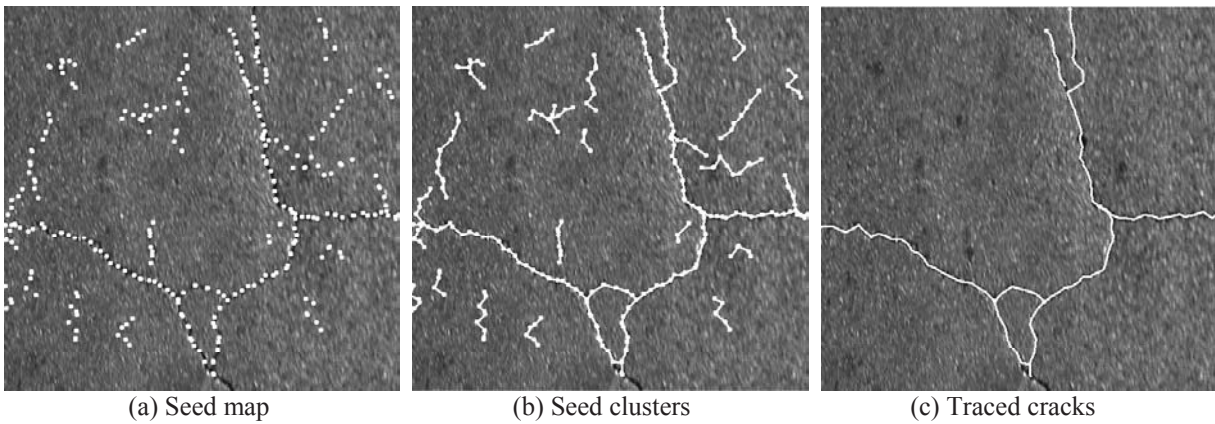


FIG. 5—Crack detection steps.

The next step is to connect individual seeds into seed clusters as shown in Fig. 5b. Each seed cluster contains information of its weight or the number of seeds in the cluster, all seed parameters on its path, the direction, and the start and end coordinates. Seed clusters provide a guide for crack tracing. When there is more than one path to trace a crack, the process will follow the seed clusters that provide the resultant crack with the maximum length.

Cracks could be traced by connecting seed clusters into a single object. The connection is based on the distance and direction of neighboring seed clusters. Many asphalt pavement images were used to select proper thresholds for the distance and direction checking. Three criteria are used for a validation check on all connections to eliminate falsely detected cracks. First of all, a valid crack must have a clear dark path along its axis. The contrast of pixels on a crack's axis to their neighbor pixels on both sides is checked with an adaptive threshold for the image.

Secondly, the average width, the width variation, and crack direction of an individual crack are checked to avoid shadows, pavement joints, and other non-crack objects. Finally, short cracks with lengths less than a given threshold, e.g., 75 mm (3 in.), will be removed from the cracks list. A final traced crack map is shown in Fig. 5c. The final direction of a traced crack is calculated by its start and end coordinates. A crack is then classified as longitudinal or transverse based on this direction.

As mentioned earlier, shadows are unavoidable in some pavement images under natural lighting. Shadows may be caused by overhead construction, roadside objects, and the vehicle, and the size and shape change with the driving direction. As the seed validation emphasizes the presence of dark stripes in small cells, the chance to identify a shadow as a crack is minimized. On the other hand, in a large shadow area caused by the vehicle body, cracks are still detectable if the brightness and contrast in the shadowed area can be enhanced. An equalization function is designed based on the vertical projections of the average brightness of each cell. It stretches the brightness distribution uniformly over the entire histogram so that the contrast in a shadowed area can be improved. Figure 6a shows a shadowed image. After being equalized, the cracks and lane marks are preserved, while the shadow is diminished in Fig. 6b. This equalization is performed at the grid cell level and takes only a fraction of a millisecond.

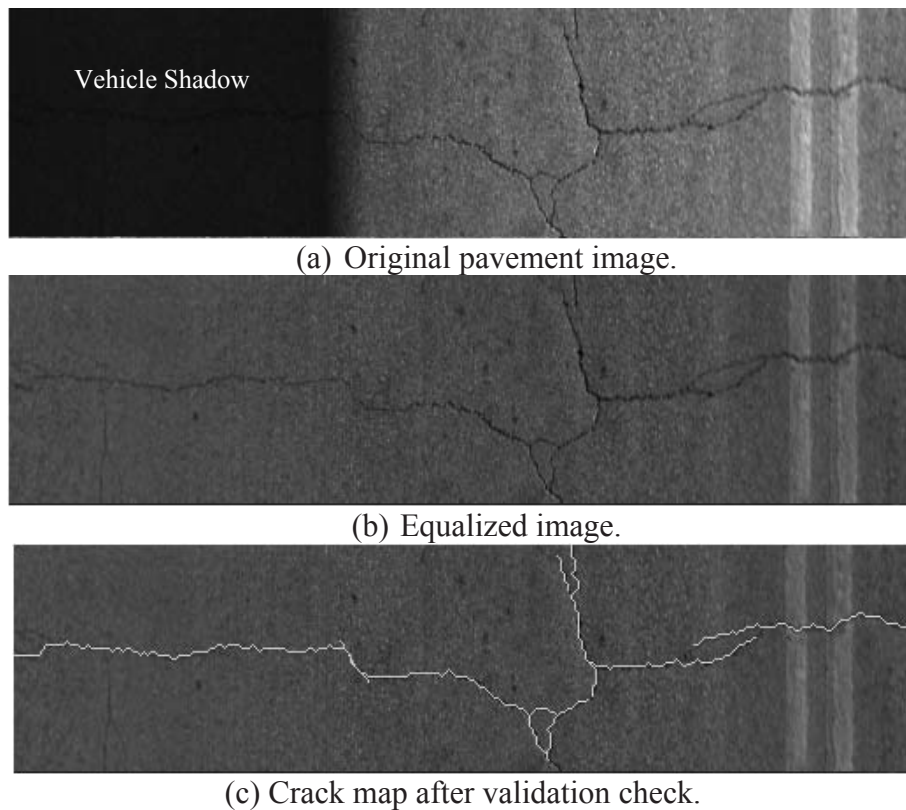


FIG. 6—A pavement image with shadow and the traced cracks.

The system offers an image-capturing function for saving long-distance images for visual confirmation of the analyzed results. It continuously grabs a one km (0.62 mile) full size image, or a 16 km (10 mile) compressed image over a full pavement lane. The full size image can be processed offline and used for visual verifications, while the compressed image can be used for training or documentation. Figure 7 shows a sample of a 10-m pavement section with its crack

map. The crack data from individual frames can be combined to show long cracks that run across multiple frames. For pavement surveys, crack length, direction, and start and end locations are useful for mapping the cracks.

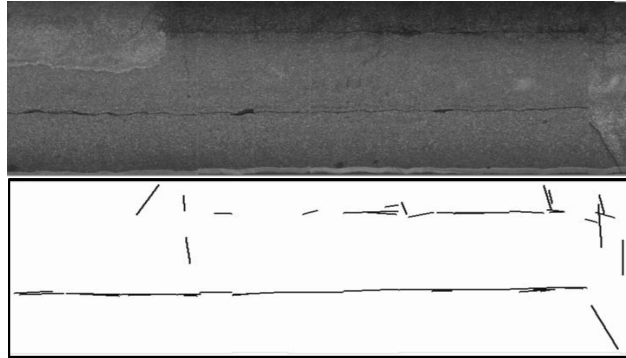


FIG. 7—Reconstructed 10 m (32 ft) pavement and crack map.

An on-screen visual assessment was conducted on 1000 full size pavement images to evaluate the accuracy of the algorithm. Images, which contain a variety of different cracks, were chosen from over 32 km (20 miles) of different pavement sections for visual and automated rating comparison. The lighting varied largely from a sunny condition to a very cloudy condition. It was found that about 75 % of wide unsealed cracks (>5 mm in width) and 65 % of small unsealed cracks (≤ 5 mm in width) can be correctly measured by this pavement distress survey algorithm.

Using grid cells rather than image pixels to process a large pavement image provides a significant advantage for real-time processing pavement images. Since the exact locations of cracks are recorded during the data extraction from each cell, cracks can be traced and checked in the original image. Therefore, the algorithm does not undermine the possible resolution and accuracy of crack detections.

Validation Test

The survey data can be reported either in the PMIS or AASHTO format. In the PMIS data format, distresses are sorted into longitudinal, transverse, alligator, and block cracking, while in the AASHTO protocol the various distresses are combined in terms of wheel paths. A full pavement lane is divided into different paths to reflect whether distresses are in the wheel paths or outside.

Many on-road surveys have been conducted to examine the performance of the system. The data were organized according to the TxDOT pavement survey protocol [6], in which a data are defined over one survey station of 30.5 m (100 ft). Then, all data for every 0.8 km (0.5 mile) are averaged to provide a section statistical record. The tests included the evaluations of the repeatability of the system under different weather, lighting, and vehicle speed conditions.

Figure 8 shows the results of a repeatability test of multiple scans. Surveys were repeated on the same pavement section at nearly constant speed of 88 km/h (55 mph) in a short period of time. The high correlations among the three scans indicate that the system is capable of providing coherent results for the same pavement distress under similar conditions. The shift of the driving path in different scans is one of the main sources of variations in the output.

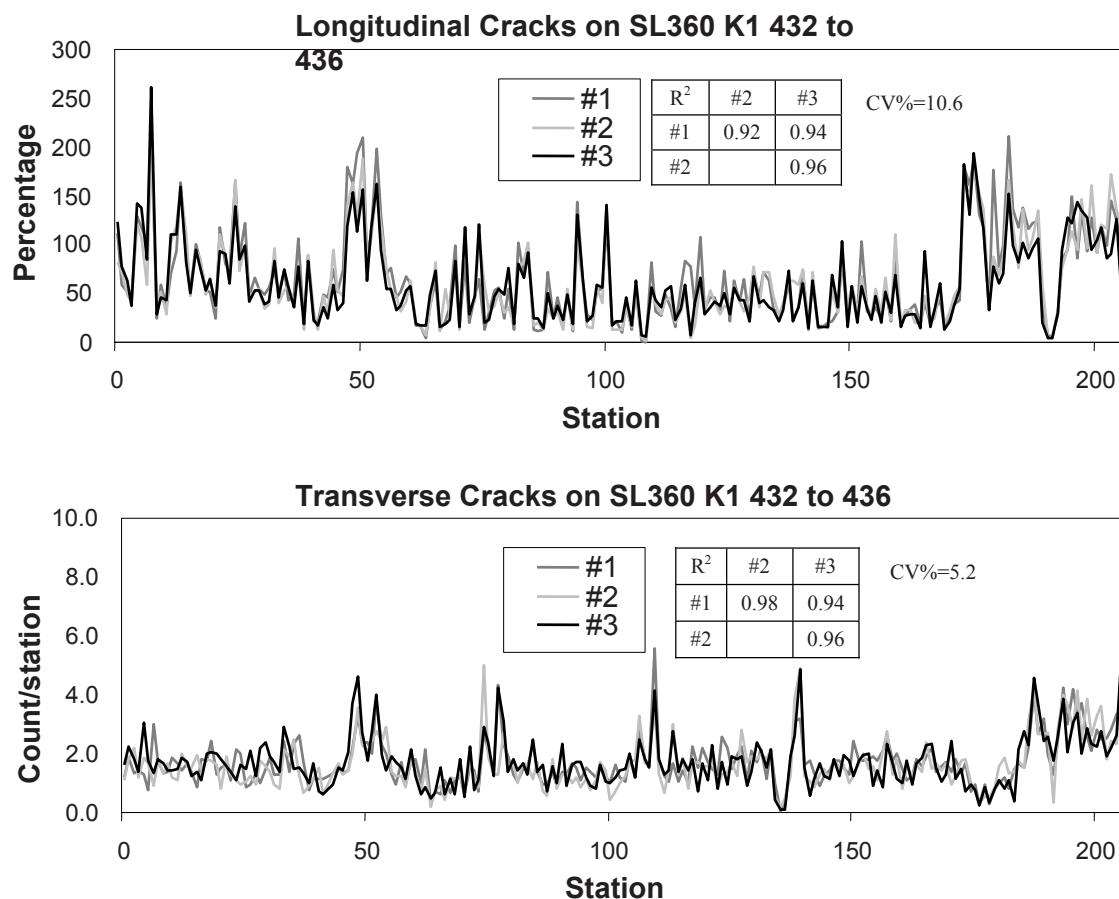


FIG. 8—Repeatability test with multiple scans.

Surveys at different travel speeds were conducted over a 30-station long pavement section, a relatively short distance to avoid traffic lights or other speed disturbances. Since the data were processed at the station level, details of distresses for each station are emphasized. It is understandable that data at the station level have larger variations than those at the record level. Both data plots and the statistical results in Fig. 9 indicate an acceptable level of correlations between surveys at different speeds. In addition, as there are only few transverse cracks existing in the scanned pavement, a small number of false positive or negative records may change the station level data appreciably. However, the value of this change is limited and will not affect the overall result of the distress magnitude at the record level.

The weather and lighting conditions are the most important factors to the image quality for a system that uses natural lighting. Although the image processing algorithm can give consistent results to every pass, it could rate differently on the same pavement when the image quality changes. Figure 10 shows survey results in three extremely different weather conditions. It shows the system performance under the influence of all environmental conditions, which include lighting, speed, and multiple passes. The correlations and coefficients of variation are acceptable for such a complicated survey system. More accuracy and consistent results can be achieved if the environmental conditions are controlled.

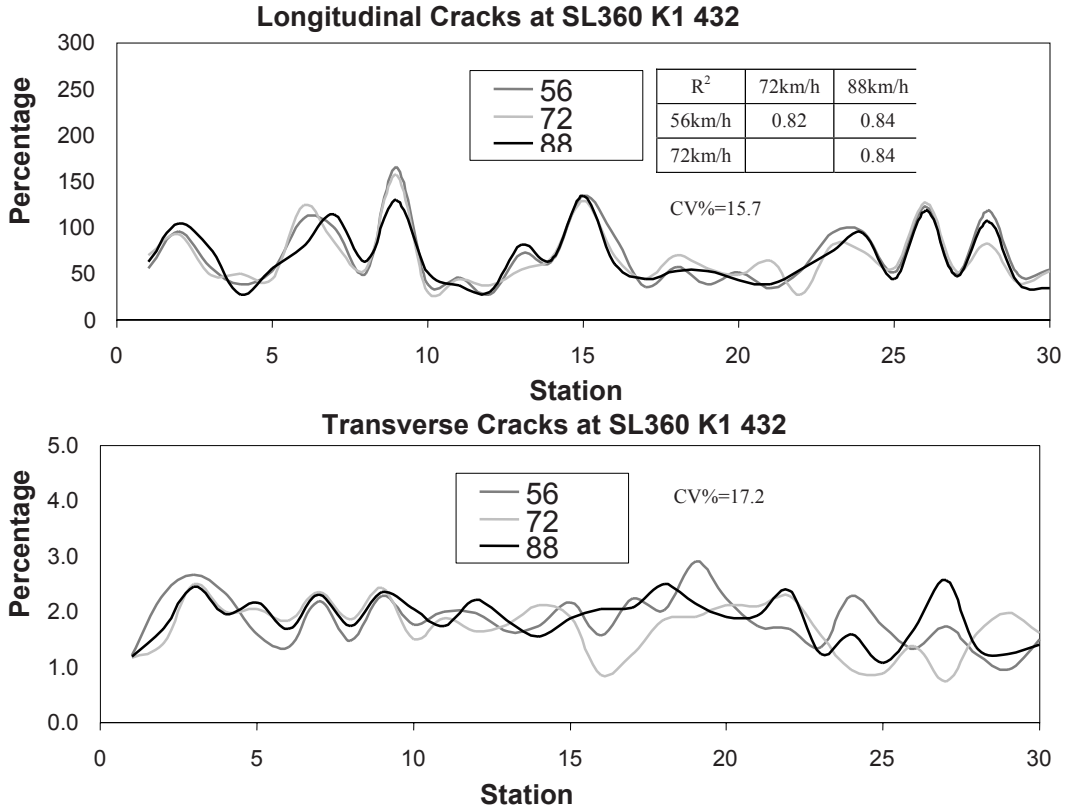


FIG. 9—Survey at different travel speeds.

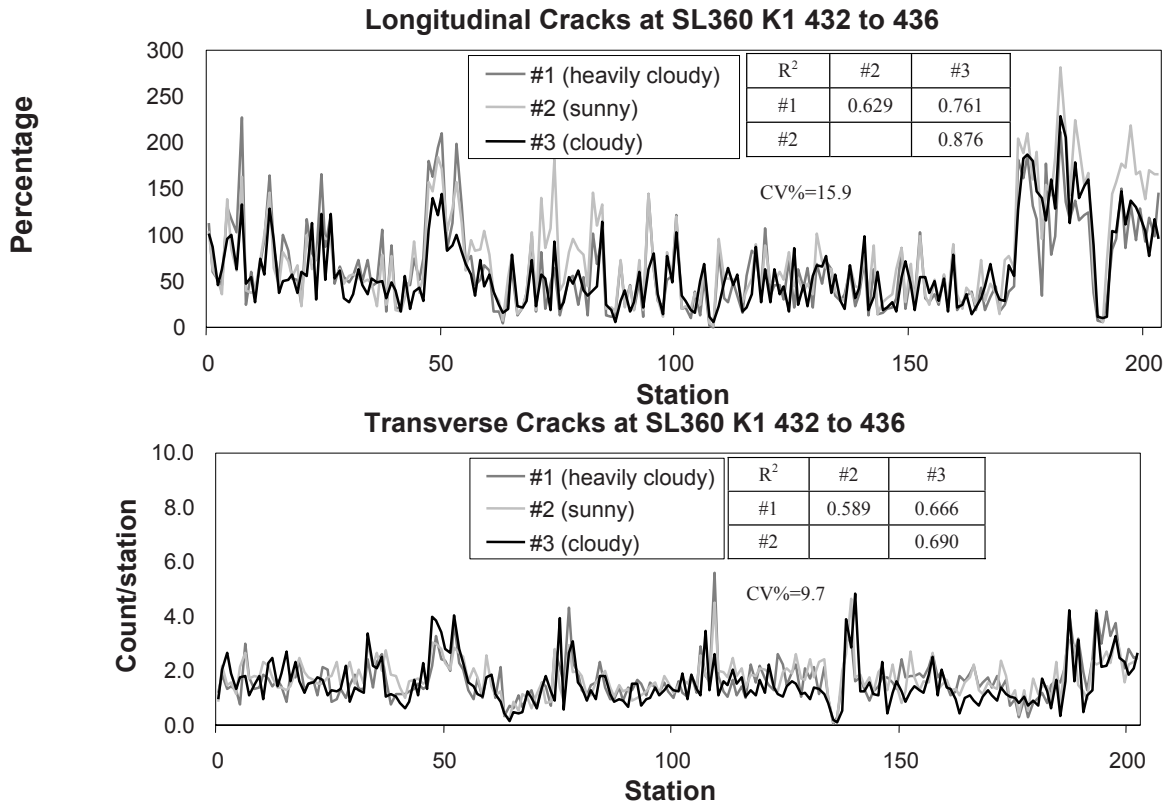


FIG. 10—Surveys under different weather conditions.

Conclusions

The GCA algorithm utilizes reduced grid cell data, permitting real-time processing of pavement images. It records the locations of cracks on the pavement surface so that the data can be reported in both PMIS and AASHTO formats. It can detect a fine crack as narrow as one pixel in the original image. The original image can also be preserved for the purpose of visual crack validation.

The GCA algorithm is designed particularly for tracking crack distresses in a pavement image, as a crack always shows varying darkness, width, and direction. It is not unusual for a crack to be broken in segments in a grayscale image. Special techniques are required to trace the maximum length of a crack within a very limited period of time. GCA is a two step process of crack detection. The first step processes individual cells in the original image. A cell is classified as either a non-crack cell or a crack seed according to certain criteria. The seed location is the coordinate of the darkest pixel inside the seed. This pixel coordinate makes it possible for a crack trace to occur at the same resolution as the original pavement image. In a distressed area, seed clusters can be found along crack paths. A few seeds caused by non-crack objects may spread across a large area. The second GCA step groups seed clusters into a crack segment and then connects segments to a full crack. The direction, contrast, and distance of seed clusters are the key factors in this process.

Considering the complexity of highway pavement surface conditions, both crack segments and cracks have to be validated. A valid crack segment shows a certain level of local contrast and presents a dark strip. Besides these two conditions, a crack also shows a clear dark path along its trace. These two processes are useful to eliminate falsely identified cracks from a complicated pavement background.

Visual assessment and field survey tests have proved that the GCA algorithm is accurate for measuring different cracks. Consistent results can be obtained from surveys conducted at different times and travel speeds. This study has verified that pavement distress may appear differently under different weather, i.e., lighting, conditions. Although an acceptable level of confidence was demonstrated by this system for its well-designed camera control ability, the results can be better if surveys are conducted under controlled lighting or weather conditions.

Acknowledgments

The authors are grateful for the financial support provided by TxDOT, and would like to thank Brian Michalk, Carl Bertrand, and many other members at the Pavement Design Section of TxDOT for their guidance and assistance in the system testing.

References

- [1] Fukuhara, T., Terada, K., Nagao, M., Kasahara, A., and Ichihashi S., "Automatic Pavement-Distress-Survey System," *J. Transportation Engineering*, ASCE 116, Vol. 3, 1990, pp. 280–286.
- [2] McNeil, S. and Humplick, F., "Evaluation of Errors in Automated-Distress Data Acquisition," *J. Transportation Engineering*, ASCE, Vol. 117, No. 2, 1991, pp. 224–241.
- [3] Wang, K., "Design and Implementation of Automated System for Pavement Surface Distress Survey," *Journal of Infrastructure System*, Vol. 6, No. 1, 2000, pp. 24–32.

- [4] Sjogren, L., "State of the Art: Automated Crack Measurement of Road Surface," Research Project Report, Swedish National Road and Transportation Research Institute (VTI), 2002.
- [5] Pynn, J., Wright, A., and Lodge, R., "Automated Identification of Crack in Road Surface, Image Processing and Its Application," Conference Publication No. 465, 671-675, IEEE, 1999.
- [6] Pavement Management Information System, Rater's Manual for Fiscal Year 2001, Texas Department of Transportation, June 2000.

Hosin Lee¹ and Jungyong Kim¹

Analysis of Error in Pavement Ground Truth Indicators for Evaluating the Accuracy of Automated Image Collection and Analysis System

ABSTRACT: The main purpose of this paper is to present the Automated Image Collection System (AICS) and Manual Image Analysis System (MIAS) as “ground-truth” for evaluating Automated Image Collection System (AICS) and Automated Image Analysis System (AIAS) for highway asset management. The proposed “ground-truth” is evaluated with respect to its repeatability against a traditional “ground-truth” procedure based on Manual Distress Collection System (MDCS) and Manual Distress Analysis System (MDAS). To capture digital images automatically, a vehicle mounted with a digital video camera was driven on the pavement test section. To determine the repeatability of MIAS, the images were evaluated by three individuals twice per individual. To determine the repeatability of MDCS/MDAS, the same individuals were asked to evaluate the same pavement section in the field twice per individual. Repeatability on three crack types was evaluated for two survey methods and three individuals. Overall, the average relative precisions of AICS/MIAS-based procedure by three individuals were 10, 8, and 19 % for longitudinal, transverse, and block cracks, respectively, whereas those of MDCS/MDAS-based procedure were 43, 45, and 41 % for longitudinal, transverse, and block cracks, respectively. In conclusion, the proposed AICS/MIAS-based “ground-truth” measurements can be considered as more repeatable by human operators than MDCS/MDAS-based “ground-truth” measurements.

KEYWORDS: pavement management, asset management, Manual Distress Collection System (MDCS), Manual Distress Analysis System (MDAS), Automated Image Collection System (AICS), Automated Image Analysis System (AIAS), Manual Image Analysis System (MIAS)

Introduction

Over the past two decades, significant efforts have been made on evaluating the accuracy of Automated Image Collection System (AICS) and Automated Image Analysis System (AIAS) based on the “ground-truth” data obtained from Manual Distress Collection System (MDCS) and Manual Distress Analysis System (MDAS) [1,2]. MDCS is composed of the grid paper for distress mapping and MDAS is performed following a set of rules interpreting the drawings of distresses on the grid papers. AICS is composed of a video digital camera mounted on a vehicle; AIAS is typically based on an automated digital image processing algorithm. The MDCS and MDAS process involves hand-drawings of distresses on the grid paper in the field and quantifying them in the numerical scale in the office. Major limitations of the MDCS are a boredom attendant on such a mundane task and a danger associated with an exposure to the high-speed traffic. Due to its high level of subjectivity and inconsistency within and among evaluators, in some cases, the MDCS and MDAS could not be considered as a “ground-truth” for evaluating AICS and AIAS. Thus, it has become necessary to define a consistent “ground-truth” for evaluating the accuracy of AICS and AIAS, which would allow researchers to isolate various sources of error.

The main purpose of this paper is to present a new “ground-truth” procedure based on Automated Image Collection System (AICS) and Manual Image Analysis System (MIAS) and its comparison against a traditional “ground-truth” method in terms of its repeatability. In this paper, the proposed AICS/MIAS-based evaluation process is compared against a traditional evaluation procedure based on MDCS and MDAS. First, to capture digital images, a vehicle mounted with a digital video camera was driven on the pavement test section. Second, three individuals evaluated the collected images using MIAS software

Manuscript received October 15, 2004; accepted for publication February 14, 2006; published online April 2006. Presented at ASTM Symposium on Pavement Surface Condition/Performance Assessment on 07 December 2004 in Washington, DC; B. Choubane, Guest Editor.

¹ Public Policy Center, Department of Civil and Environmental Engineering, University of Iowa, Iowa City, Iowa.

following the Strategic Highway Research Program's (SHRP) pavement distress evaluation protocol. The images were then randomly shuffled and evaluated again by the same three individuals. Third, they went to the same pavement section in the field and evaluated the pavement condition based on MDCS and MDAS following the SHRP protocol. They evaluated the same pavement sections one more time in the opposite direction to prevent them from recollecting the distress information from the previous survey.

Based on this new AICS/MIAS-based "ground-truth" procedure, mainly, two sources of error were identified in this research: (1) human error in observing and interpreting pavement conditions in the field, and (2) human error in observing pavement images and interpreting pavement conditions using MIAS software in the office.

Background

The MDCS and MDAS techniques for manually collecting and analyzing pavement distress data are subjective, labor-intensive, and dangerous. The major efforts were directed towards developing AICS and AIAS approaches to automatically collect and analyze the pavement distress data [3]. To compare the effectiveness of these AICS approaches, a set of criteria were proposed [4]. The Federal Highway Administration (FHWA) has conducted three major studies comparing AICS against MDCS results, which concluded that better techniques were needed to evaluate AICS [5]. Although there is a variability associated with distress data, a study reported that a reasonable level of precision for MDCS is attainable with a focus on essential distresses [6]. Additional studies reported that there is no difference in distress data between MDCS and 35 mm photograph AICS [7,8] or digital line scan AICS [9,10].

Recently, a number of research projects have been carried out to address the issues associated with QA/QC of pavement distress data [11]. As a result, different QA/QC procedures were developed for pavement distress data in Virginia [12,13], Maryland [14], British Columbia, and Canada [15]. Maryland DOT focused their QA/QC efforts on AIAS by requiring 80 % crack detection rate. An application of QA testing methodology was presented to evaluate the quality of the pavement condition data automatically collected and processed for the National Park Service (NPS) Road Inventory Program [16]. However, most of them adopted the MDCS as "ground-truth" data to perform QA/QC for their AICS and AIAS. A guideline to develop a QA/QC procedure was also proposed for highway agencies that contract pavement distress data collection [17]. It was also pointed out that the main problem associated with QA/QC for AICS is that most agencies do not know the accuracy, precision, and resolution they need. It was recommended that each highway agency should conduct detailed MDCS of the predetermined test sections and use it as "ground-truth" to evaluate AICS.

Although many highway agencies maintained their own QA/QC procedures for AICS/AIAS, their QA/QC procedures rely on the subjective MDCS as their "ground-truth." Besides, some highway agencies use a composite index as their evaluation criteria for AICS/AIAS. Given the complex AICS hardware and sophisticated AIAS software, the current QA/QC approaches based on MDCS/MDAS could lead to erroneous results if the proposed MIAS is not properly incorporated into their QA/QC procedures. Many highway agencies are often provided with the AIAS results in hard copies without corresponding images. As a result, it became difficult for the owner agencies to verify the outputs provided by contractors using their own AIAS. To improve the accuracy of the results generated by AIAS, several highway agencies adopted an MIAS as a production tool.

Pavement Distress Survey Systems

This section describes three pavement distress survey systems adopted for this study, which include Automated Image Collection System (AICS), Manual Distress Collection System (MDCS), and Manual Image Analysis System (MIAS).

Automated Image Collecting System

As shown in Fig. 1, the AICS adopted for this study is composed of the off-the-shelf area scan digital video camera mounted on a vehicle, DMI, and a PC with image processing board. This digital area scan camera can capture an image with 776×582 pixel resolution at 0.001 s of exposure time. The DMI

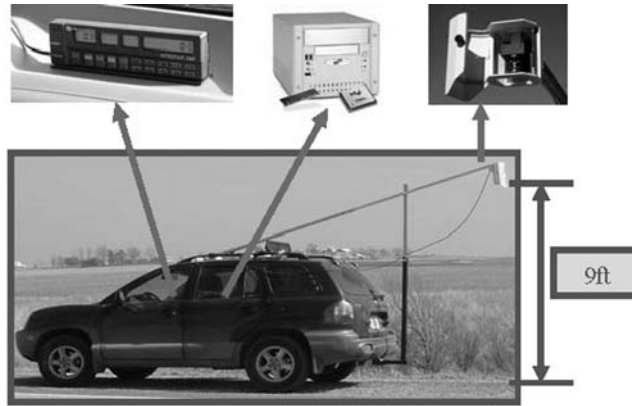


FIG. 1—Automated Image Collection System (AICS) adopted for this study.

provides a distance signal at 1 ft (0.3 m) interval to a computer controller to capture the image at a predetermined fixed distance. Figure 2 shows an image of 11 ft (3.4 m) in width by 9 ft (2.7 m) in length on the pavement surface as captured by the digital video camera mounted on top of a vehicle at approximately 9 ft (2.7 m) from the ground. As a result, each pixel would represent approximately 0.2 in. (5 mm) \times 0.2 in. (5 mm) terms of area of pavement surface. In order to cover 100 % of the pavement surface, the images were collected every 9 ft (2.7 m) at a highway speed. However, due to the inaccuracy associated with the DMI, there were some overlaps or skipped sections between successive images. As can be seen from Fig. 2, the edges of the image were distorted because a wide-angle camera lens was used to cover the full-lane width of 11 ft (3.4 m).

Manual Data Collection System

As shown in Fig. 3, the pavement test section was evaluated by three individuals following the SHRP distress evaluation protocol [18]. As shown in Fig. 4, the distresses were drawn on the grid paper following the SHRP guideline. The completed grid papers were later analyzed in the office.

Manual Image Analysis System

MIAS allows an operator to measure the extent and severity of various types of distress from a computer screen. As shown in Fig. 5(a), an operator can measure a length of a crack by tracing a crack using a mouse on a computer screen. From the starting point of a crack a user holds down the left mouse button and drags the mouse to the ending point of a crack. In order to measure the extent of alligator cracking, as shown in Fig. 5(b), the operator can draw a polygon along the boundary of cracked area. The MIAS automatically computes the extent of an alligator crack as measured in the field. To measure the severity of cracking, the image is zoomed at the predetermined level and the operator can measure a crack width

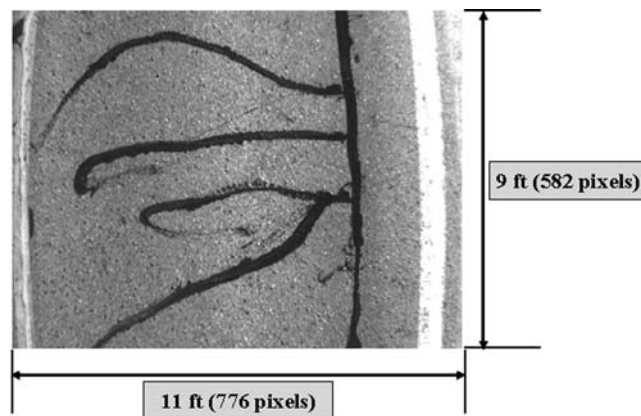


FIG. 2—Sample Pavement Surface Image captured by the AICS.



FIG. 3—Picture of the MDCS process of the pavement test section in the field.

using a mouse. The information window also shows necessary information on a computer screen such as a full path of the image file, location information from DMI, and actual dimension of pavement surface.

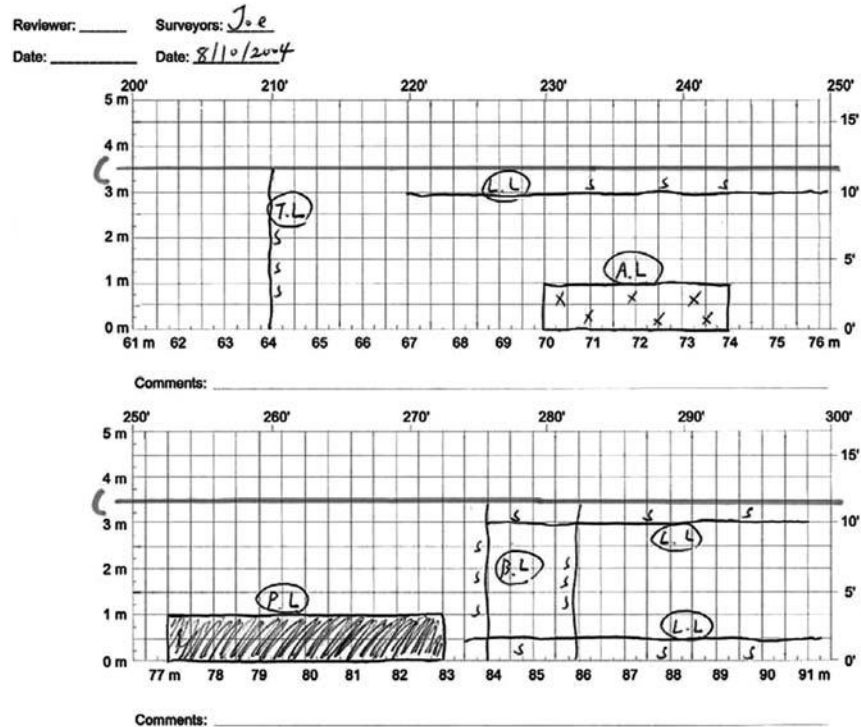


FIG. 4—Distress map drawn on grid paper using MDCS based on SHRP protocol.

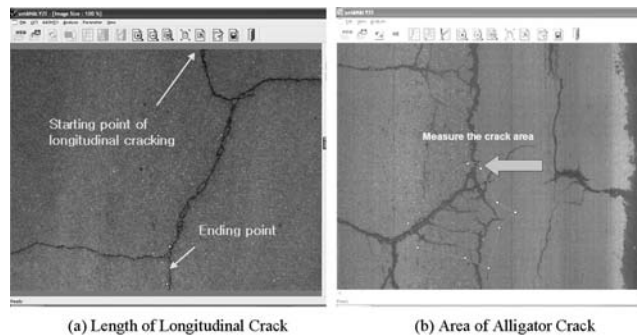


FIG. 5—MIAS screen shots demonstrating crack measuring process.

TABLE 1—Two test results of MDAS done by Investigator A.

No.	Station	Longitudinal Crack, m				Transverse Crack, m				Block Crack, m ²			
		A1	A2	A1-A2	A1-A2	A1	A2	A1-A2	A1-A2	A1	A2	A1-A2	A1-A2
1	0-100	29.2	29.6	-0.4	0.4	51.3	59.9	-8.6	8.6	0.0	0.0	0.0	0.0
2	100-200	32.3	43.8	-11.5	11.5	66.5	80.6	-14.0	14.0	0.0	0.0	0.0	0.0
3	200-300	46.2	45.5	0.7	0.7	81.5	89.1	-7.6	7.6	0.0	0.0	0.0	0.0
4	300-400	25.4	58.0	-32.6	32.6	30.3	74.7	-44.4	44.4	34.6	18.4	16.1	16.1
5	400-500	4.6	52.6	-48.1	48.1	63.5	132.9	-69.4	69.4	34.2	2.7	31.5	31.5
6	500-600	35.5	28.5	6.9	6.9	53.6	58.9	-5.3	5.3	0.0	0.0	0.0	0.0
7	600-700	19.1	28.7	-9.6	9.6	33.8	38.1	-4.3	4.3	0.0	13.0	-13.0	13.0
8	700-800	13.2	15.5	-2.3	2.3	24.2	19.8	4.4	4.4	43.2	46.1	-2.8	2.8
9	800-900	24.5	4.9	19.6	19.6	13.7	16.3	-2.5	2.5	47.1	62.2	-15.1	15.1
10	900-1000	5.6	3.9	1.7	1.7	0.0	15.2	-15.2	15.2	68.7	58.0	10.7	10.7
11	1000-1100	0.0	0.0	0.0	0.0	0.0	0.0	0.0	0.0	64.5	66.1	-1.6	1.6
12	1100-1200	2.7	33.8	-31.1	31.1	27.4	83.4	-56.0	56.0	54.0	28.2	25.8	25.8
13	1200-1300	3.6	22.4	-18.8	18.8	16.8	65.0	-48.3	48.3	50.5	21.7	28.8	28.8
14	1300-1400	0.0	0.0	0.0	0.0	0.0	0.0	0.0	0.0	61.6	5.5	56.1	56.1
15	1400-1500	0.0	0.0	0.0	0.0	0.0	0.0	0.0	0.0	65.9	7.6	58.3	58.3
	Average	16.1	24.5	-8.4	12.2	30.8	48.9	-18.1	18.7	35.0	22.0	13.0	17.3
	Relative Precision	20.3		-0.41	0.60	39.9		-0.45	0.47	28.5		0.46	0.61

Evaluation of Pavement Test Section Using Both MDCS/MDAS and AICS/MIAS

To determine the repeatability of the both MDCS/MDAS and AICS/MIAS procedures, the 1500-ft (457.2-m) test section was selected which mainly included longitudinal, transverse, and block cracks. Three individuals were asked to survey the pavement distress condition twice using both MDCS/MDAS and AICS/MIAS following the SHRP Distress Identification Manual [18]. To randomize the process, they were asked to survey the pavement section twice in the opposite directions. The digital images were captured from the same pavement section using the AICS at a highway speed and the same individuals were asked to evaluate the images projected on the computer screen twice using the MIAS. To randomize the process, they were asked to evaluate the images after the images were randomly shuffled.

Repeatability of MDCS/MDAS

To evaluate the repeatability of MDAS/MDAS, the survey results from the three individuals, designated as A, B, and C, are summarized in Tables 1-3, and plotted in Figs. 6-8, respectively.

TABLE 2—Two test results of MDAS Done by Investigator B.

No.	Station	Longitudinal Crack, m				Transverse Crack, m				Block Crack, m ²			
		B1	B2	B1-B2	B1-B2	B1	B2	B1-B2	B1-B2	B1	B2	B1-B2	B1-B2
1	0-100	32.9	31.0	1.9	1.9	57.8	72.7	-14.9	14.9	0.0	0.0	0.0	0.0
2	100-200	56.6	56.0	0.6	0.6	74.9	62.4	12.5	12.5	0.0	0.0	0.0	0.0
3	200-300	43.0	45.5	-2.5	2.5	95.6	93.2	2.4	2.4	0.0	0.0	0.0	0.0
4	300-400	27.3	23.0	4.4	4.4	34.8	27.7	7.1	7.1	34.7	25.1	9.7	9.7
5	400-500	14.0	25.7	-11.7	11.7	40.2	107.8	-67.6	67.6	36.7	7.6	29.1	29.1
6	500-600	36.5	37.7	-1.2	1.2	71.3	53.2	18.1	18.1	0.0	0.0	0.0	0.0
7	600-700	19.1	18.1	1.0	1.0	35.8	43.1	-7.3	7.3	13.3	9.7	3.7	3.7
8	700-800	8.2	12.3	-4.1	4.1	5.6	24.4	-18.8	18.8	53.9	32.6	21.3	21.3
9	800-900	22.7	1.5	21.1	21.1	21.7	17.0	4.8	4.8	47.8	45.2	2.6	2.6
10	900-1000	5.1	4.8	0.3	0.3	0.0	29.4	-29.4	29.4	49.4	31.7	17.7	17.7
11	1000-1100	0.0	0.0	0.0	0.0	0.0	17.5	-17.5	17.5	65.4	47.2	18.2	18.2
12	1100-1200	9.2	31.9	-22.7	22.7	23.0	79.3	-56.4	56.4	49.8	21.4	28.4	28.4
13	1200-1300	0.0	26.5	-26.5	26.5	0.0	59.0	-59.0	59.0	66.3	31.9	34.4	34.4
14	1300-1400	0.0	0.0	0.0	0.0	0.0	13.2	-13.2	13.2	63.6	47.2	16.4	16.4
15	1400-1500	0.0	0.0	0.0	0.0	0.0	20.3	-20.3	20.3	66.3	47.2	19.1	19.1
	Average	18.3	20.9	-2.6	6.5	30.7	48.0	-17.3	23.3	36.5	23.1	13.4	13.4
	Relative Precision	19.6		-0.13	0.33	39.4		-0.44	0.59	29.8		0.45	0.45

TABLE 3—Two test results of MDAS done by Investigator C.

No.	Station	Longitudinal Crack, m				Transverse Crack, m				Block Crack, m ²			
		C1	C2	C1-C2	C1-C2	C1	C2	C1-C2	C1-C2	C1	C2	C1-C2	C1-C2
1	0-100	39.1	30.3	8.8	8.8	63.6	55.0	8.6	8.6	0.0	7.0	-7.0	7.0
2	100-200	62.3	48.1	14.3	14.3	90.3	64.5	25.8	25.8	0.0	5.5	-5.5	5.5
3	200-300	42.0	56.8	-14.8	14.8	132.2	103.4	28.8	28.8	0.0	0.0	0.0	0.0
4	300-400	39.6	24.9	14.7	14.7	52.7	54.4	-1.6	1.6	25.3	28.7	-3.4	3.4
5	400-500	23.3	43.5	-20.3	20.3	81.2	127.1	-45.9	45.9	24.1	10.2	13.9	13.9
6	500-600	30.8	18.4	12.4	12.4	88.9	60.0	28.9	28.9	0.0	0.0	0.0	0.0
7	600-700	22.1	28.0	-5.8	5.8	43.7	44.4	-0.7	0.7	11.4	11.1	0.2	0.2
8	700-800	23.2	30.4	-7.2	7.2	26.5	22.0	4.5	4.5	33.1	25.4	7.6	7.6
9	800-900	16.7	8.2	8.4	8.4	12.0	9.8	2.2	2.2	53.1	49.5	3.6	3.6
10	900-1000	14.9	4.6	10.4	10.4	7.1	22.2	-15.1	15.1	49.5	45.7	3.8	3.8
11	1000-1100	0.0	1.4	-1.4	1.4	0.0	14.3	-14.3	14.3	64.3	53.1	11.2	11.2
12	1100-1200	34.1	25.6	8.5	8.5	73.9	59.4	14.4	14.4	33.1	30.8	2.3	2.3
13	1200-1300	43.7	34.8	8.9	8.9	63.9	56.8	7.1	7.1	23.3	22.8	0.5	0.5
14	1300-1400	0.0	0.0	0.0	0.0	0.0	7.6	-7.6	7.6	66.1	57.1	9.0	9.0
15	1400-1500	0.0	0.0	0.0	0.0	0.0	8.3	-8.3	8.3	66.1	58.1	8.0	8.0
Average		26.1	23.7	2.5	9.1	49.1	47.3	1.8	14.3	30.0	27.0	2.9	5.1
Relative Precision		24.9		0.10		48.2		0.04		28.5		0.18	

As shown in Fig. 6, for all three cracking types, longitudinal, transverse, and block, measurements by individual A are scattered away from the 45-deg equality line. It is interesting to note that, in the second round, individual A identified more longitudinal and transverse cracks whereas he identified less block cracks. It can be postulated that he could have misclassified some block cracks as either longitudinal or

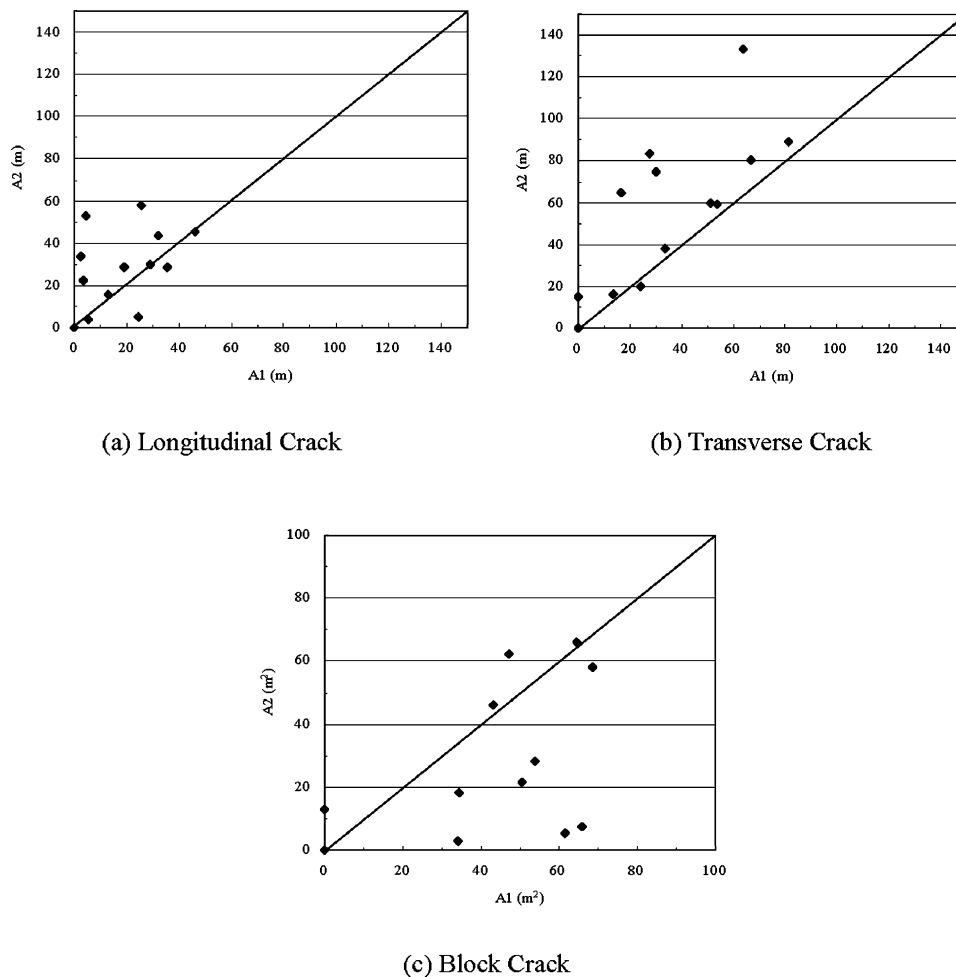


FIG. 6—Comparison between first and second Data of MDAS by Investigator A.

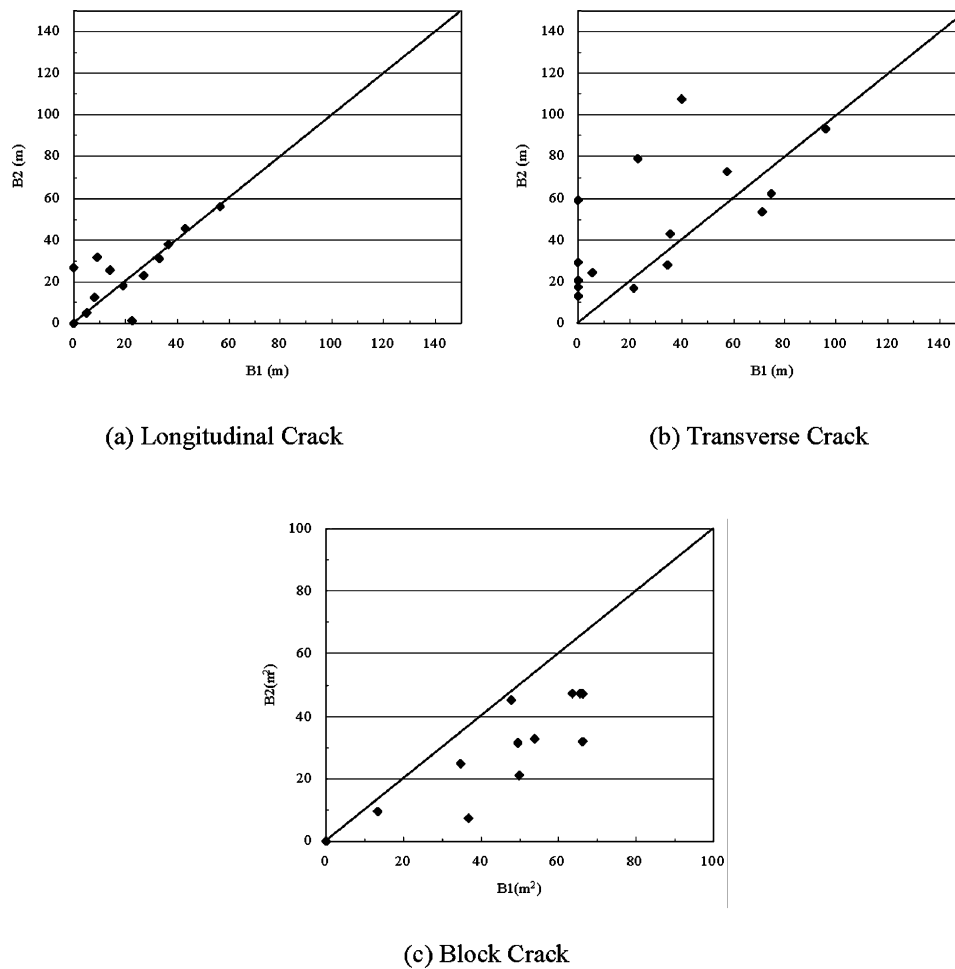


FIG. 7—Comparison between first and second Data of MDAS by Investigator B.

transverse cracks in the second round. It can be shown from Table 1 that, on the average in the second round, he overestimated longitudinal cracks by 8.4 m and transverse crack by 18.1 m per 100-ft (30.5-m) station whereas he underestimated block cracks by 13.0 m². To determine the repeatability of the individual A, the average values of the absolute difference between two measurements were computed as 12.2 m for longitudinal cracks, 18.7 m for transverse cracks, and 17.3 m² for block cracks. These values are quite large given that the average lengths of these cracks were 20.3 m, 39.9 m, and 28.5 m² per 100-ft (30.5-m) station, respectively. We then computed the relative precisions for three cracking types by dividing the average absolute difference by the average value resulting in 60, 47, and 61 %, respectively. These large relative precision values indicate that the distress collection and analysis result from individual A using MDCS/MDAS is not repeatable.

As shown in Fig. 7, individual B repeated the two measurements consistently for longitudinal crack, overestimated transverse cracks, and underestimated block cracks in the second round. It can be postulated that he could have misclassified some block cracks as transverse cracks in the second round. It can be shown from Table 2 that, on the average in the second round, he overestimated longitudinal cracks by 2.6 m and transverse crack by 17.3 m per 100-ft (30.5-m) station whereas he underestimated block cracks by 13.4 m². To determine the repeatability of individual B, the average values of the absolute difference between two measurements were computed as 6.5 m for longitudinal cracks, 23.3 m for transverse cracks, and 13.4 m² for block cracks. These values are relatively large given that the average lengths of these cracks were 19.6 m, 39.4 m, and 29.8 m² per 100-ft (30.5-m) station, respectively. We then computed the relative precisions for three cracking types by dividing the average absolute difference by the average value resulting in 33, 59, and 45 %, respectively. Compared to the individual A, the repeatability of the individual was better in longitudinal and block cracks but worse in transverse cracks. These large relative precision values indicate that the distress collection and analysis result from individual B using MDCS/MDAS should not be considered repeatable.

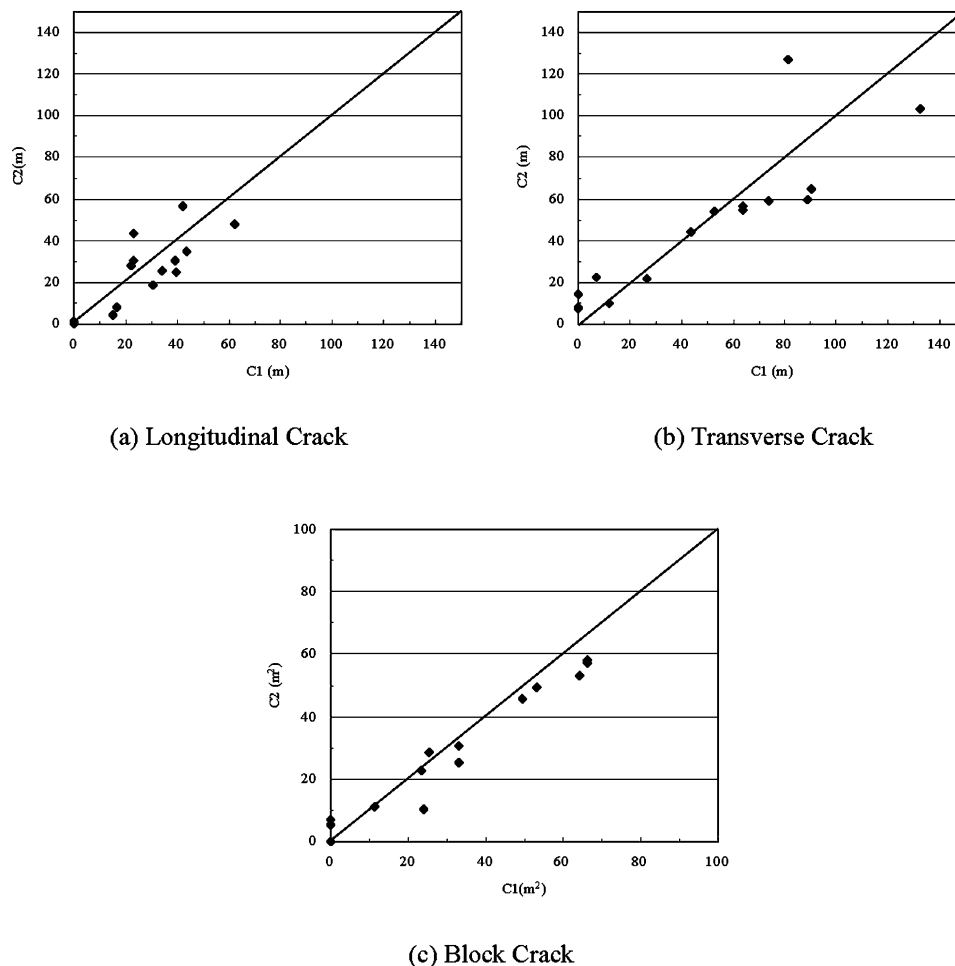


FIG. 8—Comparison between first and second Data of MDAS by Investigator C.

As shown in Fig. 8, compared to two previous individuals, individual C repeated the two measurements consistently for all three distress types. It can be shown from Table 3 that, on the average in the second round, she underestimated all distress types, by 2.5 m for longitudinal cracks, by 1.8 m for transverse cracks and by 2.9 m² for block cracks per 100-ft (30.5-m) station. To determine the repeatability of individual C, the average values of the absolute difference between two measurements were computed as 9.1 m for longitudinal cracks, 14.3 m for transverse cracks, and 5.1 m² for block cracks. These values are relatively small given that the average lengths of these cracks were 24.9 m, 48.2 m, and 28.5 m² per 100-ft (30.5-m), respectively. We then computed the relative precisions for three cracking types by dividing the average absolute difference by the average value resulting in 36, 30, and 18 %, respectively. Compared to the two previous individuals, the repeatability of individual C was much better in all three distress types. These relatively small precision values compared to two previous individuals indicate that the distress collection and analysis result from individual C using MDCS/MDAS can be considered more repeatable than other individuals.

Evaluating the Repeatability of MIAS

To evaluate the repeatability of AICS/MIAS, the survey results from the three individuals, designated as A, B, and C, are summarized in Tables 4–6, and plotted in Figs. 9–11, respectively. Overall, it should be noted that all distress measurement values using AICS/MIAS are significantly larger than the ones measured using MDCS/MDAS. This indicates that people can see more distresses in all types using AICS/MIAS.

As shown in Fig. 9, for all three cracking types, longitudinal, transverse, and block, measurements by individual A are scattered near from the 45-deg equality line. It can be shown from Table 4 that, on the average in the second round, he underestimated longitudinal cracks by 4.7 m and transverse crack by 4.8 m per 100-ft (30.5-m) station whereas he overestimated block cracks by 3.6 m². To determine the

TABLE 4—Two test results of MIAS done by Investigator A.

No.	Station	Longitudinal Crack, m				Transverse Crack, m				Block Crack, m ²			
		A1	A2	A1-A2	A1-A2	A1	A2	A1-A2	A1-A2	A1	A2	A1-A2	A1-A2
1	0-100	44.8	44.4	0.4	0.4	60.9	61.8	-0.9	0.9	2.0	1.9	0.1	0.1
2	100-200	60.7	63.6	-2.9	2.9	65.0	64.7	0.3	0.3	2.2	2.1	0.1	0.1
3	200-300	33.3	28.9	4.4	4.4	62.4	66.3	-3.9	3.9	8.8	8.9	-0.2	0.2
4	300-400	59.7	73.9	-14.1	14.1	70.7	69.1	1.6	1.6	26.6	24.0	2.6	2.6
5	400-500	28.4	26.5	1.9	1.9	74.2	67.9	6.3	6.3	52.4	54.5	-2.1	2.1
6	500-600	37.3	39.4	-2.0	2.0	64.8	64.6	0.2	0.2	0.0	0.0	0.0	0.0
7	600-700	45.6	42.5	3.1	3.1	59.8	55.7	4.1	4.1	6.3	12.0	-5.7	5.7
8	700-800	86.7	79.0	7.7	7.7	45.5	44.9	0.6	0.6	31.4	35.1	-3.7	3.7
9	800-900	96.8	77.9	18.9	18.9	59.8	52.5	7.3	7.3	54.2	56.9	-2.8	2.8
10	900-1000	94.4	84.0	10.3	10.3	85.5	76.5	9.1	9.1	23.2	36.1	-12.9	12.9
11	1000-1100	93.3	86.7	6.6	6.6	79.2	74.3	5.0	5.0	16.9	24.0	-7.1	7.1
12	1100-1200	75.0	67.6	7.4	7.4	72.5	57.6	14.9	14.9	41.8	46.3	-4.4	4.4
13	1200-1300	65.9	65.4	0.5	0.5	88.0	78.1	9.9	9.9	38.2	40.9	-2.7	2.7
14	1300-1400	144.1	127.1	17.0	17.0	76.0	63.4	12.6	12.6	9.1	22.1	-13.0	13.0
15	1400-1500	99.3	87.9	11.4	11.4	86.1	81.4	4.7	4.7	11.4	14.3	-2.9	2.9
	Average	71.0	66.3	4.7	7.3	70.0	65.2	4.8	5.4	21.6	25.3	-3.6	4.0
	Relative Precision	68.7		0.07	0.11	67.6		0.07	0.08	23.4		-0.16	0.17

repeatability of individual A, the average values of the absolute difference between two measurements were computed as 7.3 m for longitudinal cracks, 5.4 m for transverse cracks, and 4.0 m² for block cracks. These values are quite small given that the average lengths of these cracks were 68.7 m, 67.6 m, and 23.4 m² per 100-ft (30.5-m) station, respectively. We then computed the relative precisions for three cracking types by dividing the average absolute difference by the average value resulting in 11, 8, and 17 %, respectively. These values are a significant improvement over the relative precisions of MDCS/MDAS by the same person of 60, 47, and 61 %, respectively. These small relative precision values indicate that the distress collection and analysis result from individual A using AICS/MIAS is more repeatable than MDCS/MDAS.

As shown in Fig. 10, for all three cracking types, longitudinal, transverse, and block, measurements by individual B are plotted very near from the 45-deg equality line. It can be shown from Table 5 that, on the average in the second round, he underestimated longitudinal cracks by 2.8 m and transverse crack by 4.7 m per 100-ft (30.5-m) station whereas he overestimated block cracks by 0.8 m². To determine the repeatability of individual B, the average values of the absolute difference between two measurements were computed as 5.7 m for longitudinal cracks, 7.4 m for transverse cracks, and 2.1 m² for block cracks.

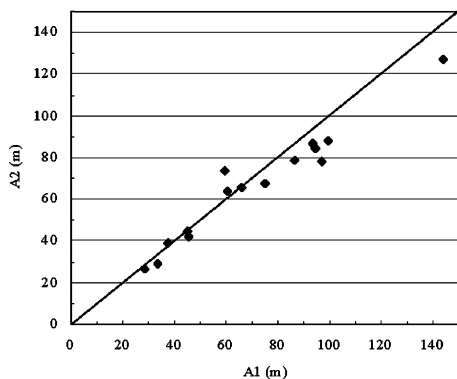
TABLE 5—Two test results of MIAS Done by Investigator B.

No.	Station	Longitudinal Crack, m				Transverse Crack, m				Block Crack, m ²			
		B1	B2	B1-B2	B1-B2	B1	B2	B1-B2	B1-B2	B1	B2	B1-B2	B1-B2
1	0-100	66.5	66.3	0.2	0.2	65.6	48.4	17.2	17.2	5.6	12.7	-7.1	7.1
2	100-200	71.2	75.2	-4.0	4.0	67.6	62.7	5.0	5.0	2.7	2.6	0.1	0.1
3	200-300	33.4	35.4	-2.0	2.0	80.7	65.6	15.0	15.0	5.0	6.4	-1.3	1.3
4	300-400	86.2	79.9	6.3	6.3	103.7	104.6	-0.9	0.9	9.8	9.4	0.4	0.4
5	400-500	64.7	60.5	4.2	4.2	96.7	86.6	10.1	10.1	17.2	22.1	-4.9	4.9
6	500-600	47.9	46.7	1.2	1.2	65.9	62.5	3.4	3.4	1.1	1.2	-0.1	0.1
7	600-700	53.1	54.9	-1.8	1.8	53.7	52.3	1.4	1.4	9.0	8.5	0.5	0.5
8	700-800	112.3	104.9	7.4	7.4	59.3	57.4	1.9	1.9	13.5	14.1	-0.7	0.7
9	800-900	139.5	129.7	9.8	9.8	64.6	77.0	-12.4	12.4	23.7	23.9	-0.1	0.1
10	900-1000	93.6	107.1	-13.5	13.5	86.0	79.9	6.1	6.1	26.4	20.1	6.3	6.3
11	1000-1100	122.9	107.8	15.0	15.0	89.5	96.0	-6.5	6.5	13.3	12.1	1.2	1.2
12	1100-1200	106.7	101.1	5.5	5.5	87.8	80.8	7.1	7.1	17.2	19.5	-2.4	2.4
13	1200-1300	99.5	99.4	0.2	0.2	107.2	87.5	19.7	19.7	19.5	24.7	-5.2	5.2
14	1300-1400	141.2	135.1	6.1	6.1	76.0	71.6	4.4	4.4	6.7	6.9	-0.2	0.2
15	1400-1500	101.5	93.5	8.0	8.0	101.2	102.0	-0.8	0.8	9.8	8.4	1.4	1.4
	Average	89.3	86.5	2.8	5.7	80.4	75.7	4.7	7.4	12.0	12.8	-0.8	2.1
	Relative Precision	87.9		0.03	0.06	78.0		0.06	0.10	12.4		-0.06	0.17

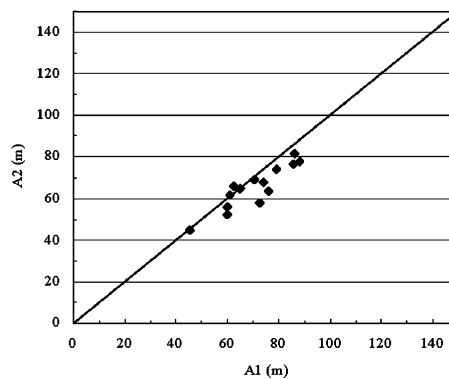
TABLE 6—Two test results of MIAS done by Investigator C.

No.	Station	Longitudinal Crack, m				Transverse Crack, m				Block Crack, m ²			
		C1	C2	C1-C2	C1-C2	C1	C2	C1-C2	C1-C2	C1	C2	C1-C2	C1-C2
1	0-100	52.2	51.8	0.4	0.4	86.5	86.0	0.5	0.5	2.9	2.9	0.0	0.0
2	100-200	62.1	62.5	-0.4	0.4	67.4	64.3	3.1	3.1	7.0	7.1	-0.1	0.1
3	200-300	44.7	40.0	4.7	4.7	74.5	75.2	-0.7	0.7	3.2	3.3	0.0	0.0
4	300-400	89.8	45.5	44.3	44.3	119.1	92.1	27.0	27.0	8.0	37.0	-28.9	28.9
5	400-500	46.3	48.5	-2.2	2.2	130.6	133.5	-2.9	2.9	13.6	12.3	1.3	1.3
6	500-600	38.5	37.0	1.5	1.5	70.5	72.5	-2.0	2.0	0.0	0.0	0.0	0.0
7	600-700	43.7	49.2	-5.5	5.5	65.7	60.8	4.9	4.9	12.4	11.6	0.8	0.8
8	700-800	63.2	70.7	-7.5	7.5	38.8	47.3	-8.5	8.5	48.8	40.0	8.9	8.9
9	800-900	84.9	110.9	-26.0	26.0	62.3	63.6	-1.2	1.2	53.5	38.2	15.3	15.3
10	900-1000	33.8	43.0	-9.3	9.3	56.7	57.3	-0.6	0.6	86.9	77.6	9.3	9.3
11	1000-1100	59.7	50.5	9.2	9.2	56.1	51.6	4.5	4.5	65.1	76.4	-11.3	11.3
12	1100-1200	79.8	86.3	-6.5	6.5	93.2	98.2	-5.0	5.0	29.2	25.2	4.0	4.0
13	1200-1300	65.4	70.2	-4.8	4.8	108.6	105.5	3.1	3.1	29.9	29.4	0.5	0.5
14	1300-1400	142.8	138.4	4.4	4.4	93.9	91.6	2.3	2.3	8.7	13.0	-4.3	4.3
15	1400-1500	115.9	116.0	-0.1	0.1	106.4	106.5	-0.1	0.1	3.9	4.0	-0.1	0.1
Average		68.2	68.0	0.1	8.4	82.0	80.4	1.6	4.4	24.9	25.2	-0.3	5.7
Relative Precision		68.1		0.00	0.12	81.2		0.02	0.05	25.0		-0.01	0.23

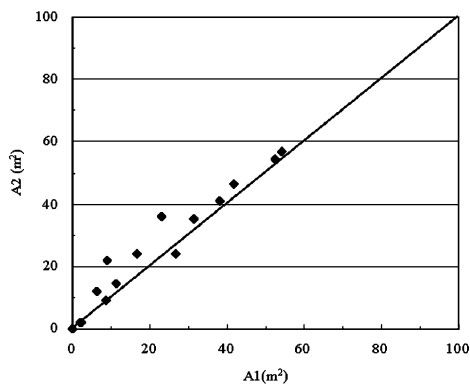
These values are relatively small given that the average lengths of these cracks were 87.9 m, 78.0 m, and 12.4 m² per 100-ft (30.5-m) station, respectively. We then computed the relative precisions for three cracking types by dividing the average absolute difference by the average value resulting in 6, 10, and 17 %, respectively. These values are a significant improvement over the relative precisions of MDCS/



(a) Longitudinal Crack



(b) Transverse Crack



(c) Block Crack

FIG. 9—Comparison between first and second data of MIAS by Investigator A.

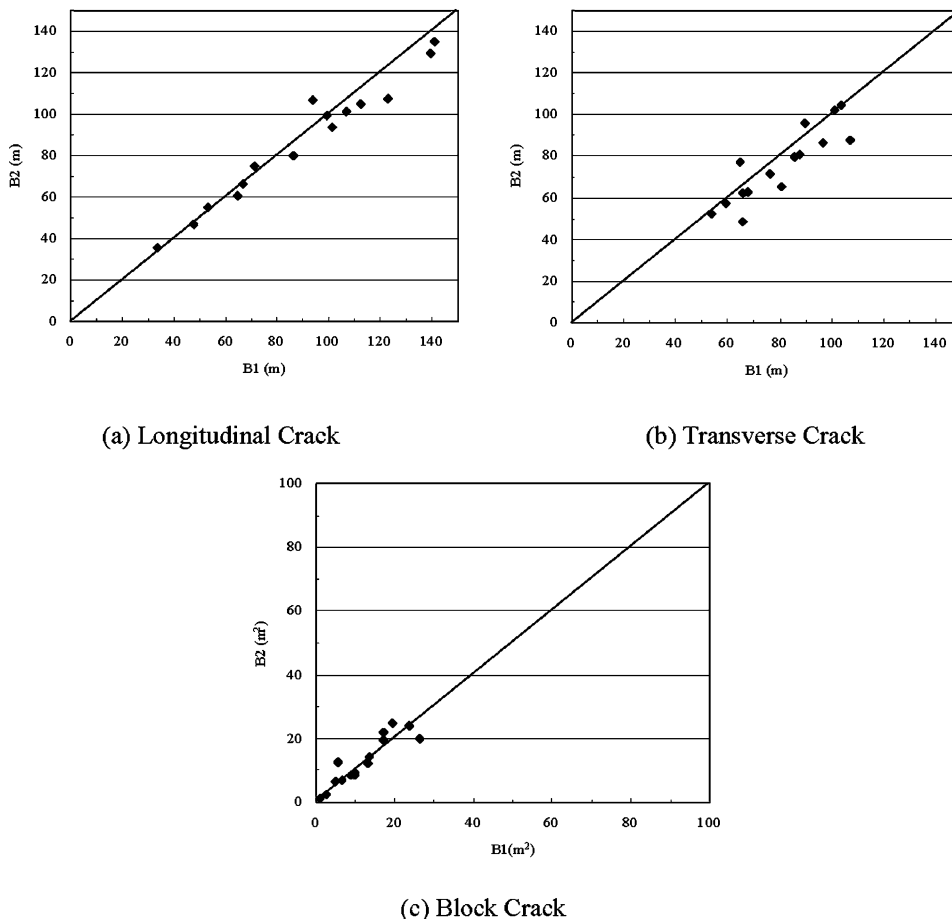


FIG. 10—Comparison between first and second data of MIAS by Investigator B.

MDAS by the same person of 33, 59, and 45 %, respectively. These small relative precision values indicate that the distress collection and analysis result from individual B using AICS/MIAS is more repeatable than MDCS/MDAS.

As shown in Fig. 11, for all three cracking types, longitudinal, transverse, and block, measurements by individual C are plotted very near from the 45-deg equality line. It can be shown from Table 6 that, on the average in the second round, she underestimated longitudinal cracks by 0.1 m and transverse crack by 1.6 m per 100-ft (30.5-m) station whereas she overestimated block cracks by 0.3 m². To determine the repeatability of individual C, the average values of the absolute difference between two measurements were computed as 8.4 m for longitudinal cracks, 4.4 m for transverse cracks, and 5.7 m for block cracks. These values are relatively small given that the average lengths of these cracks were 68.1 m, 81.2 m, and 25.0 m² per 100-ft (30.5-m) station, respectively. We then computed the relative precisions for three cracking types by dividing the average absolute difference by the average value resulting in 12, 5, and 23 %, respectively. These values are a significant improvement over the relative precisions of MDCS/MDAS by the same person of 36, 30, and 18 %, respectively. These small relative precision values indicate that the distress collection and analysis result from individual C using AICS/MIAS is more repeatable than MDCS/MDAS except for block cracks.

Comparison Between MDCS/MDAS and AICS/MIAS

To compare consistency between MDCS/MDAS and AICS/MIAS, average values of six distress measurements by three individuals using these two distress survey methods are summarized in Table 7 and plotted in Fig. 12.

As shown in Fig. 12, for all three cracking types, longitudinal, transverse, and block, average measurements by two methods are scattered away from the 45-deg equality line. It is interesting to note that, using the AICS/MIAS, all three individuals identified many more cracks in longitudinal and transverse

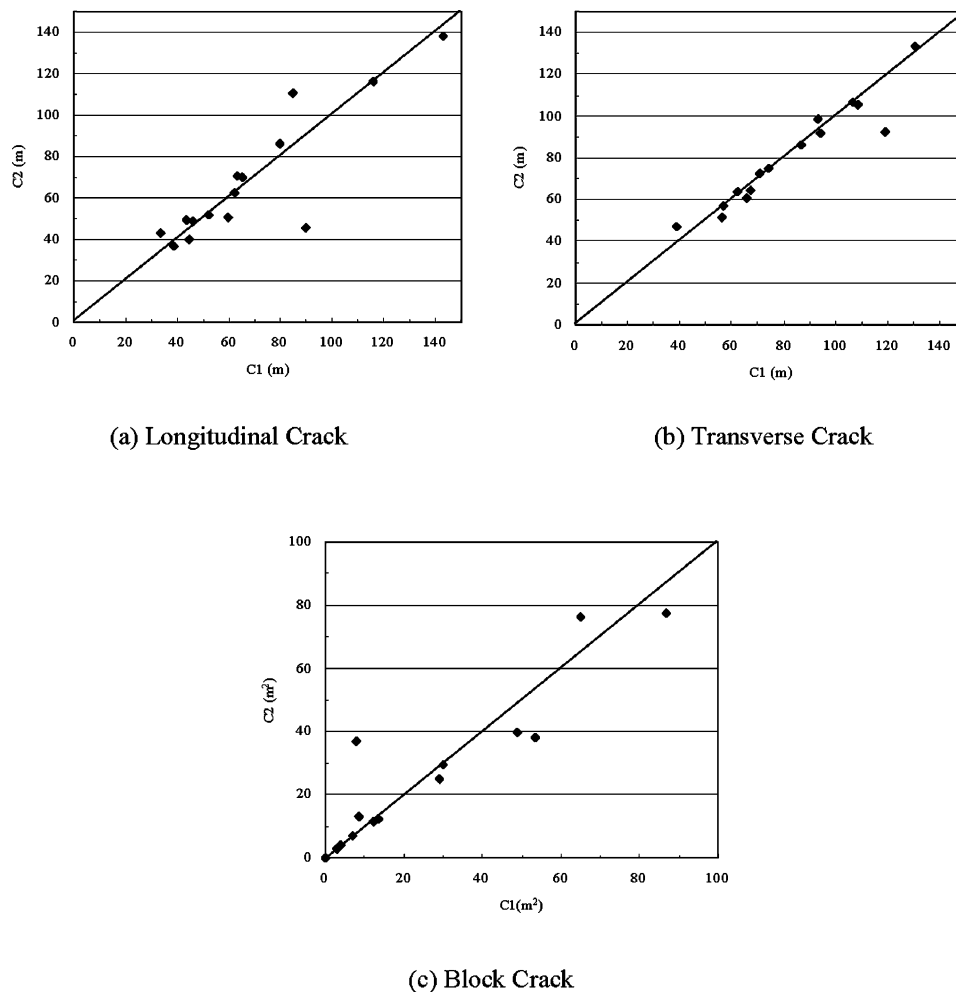


FIG. 11—Comparison between first and second data of MIAS by Investigator C.

cracks although they observed slightly less block cracks. It seems reasonable because people can see cracks better using AICS/MIAS rather than MDCS/MDAS. It can be shown from Table 7 that, on the average using AICS/MIAS, three individuals overestimated longitudinal cracks by 53.3 m and transverse

TABLE 7—Comparison between MDAS and MIAS.

No.	Station	Longitudinal Crack, m				Transverse Crack, m				Block Crack, m ²			
		MDAS	MIAS	MDAS- MIAS	MDAS- MIAS	MDAS	MIAS	MDAS- MIAS	MDAS- MIAS	MDAS	MIAS	MDAS- MIAS	MDAS- MIAS
1	0–100	32.0	54.3	-22.3	22.3	60.1	68.2	-8.1	8.1	1.2	4.7	-3.5	3.5
2	100–200	49.8	65.9	-16.0	16.0	73.2	65.3	7.9	7.9	0.9	4.0	-3.0	3.0
3	200–300	46.5	36.0	10.6	10.6	99.2	70.8	28.4	28.4	0.0	5.9	-5.9	5.9
4	300–400	33.0	72.5	-39.5	39.5	45.8	93.2	-47.4	47.4	27.8	19.1	8.7	8.7
5	400–500	27.3	45.8	-18.5	18.5	92.1	98.2	-6.1	6.1	19.2	28.7	-9.4	9.4
6	500–600	31.2	41.1	-9.9	9.9	64.3	66.8	-2.5	2.5	0.0	0.4	-0.4	0.4
7	600–700	22.5	48.2	-25.7	25.7	39.8	58.0	-18.2	18.2	9.8	10.0	-0.2	0.2
8	700–800	17.1	86.1	-69.0	69.0	20.4	48.9	-28.5	28.5	39.0	30.5	8.6	8.6
9	800–900	13.1	106.6	-93.5	93.5	15.1	63.3	-48.2	48.2	50.8	41.7	9.1	9.1
10	900–1000	6.5	76.0	-69.5	69.5	12.3	73.7	-61.3	61.3	50.5	45.1	5.5	5.5
11	1000–1100	0.2	86.8	-86.6	86.6	5.3	74.4	-69.1	69.1	60.1	34.6	25.5	25.5
12	1100–1200	22.9	86.1	-63.2	63.2	57.7	81.7	-24.0	24.0	36.2	29.9	6.3	6.3
13	1200–1300	21.8	77.6	-55.8	55.8	43.6	95.8	-52.2	52.2	36.1	30.4	5.7	5.7
14	1300–1400	0.0	138.1	-138.1	138.1	3.5	78.8	-75.3	75.3	50.2	11.1	39.1	39.1
15	1400–1500	0.0	102.4	-102.4	102.4	4.8	97.3	-92.5	92.5	51.9	8.7	43.2	43.2
	Average	21.6	74.9	-53.3	54.7	42.5	75.6	-33.1	38.0	28.9	20.3	8.6	11.6
	Relative Precision		48.3	-1.10	1.13		59.1	-0.56	0.64		24.6	0.35	0.47

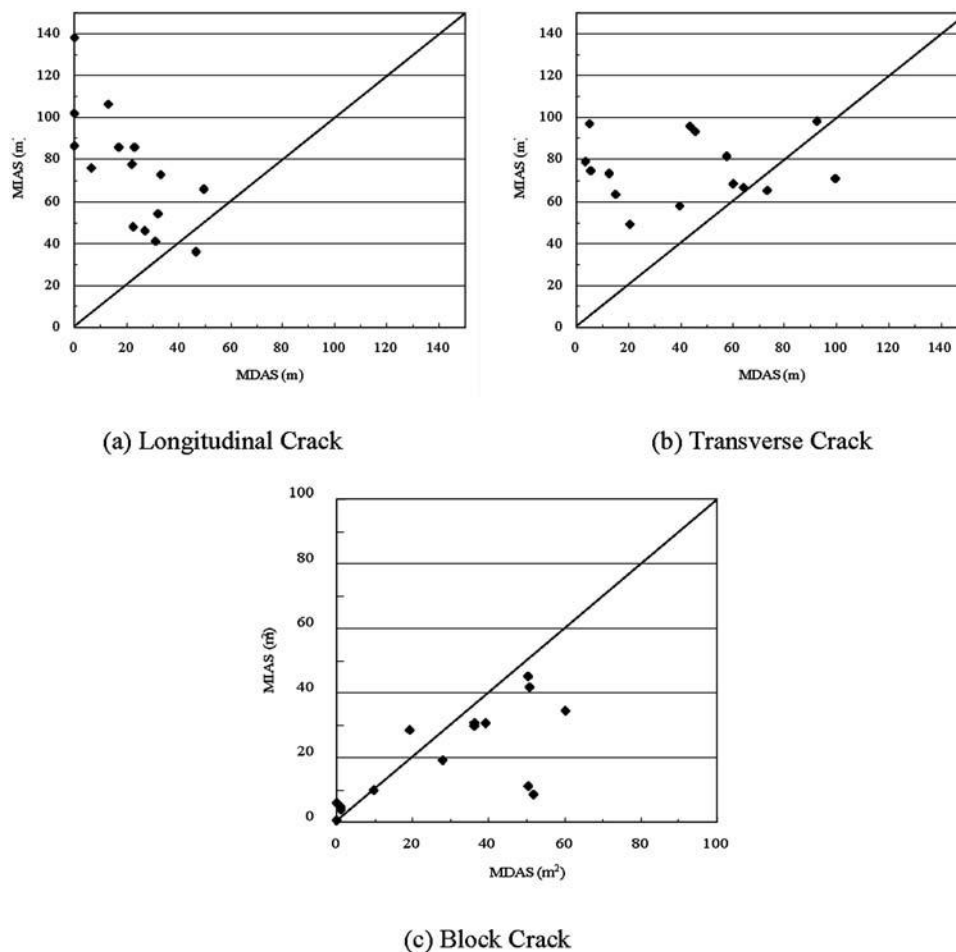


FIG. 12—Comparison between MDAS and MIAS.

crack by 33.1 m per 100-ft (30.5-m) station whereas they underestimated block cracks by 8.6 m². The average values of the absolute difference between two measurements were computed as 54.7 m for longitudinal cracks, 38.0 m for transverse cracks, and 11.6 m² for block cracks. These values are quite large given that the average lengths of these cracks were 48.3 m, 59.1 m, and 24.6 m² per 100-ft (30.5-m) station, respectively. We then computed the relative precisions for three cracking types by dividing the average absolute difference by the average value resulting in 113, 64, and 47 %, respectively. These very large relative precision values indicate that the distress measurements using ACIS/MIAS are significantly different from those obtained using MDCS/MDAS, particularly in longitudinal cracks.

Summary and Conclusions

In the past, many highway agencies relied on the Manual Distress Collection System (MDCS) and Manual Distress Analysis System (MDAS) as “ground-truth” for evaluating Automated Image Collection System (AICS) and Automated Image Analysis System (AIAS). However, both MDCS and MDAS have a number of limitations, which include subjectivity and inconsistency. This paper presents Manual Image Analysis System (MIAS) as “ground-truth” for evaluating different pavement distress analysis systems such as AIAS. Given the black-box nature of most AIAS’s available in the market today, it is critical for owner agencies to develop an objective QA/QC procedure based on MIAS. In addition, the proposed MIAS-based QA/QC procedure can be used to isolate various sources of error associated with different distress collection equipment and automatic analysis software.

For this study, first, the images were collected using the AICS. The images were then analyzed using MIAS by three different individuals. To determine the repeatability of each individual in the MIAS process, they were asked to evaluate the same images twice after the images were randomly shuffled. The same individuals were asked to collect distress information from the same pavement section in the field by

drawing distress maps on the grid papers. They later analyzed the distress maps in the office. To determine the repeatability of each individual in the MDCS/MDAS process, they were asked to conduct the survey twice in the opposite direction.

In all cases, repeatability of the three individuals was consistently better when they were using the AICS/MIAS approach rather than the MDCS/MDAS approach. This indicates that AICS/MIAS is a more consistent method in evaluating pavement distresses compared to MDCS/MDAS. In addition, using the AICS/MIAS, all three individuals identified many more cracks in longitudinal and transverse cracks although they observed slightly less block cracks. It seems reasonable because people can see cracks better using AICS/MIAS rather than using MDCS/MDAS in the field.

Given the high repeatability error of MDCS/MDAS reported in this study, it should not be considered as “ground-truth” for evaluating Automated Image Collection System (AICS) and Automated Image Analysis System (AIAS). Instead, given its better repeatability and visibility, the proposed AIAS/MIAS method should be adopted as “ground-truth” for evaluating other evaluation methods such as AIAS.

This paper addressed the main source of error associated with the human operators in collecting and interpreting the pavement distresses. The paper did not address the source of error associated with distress collection equipment and automated image analysis algorithms. Therefore, precautions should be taken to account for the variability under different distress collection equipment and lighting conditions. In the future, it is recommended that the effect of ambient illumination on crack visibility should be considered by using different image collection equipment in different ambient lighting conditions.

References

- [1] Lee, H., *Standardization of Distress Measurements for the Network-Level Pavement Management System, ASTM STP 1121*, ASTM International, West Conshohocken, PA, 1992, pp. 424–436.
- [2] Paterson, W. D., “Proposal of Universal Cracking Indicator for Pavements,” *Transp. Res. Rec.*, No. 1455, 1994.
- [3] Wang, K. C. P. and Gong, W., “Automated Pavement Distress Survey: A Review and A New Direction,” Pavement Evaluation Conference, 2002.
- [4] Haas, C. and McNeil, S., “Criteria for Evaluating Pavement Imaging Systems,” *Transp. Res. Rec.*, No. 1260, 1990.
- [5] Luhr, D. R., “A Proposed Methodology to Quantify and Verify Automated Crack Survey Measurements,” the 78th Annual TRB Meeting, Washington, DC, January 1999.
- [6] Daleiden, J. F. and Simpson, A. L., “Off-the-Wall Pavement Distress Variability Study,” *Transp. Res. Rec.*, No. 1643, 1998.
- [7] Richter, C., “Key Findings from LTPP Distress Data,” FHWA-RD-02-031, 2002.
- [8] Rada, G. R., Wu, C. L., Elkins, G. E., Bhandari, R. K., and Bellinger, W. Y., “Update of Long-Term Pavement Performance Manual Distress Data Variability, Bias and Precision,” *Transp. Res. Rec.*, No. 1643, 1998.
- [9] Miller, W. R., Raman, M., Hossain, M., Cumberledge, G., Reigle, J., Lee, H., and Kang, K., “Comparison of Image-Based Distress Survey Results with Manual Distress Surveys for Transverse Cracking,” the 82nd Annual TRB Meeting, Washington, DC, January 2003.
- [10] Cline, G. D., Shahin, M. Y., and Burkhalter, J. A., “Automated Pavement Condition Index Survey,” the 82nd Annual TRB Meeting, Washington, DC, January 2003.
- [11] Smith, K. L., Stivers, M. L., Hoerner, T. E., and Romine, A. R., “Highway Maintenance Quality Assurance,” ERES Consultants, Inc, ERES Project 086-R1-94, April 1997.
- [12] Morian, D., Stoffels, S., and Frith, D. J., “Quality Management of Pavement Performance Data,” the 82nd Annual TRB Meeting, Washington, DC, January 2003.
- [13] Larson, C. D., Sami, N., and Luhr, D. R., “Structured Approach to Managing Quality of Pavement Distress Data,” *Transp. Res. Rec.*, No. 1699, 2000.
- [14] Groeger, J. L., Stephanos, P., Dorsey, P., and Chapman, M., “Implementation of Automated Network Level Crack Detection Processes in the State of Maryland,” the 82nd Annual TRB Meeting, Washington, DC, January 2003.
- [15] Landers, S., Bekheet, W., and Falls, L. C., “The Use of Cohen’s Weighted Kappa Statistic in Quality Control/Quality Assurance Procedures for Network Level Contract Pavement Surface Condition

Surveys in British Columbia,” the 82nd Annual TRB Meeting, Washington, DC, January 2003.

- [16] Selezneva, O., Mladenovic, G., Speir, R., Amenta, J., and Kennedy, J., “QA Sampling Considerations for Automated Distress Data Collection and Processing for National Park Service Road Inventory Program,” the 83rd Annual TRB Meeting, Washington, DC, January 2004.
- [17] Smith, R. E., Freeman, T. J., and Pendleton, O. J., “Contracting for Pavement Distress Data Collection,” *Transp. Res. Rec.*, No. 1643, 1998.
- [18] LTPP Distress Identification Manual for the Long-Term Pavement Performance Project, SHRP-P-338, National Research Council, Washington, DC, 1993.

Nicolas Gagarin¹ and James R. Mekemson¹

Analysis of Surface Inertial Profiles Measured on Jointed Portland Cement Pavements

ABSTRACT: The feasibility of measuring slab curling using high-speed profilers was assessed by the Turner-Fairbank Highway Research Center of the Federal Highway Administration. The primary objectives of the study were to: (1) measure the surface profile of the concrete slabs using state-of-the-art profiling technology, (2) establish a standard procedure to identify warping and curling of the slabs using the measured surface profiles, (3) relate the changes in pavement surface profiles to the change in surface temperature, (4) determine the relationship between changes in pavement surface profile, roughness, premature transverse cracking, and construction condition, and (5) establish a standard procedure to analyze the condition of joints, including rotation and faulting, and determine the relationship between joint condition, and roughness. The paper discusses data mining on a database of 16 000 slabs measured during four time windows in a 24-h period. A visualization of all parameters and samples at all four times of the day show the groups of slabs which have cracked and are likely to crack shown by the divergence from the normal response measured in most slabs.

KEYWORDS: inertial, profile, warping, curl, concrete slabs, joints, roughness, empirical mode decomposition

Introduction

Inertial profile measurements are used mainly in practice to compute roughness parameters such as the International Roughness Index (IRI). In the case of profiles measured on Portland Concrete Cement (PCC) pavements made of jointed slabs, the patterns of slab curling due to daily changes in surface temperature, and the sag in the string lines used to guide the equipment at construction are recognizable features in the inertial profile measurements.

Figure 1 is comprised of two plots. The top plot is the inertial profile of a PCC pavement and the bottom plot is a nonlinear, nonstationary decomposition of that inertial profile. Elevation in millimetres is plotted against distance in metres. The bottom plot has three curves. They are summations of some of the intrinsic mode functions produced by the empirical mode decomposition method used by the Hilbert-Huang Transform [1,2]. The top curve captures the wavelength that corresponds to a sagging string line used during construction of the concrete slab pavement. The middle curve shows the amount of curling of the individual slabs. The bottom curve shows the pavement texture, joints spaced at 6.1 m, and a crack in the middle of a slab. This paper discusses the analysis of inertial profiles to estimate changes in slab shape and joint geometry due to surface temperature variations.

Background

The first attempt to utilize inertial profiles for measuring slab curvature was made by Byrum [3]. Using historical data from the Long-Term Pavement Performance (LTPP) database, curvature was estimated by performing a prescribed series of estimations at different sampling intervals and averaging them a few times. Before the Byrum estimates of the curvature could be made, the data near the joints were truncated to stabilize the computation. The sampling interval of the data used in this work was 150 mm. In the theory of plates and shells, and infinite foundations, with mechanics of materials in the elastic range, slab curvature is related to the modulus of elasticity, moment of inertia, and the second derivative of the vertical

Manuscript received October 20, 2004; accepted for publication February 17, 2006; published online March 2006. Presented at ASTM Symposium on Pavement Surface Condition/Performance Assessment: Procedures and Technologies on 07 December 2004 in Washington, DC; B. Choubane, Guest Editor.

¹ President and Research Engineer, respectively, Starodub, Inc., Kensington, MD 20895.

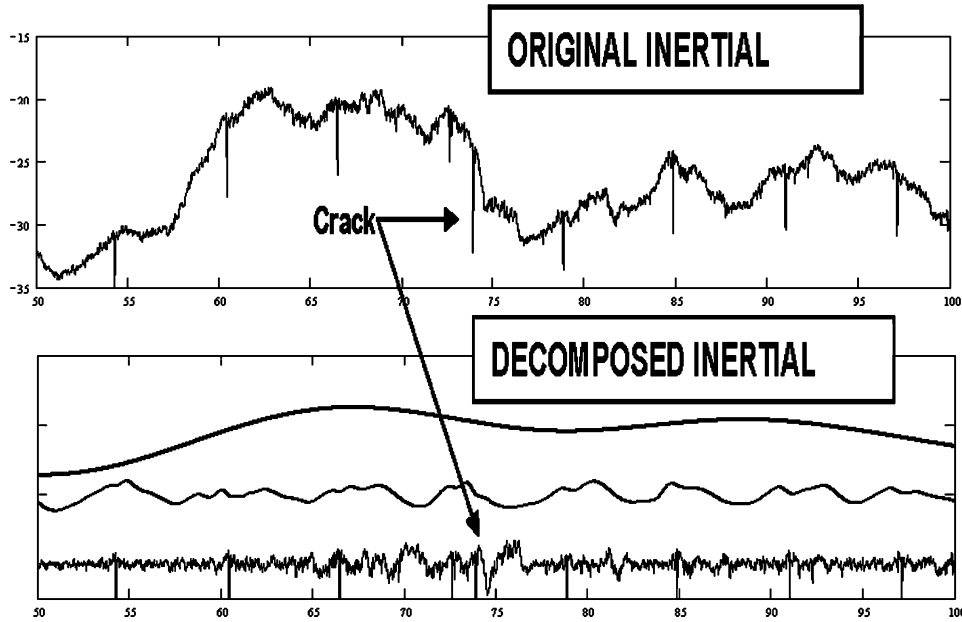


FIG. 1—Plots of inertial profile, string line sag, warp and curl, and other components.

deflection of the slab. Byrum's assumption is that the measured surface profile is directly related to the curvature of the slab. Given the other irregularities of the concrete surfaces that exist, this assumption may not be correct in many if not most cases. Slab curvature measurement would also require measuring the surface profile of the slab underside.

A new effort to utilize inertial profile measurements to capture changes in surface profiles was made by Sixbey et al. [4]. The primary objectives of the study were to:

- (1) measure the surface curvature of the concrete slabs using existing profiling technology;
- (2) establish a standard procedure to identify warp and curl from profiler data;
- (3) quantify the change in curvature due to temperature changes;
- (4) determine the sampling interval required to measure curvature;
- (5) determine the relationship between curvature and roughness measurements; and
- (6) relate curvature data to premature transverse pavement cracking and construction conditions.

Four separate surveys were conducted on 25.6 km of a four-lane interstate highway within a 24-h time period (4/30/2000–5/1/2000). Each survey consisted of collecting data on each of the four lanes (totaling 102.5.lane-km for each survey) within a specific 2-h window. The time windows for the surveys were: 6–8 p.m., 4–6 a.m., 6–8 a.m., and 11 a.m.–1 p.m.. In Fig. 2, the range of temperatures were 3 to 23°C for air, 8 to 30°C for pavement surface, and 14 to 19°C for subsurface from a nearby weather station near the site. The coolest surface temperatures were recorded in the 4–6 a.m. time window and the hottest surface temperatures were recorded in the 11 a.m.–1 p.m. time window. As warping is related to temperature gradients, it should be noted that a 22°C pavement surface temperature differential was recorded within a 24-h period.

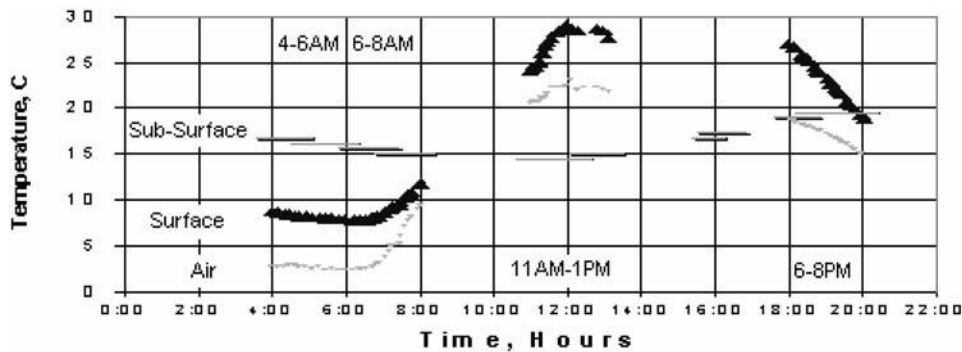


FIG. 2—Air, surface, and subsurface temperatures versus time of day from the weather station.

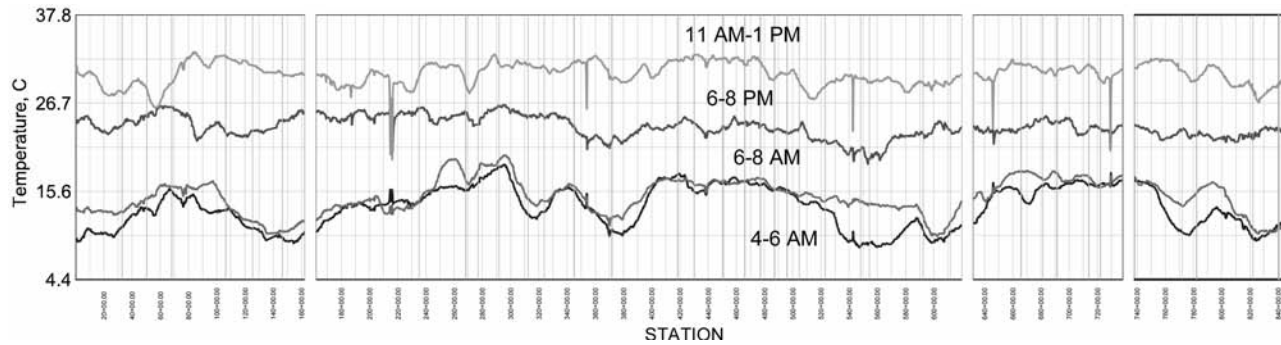


FIG. 3—Pavement surface passing lane temperature versus station (0+00–840+00).

Surface temperatures were recorded with an infrared sensor during each of the four time windows. Figure 3 shows that the surface temperatures measured in the passing lane were very similar in 4–6 a.m. and 6–8 a.m. time windows. The 11 a.m.–1 p.m. and 6–8 p.m. time windows are distinct from all others. As shown in Fig. 3, the pavement surface temperature in the 6–8 p.m. time window is decreasing faster relative to the other three time windows. The pavement surface temperature slowly decreased as the four lanes were being surveyed within this 2-h window. Similar to the weather station data, the coolest pavement surface temperatures were recorded in the 4–6 a.m. time window and the hottest surface temperatures were recorded in the 11 a.m.–1 p.m. time window. This temperature data were used in the analysis of slab deformation. Figure 4 shows the change in surface profile of a single slab during the four time windows.

The sampling interval of the inertial profile measurements was 5 mm. The need for finer sampling interval was required by the pattern recognition method utilized to identify joints, and to match the joints in the different data collection runs in order to compare the various parameters. The inertial profiling hardware met the levels of quality necessary to capture accurate surface profiles as verified in a separate experiment. The curvature of the surface profile varies significantly along the length of the slab. Understanding that the curvature of the surface profile is not necessarily equivalent to slab curvature, a measure of the change in surface elevation of the slab along the line of the inertial profile was defined to quantify the change in slab shape with temperature. This pavement surface parameter was called “maximum deformation.” Given this empirical measure, the assumption was that the change in slab curvature is proportional to the change in this parameter. This study looked at trends between various parameters but did not relate structural slab behavior to the surface profile.

Subsequent to the work performed by Sixbey et al. [4] and Rasmussen et al. [5] proposed a new approach for identifying joints and matching two inertial profiles using a cross-correlation function. The Rasmussen et al. method assumes that the distance measurement instrument has very little variation and that the path or distance traveled in different runs is very similar. Beyond a limited length of uninterrupted

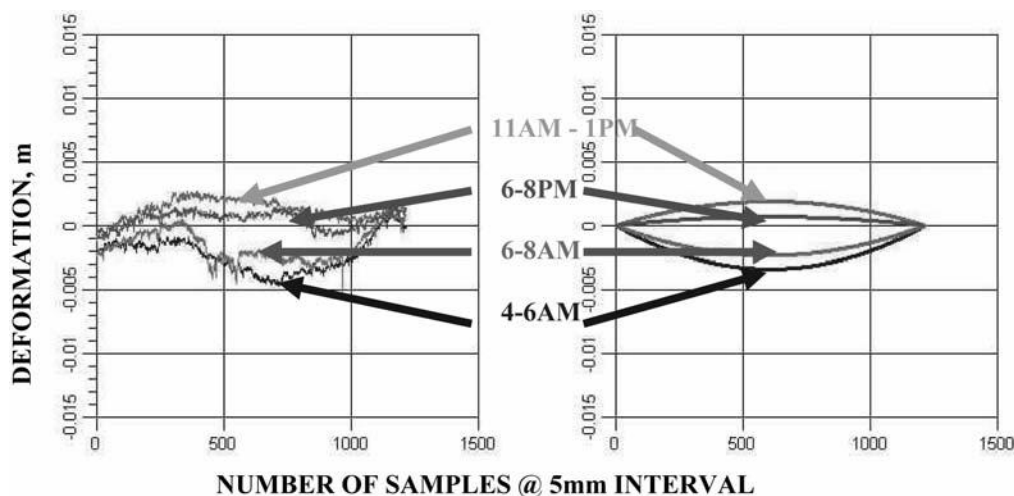


FIG. 4—Measured surface profiles and idealized shapes of one 6.1-m slab.

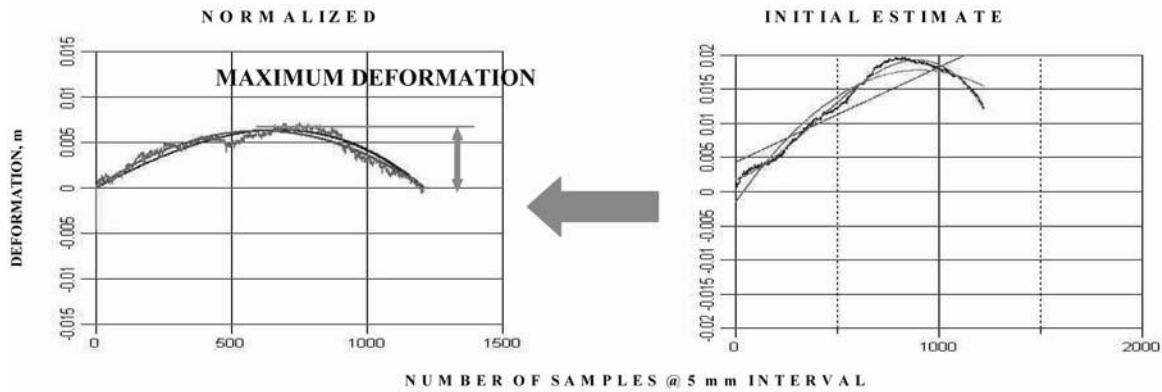


FIG. 5—Graphical definition of maximum deformation.

inertial profiles, this assumption may not hold. Using the classical definition of slab curvature at the neutral axis, it is not possible to formalize the relationship between the surface profile and the structural behavior of a slab as three-dimensional measurements are unknown. Only empirical trends in changes of curvature can be deduced.

This paper discusses the methods of analysis developed by the authors and the data mining work performed once the results of all analyses were merged.

Analysis of Slab Surface Profiles

The following procedure was used to compute the parameter “maximum surface deformation” for the quantification of the slab shape: (1) locate joints, cracks, and other surface features with 5-mm interval data; (2) identify start and end of slabs; (3) pre-process dataset keeping 5-mm interval; (4) for each slab, use 5-mm interval data from accelerometer and laser sensors to compute the slope-profile, and from the slope-profile, compute an estimate of the curvature of the surface profile; and (5) compute the profile to visualize the shape of the surface of the slab and estimate the maximum surface deformation of the slab.

Figure 5 illustrates the process used to estimate the maximum deformation of fitting quadratic and cubic curves and finding the maximum difference in elevation between the idealized profile and a reference line that passes through the end surface points near the joints.

Analysis of Joints and Slab Faulting

The procedure to estimate faulting and rotation at each joint requires the joint boundaries to be identified accurately. The boundaries include three points: the top left edge, the bottom point, and the top right edge of the joint. A linear fit of up to 50 cm on either side of the joint provides two reference lines from which rotation and faulting can be estimated.

The stability of the algorithm is a function of the span of data used to estimate the reference line on each side of the joints. Figure 6 shows the variation of the fault estimates (top half) and rotation (bottom half) for increasing data spans. The results stabilize near a span of 25 cm. One hundred randomly selected joints were used to establish the span length.

Figures 7 through 9 show the results of the boundary recognition and reference line definition steps for three joints. The abscissa is the horizontal distance in metres and the ordinate is the profile elevation in metres. Typically, the variations in profile elevations are not greater than a few centimetres, usually less than 1 cm. For example, the joint in Fig. 7 is about 10 mm deep. In Fig. 9, the joint is about 4 mm deep. Positive faulting occurs when the leading edge of the joint is higher than the trailing edge. The joint in Fig. 8 has negative faulting. Positive joint rotations are seen in Figs. 8 and 9.

Data Mining

The first phase of data mining considered the results of the analysis of surface profiles of slabs. Sixbey et al. [4] showed that: (1) the change in maximum deformation was proportional to the change in tempera-

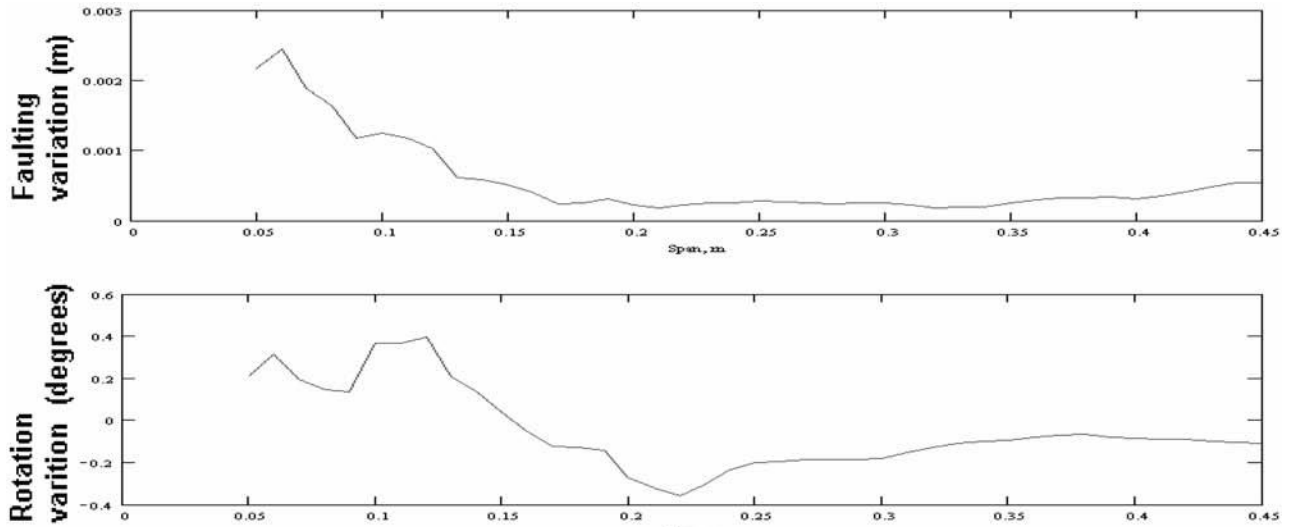


FIG. 6—Typical fault estimates and joint rotation variation versus span length.

ture; (2) the roughness of the pavement was impacted by the amount of maximum deformation but not proportional to temperature changes as some slabs flatten and others deform more; and (3) using the cases of apparently undamaged slabs to adjacent lane cracked slabs, the maximum deformation was higher for that set of slabs. Sixbey et al. also showed that temperature at the time of construction had some affect on

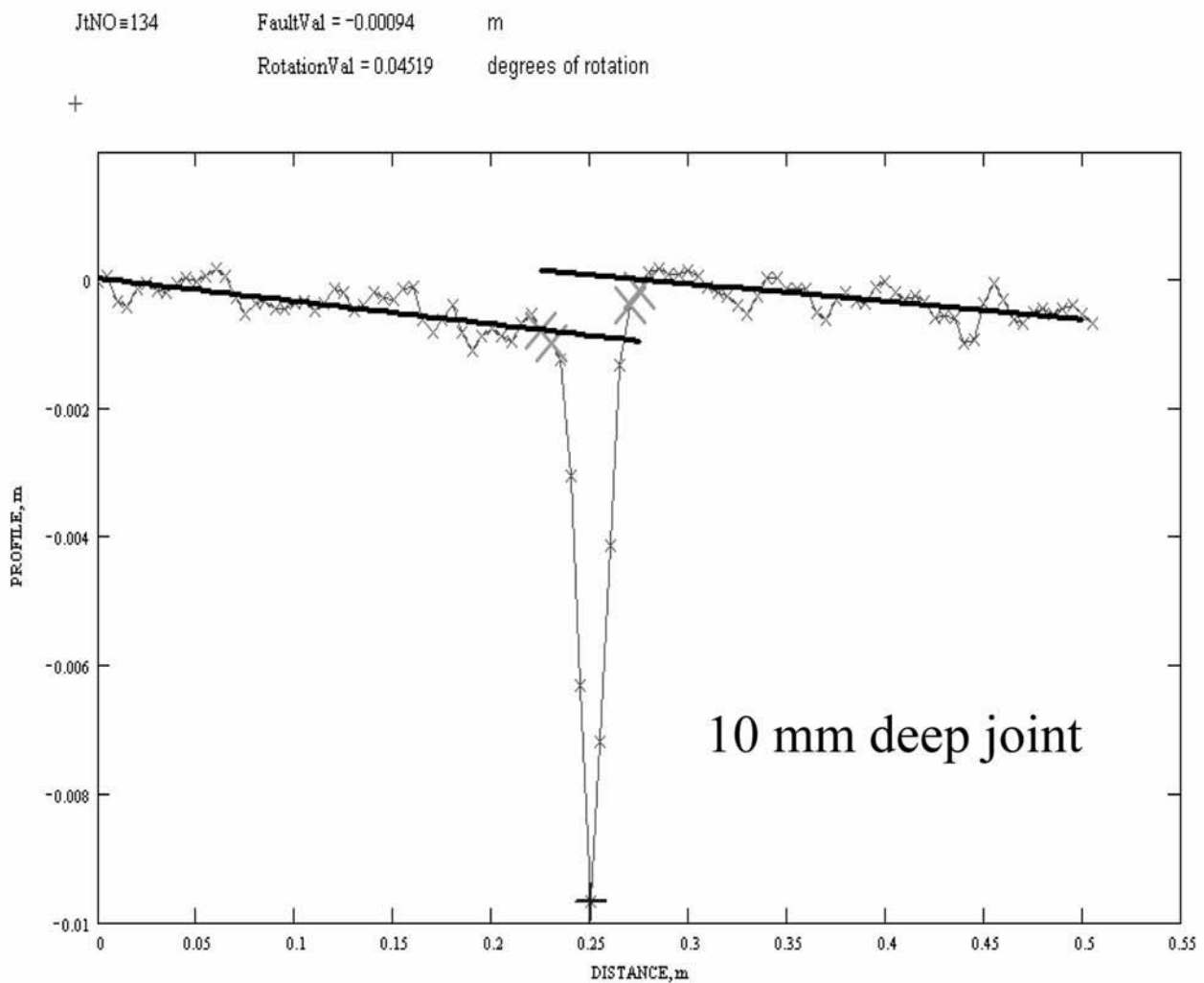


FIG. 7—Positive faulting, negative rotation.

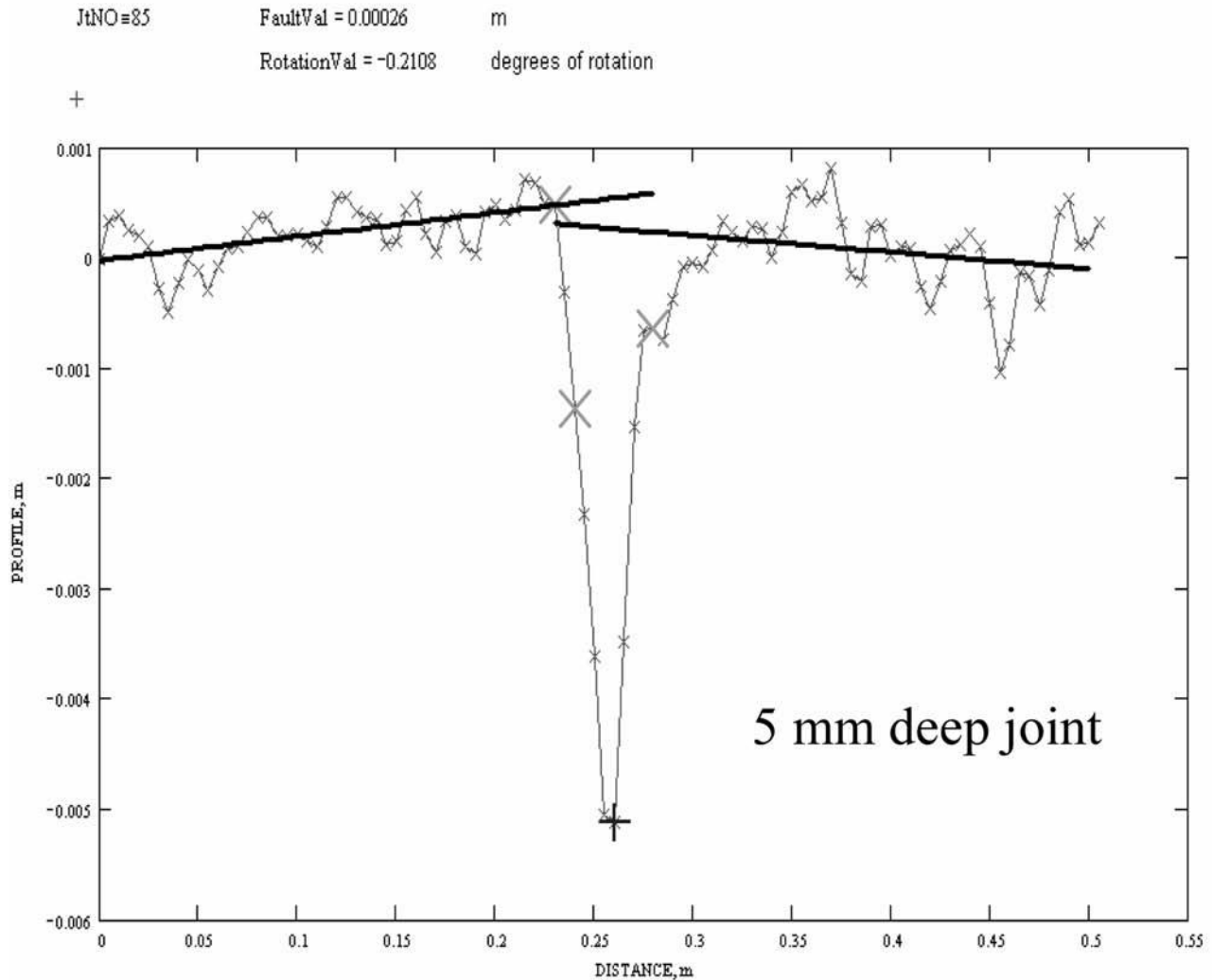


FIG. 8—Negative faulting, positive rotation.

the slab surface profile. Five sources of information were considered for data mining: (1) measured maximum deformation, (2) measured surface temperature, (3) hourly air temperature at time of construction, (4) stationing from alignment, and (5) station at boundaries of overlay and reconstruct segments. The hourly air temperatures at construction were obtained from the records of a weather station located two miles away from the site.

Figure 10 shows the five sources of information for the left lane, 6–8 p.m. time window. The upper portion of the graph shows the hourly air temperature at time of construction (points) and the pavement surface temperature at time of data collection (line). Pavement surface temperature at collection is stable around 25°C. The hourly air temperature at construction fluctuates between 10 and 40°C daily with maximum daily ranges of 20°C.

The lower portion of the graph focuses on the trend in maximum deformation of the approximately 2000 slabs over the distance of 12 km (40 000 ft=400 stations) shown on the plot. The trend was obtained by applying a median filter with a 31-slab base on the maximum deformation data.

In the second phase of data mining, joint analysis data were matched with the corresponding slab analysis data of roughness (IRI), temperature, cracks, and maximum deformation into a global database. With this new global database, a data mining plan was developed where varying levels of data subdivisions/categories were defined as shown in Fig. 11. Pavement performance measures are typically reported for summary purposes at fixed distance intervals such as 0.1 and 1.0 miles, 1 km, and overall.

The two subdivisions of the data at Level 1 are OVERLAY/RECONSTRUCT/ALL (three groups) and DRIVING LANE/PASSING LANE (two groups). The two subdivisions of Level 2 are MORNING1/MORNING2/NOON/AFTERNOON/ALL (five groups) time windows and 0.1mile/1mile/1km/ALL (four

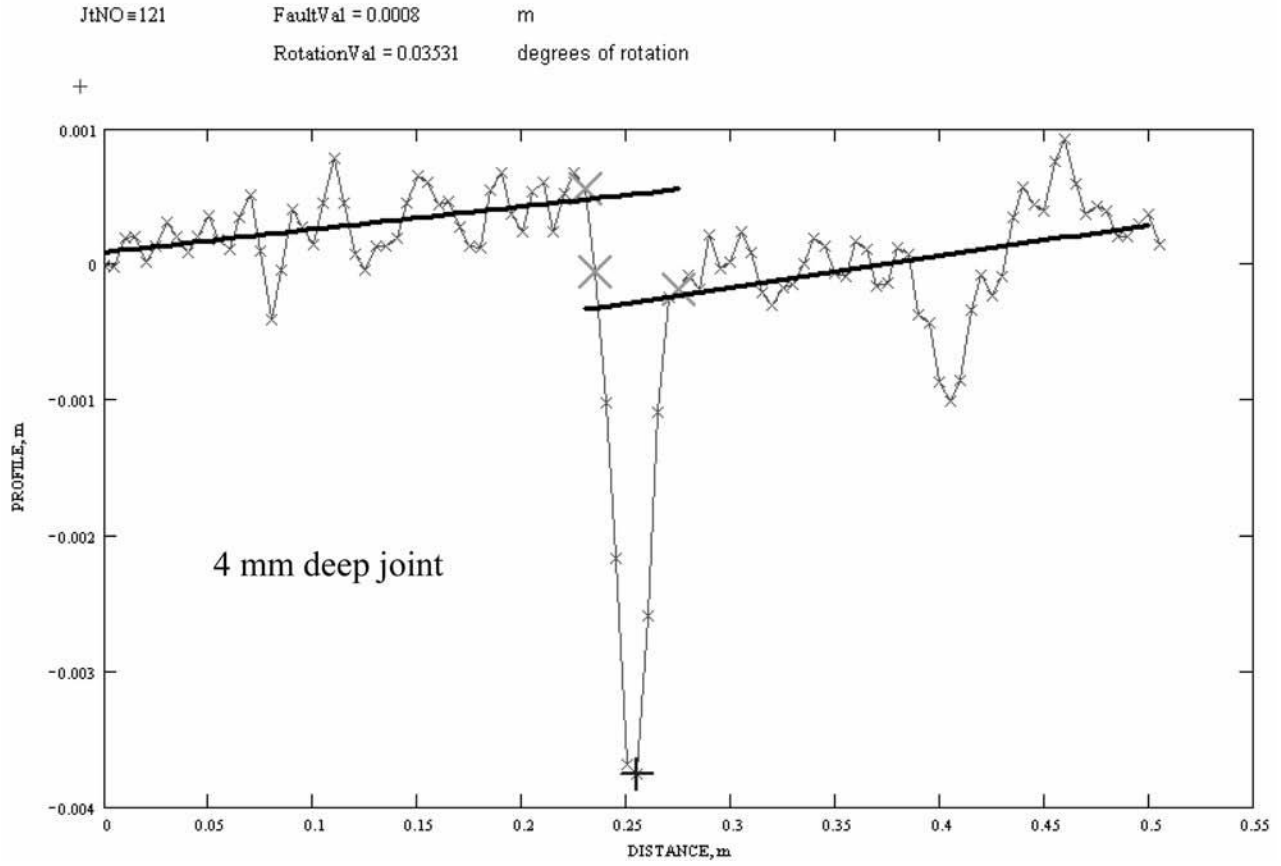


FIG. 9—Positive faulting, positive rotation.

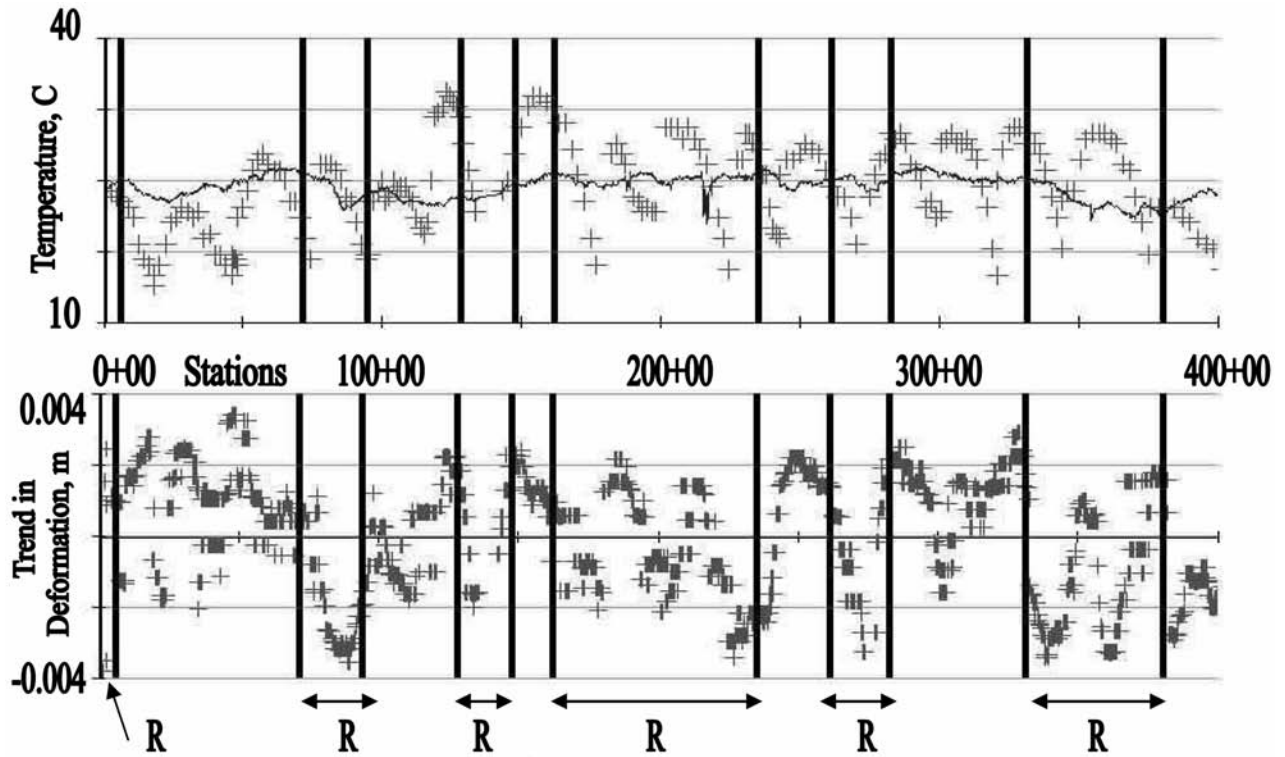


FIG. 10—Temperature at time of construction and at data collection, trend in maximum deformation (left lane, 6–8 p.m. time window), and Reconstruct (R) boundaries versus Station.

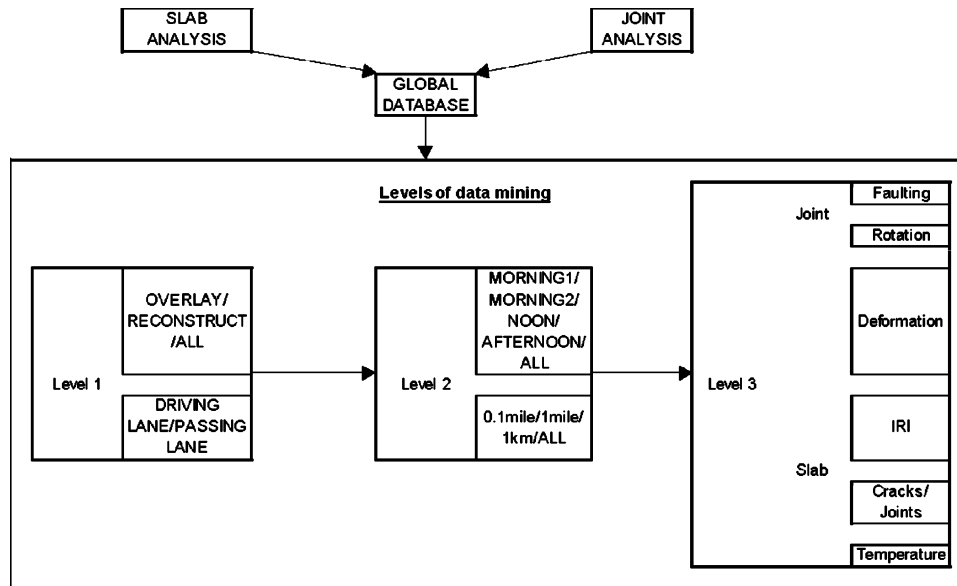


FIG. 11—Flow of data mining from fusion of analyses to levels of subdivision.

groups) distance intervals. The subdivisions of Level 3 are related to the parameters estimated in the various analyses (six groups).

Table 1 shows how the subdivision of the data into OVERLAY/RECONSTRUCT/ALL and 0.1mile/1mile/1km/ALL distance intervals provides either a single number or a vector of numbers as a result of the data mining. The data outputs with vectors of numbers were represented in graphs. The single number outputs were represented in tables.

The following data mining inquiries were made: (1) consider slab deformation versus reconstruction and overlay sections separately; (2) plot joint faulting, rotation and number cracks versus various intervals of mainline roadway—0.1 and 1.0 mile and 1 km; (3) plot average, mean, and range of joint faulting and rotation for the passing lane and driving lane separately versus various intervals of mainline roadway—0.1 and 1.0 mile and 1 km, for each of the four time windows and for the four time windows combined; (4) plot IRI for each lane for each of the four time windows and for the four time windows combined; (5) evaluate the effect of time of day on faulting and on the effect of faulting on the IRI data by lane; (6) compare the effect of faulting on IRI and the effect of slab curling on IRI by time of day for each lane in the reconstructed and overlay sections separately; and (7) for each lane and each section, identify the number and location of nonworking joints (no appreciable change in joint rotation with change in temperature) and number of cracks separately. Figure 11 shows the organization of data for the above data mining inquiries.

The relation between the data and seven data mining inquiries presented earlier is provided in Table 2. For example, inquiry 4 considers the variation of results in IRI versus time window, lane, and OVERLAY/RECONSTRUCT. In order to achieve the seven inquiries of data mining, $3 \times 2 \times 5 \times 4 \times 6 = 720$ necessary and basic comparisons of interest were needed. The 720 plots and tables did not provide clear and crisp trends and were limited in providing conclusive evidence in most cases. A sample of the results are provide in this paper.

Figure 12 shows faulting versus station by Overlay or Reconstruct. Reconstruct sections have more faulting as the number of Reconstruct spikes dominate, while Reconstruct and Overlay valleys are of approximately equal number.

TABLE 1—Number of output data points from data mining.

	0.1 mile	1 mile	1 km	All
Overlay	290	29	46	1
Reconstruct	30	3	5	1
All	320	32	51	1

TABLE 2—Correspondence between types of subdivisions and data mining inquiries.

Inquiry	Level 1		Level 2		Level 3						
	O/R	Lane	Time Window	Distance Interval	Faulting	Rotation	Maximum Def.	IRI	Cracks/ Joints	Temperature	Joint Cond.
1	Y	N	Y	N	Y	Y	Y	Y	Y	Y	N/A
2	Y	Y	N	Y	N	N	N	N	Y	N	N/A
3	Y	Y	N	Y	Y	Y	N	N	N	N	N/A
4	Y	Y	Y	N	N	N	N	Y	N	Y	N/A
5	N	Y	Y	N	Y	Y	N	Y	N	Y	N/A
6	Y	Y	Y	N	Y	Y	Y	Y	N	Y	N/A
7	N	Y	N	Y	N	N	N	N	N	N	Y

Key: Y = level/subdivision included, N = level/subdivision not included

Alternatively, groups of plots combining more than two variables provide more information: for example, in Fig. 13, faulting is plotted against temperature and IRI, where the four time windows are color-coded, having separated overlay and reconstruct into two layers of plots.

The IRI values are higher for the reconstruct sections as shown by the shift to the right by the blue arrow from overlay to reconstruct in Fig. 13. Even though Fig. 12 showed higher joint faulting values for reconstruct, such trends are not clearly visible in Fig. 13.

In Fig. 14, plotting all parameters in separate plots against station, separating overlay and reconstruct sections, the global relationship between surface profile features and roughness, becomes more apparent. Figure 14 shows overlay sections only. Six similar plots are available for reconstruct sections.

Note the dark arrows which point to the section with the most cracks. Immediately, this increase in cracks corresponds with higher joint faulting and rotations, a lack of separation between the maximum surface deformations for the four time windows as seen in other sections, and a higher IRI level. The light arrows show a section which has a local peak in the joint faulting and rotation, and a slight increase in cracks. To the right, another local fluctuation in joint rotation where the lines meet (indicated by a slanted arrow) may be an indication of locking of the joints. The dark arrows show a section where slabs have already failed, and the light arrows where the failures are beginning.

Finally, in order to identify those slabs which perform differently, parallel coordinate plots were used to visualize the relationship between all the parameters. Figure 15 shows such plots. In this case, six parameters are plotted encompassing four time windows within each parameter. Heavy vertical lines delineate each parameter. The three thin vertical lines are the three time windows, 4–6 a.m., 6–8 a.m., 11 a.m.–1 p.m., and the heavy vertical line which delineates the parameters is also the 6–8 p.m. time window. The heavy horizontal line shows the trend in the data. A cluster of slabs working similarly about the trend line become immediately apparent. Those slabs or groups of slabs that deviate from the trend correspond to those that have failed (cracked) or have non-working joints. The temperature and maximum deformation pattern are similar. The crack, fault, and IRI patterns are flat. The joint rotation pattern is the most unstable of the six parameters represented. Further work to cluster the slabs into more than two

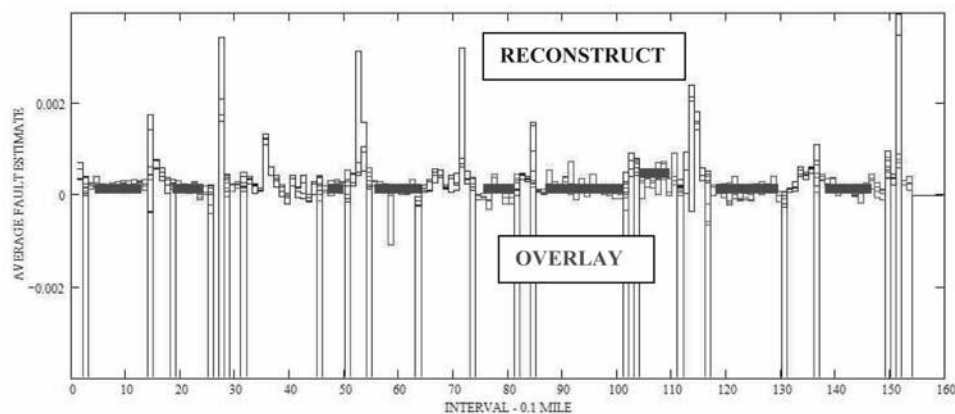


FIG. 12—Average fault estimate (m) versus interval (0.1 mile), red = overlay, blue = reconstruct.

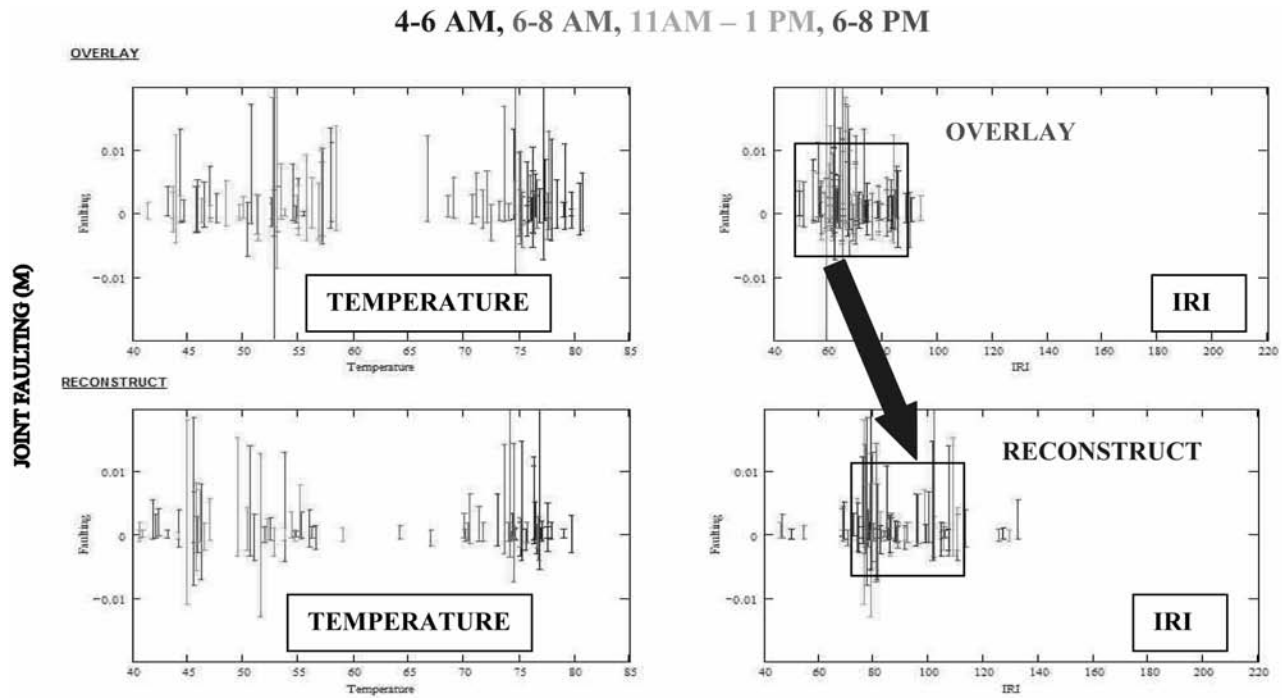


FIG. 13—Joint faulting versus temperature °C and IRI, for overlay and reconstruct sections separated—four time windows color-coded.

categories (working and non-working joints) is needed. There are additional data mining tools currently under evaluation for this future refinement.

Conclusions

Measured surface profiles can provide useful information about joint performance, roughness, and slab condition. Studying the shape of the surface profile along one path does not provide absolute answers about the curvature of the slab. Only when looking at the change in slab shape can we relate it empirically to a change in slab curvature. The paper shows how the surface profile can be used to extract a surface deformation parameter and joint rotation and faulting, along with transverse cracks. IRI values can be computed using the same profiles.

The following conclusions were derived from this empirical analysis:

- Changes in maximum surface deformation are proportional to changes in surface temperature.
- Changes in joint rotation of working joints are proportional to changes in surface temperature.
- Joint faulting of working joints and number of transverse cracks are generally invariant with changes in surface temperature.
- IRI varies slightly with changes in surface temperature. It is very much dependent upon the severity of the surface deformation at time of construction.
- The trend in surface deformation is related to the trend in temperature at construction.
- Joint faulting effects IRI but is not the driving factor.

The next four conclusions were site-specific:

- Using adjacent lane slabs, those slabs that had cracked were next to slabs with larger maximum surface deformation variations. This finding can be used to identify the next slabs most likely to fail.
- The overlay sections had little joint faulting compared to the reconstruct sections.
- The reconstruct sections had higher roughness.
- Using parallel coordinates analysis, any trace deviating from the clusters belong to slabs or sections of slabs that behave outside of the overall behavior. Working joints may be separated from non-working joints, slabs likely to fail may be isolated from the overall sample.

4-6 AM, 6-8 AM, 11AM – 1 PM, 6-8 PM

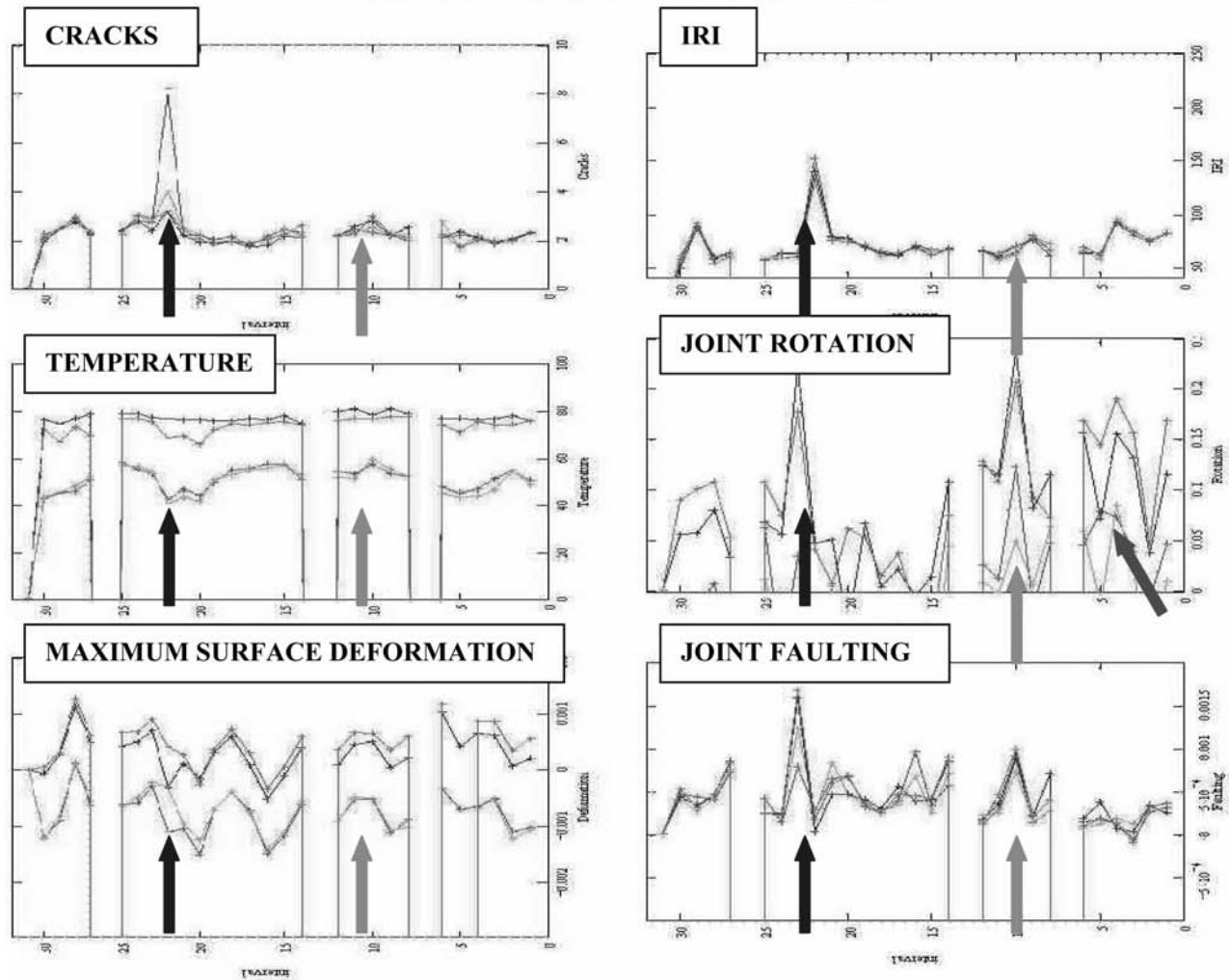


FIG. 14—Temperature °C, maximum deformation, number of cracks, joint rotation, joint faulting, and IRI versus Station for overlay sections—four time windows color-coded.

General Recommendations

Traditional signal processing using Fourier analysis that is the foundation of power spectral density analysis, averaging techniques, and linear regression are limited by their constraints of linearity and stationarity. The Hilbert-Huang Transform may allow us to explore in more detail the local wavelength content. Instead of considering average conditions provided by Fourier-based power spectral density analysis with empirical waveband filtering, more accurate estimates of the local wavelength content will provide information on the behavior of individual slabs. Combining better nonlinear analysis, cluster analysis, inertial profiling, visualization tools, and other data mining programs, the trends in the plots shown in this paper will become crisper and more conclusive.

Acknowledgments

The authors would like to acknowledge the support of the Advanced Research Team of the Turner-Fairbank Highway Research Center of the Federal Highway Administration, the relentless support of Mr. Dennis Sixbey of the Infrastructure Office of the Turner-Fairbank Highway Research Center of the Federal Highway Administration, the support by Mr. Mark Swanlund of the Office of Pavement Management of the Federal Highway Administration, and the contribution of Mr. Douglas Crowley of CACE Engineering.

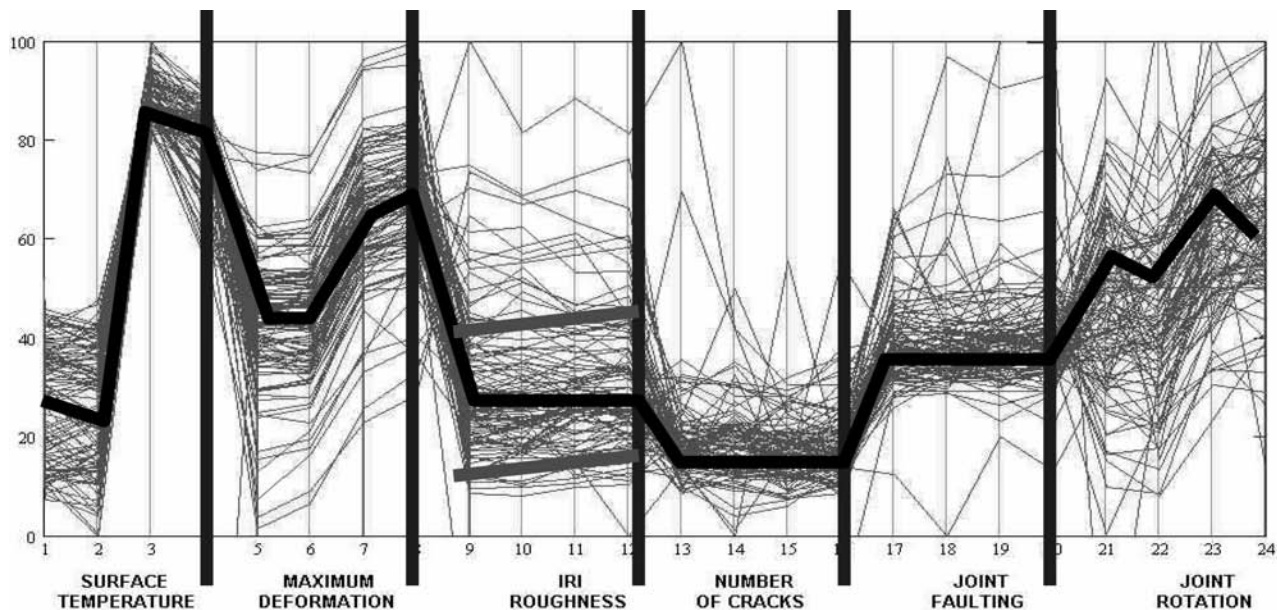


FIG. 15—Plot of six parameters for four time windows in parallel coordinate plot.

References

- [1] Gagarin, N., Mekemson, J. R., and Oskard, M., "Introduction of Non-Linear Non-Stationary Analysis into the Post-Process of Pavement Surface Profiles," *5th Symposium on Pavement Surface Characteristics*, SURF2004, June 6–10, 2004, Toronto, Canada.
- [2] Huang, N. E. et al., "The Empirical Mode Decomposition and Hilbert Spectrum for Nonlinear Non-stationary Time Series Analysis," 1998, *Proc. Roy. Soc. Lond.*, A454, pp. 903–995.
- [3] Byrum, C. R., "A High Speed Profiler Based Slab Curvature Index for Jointed Concrete Pavement Curling and Warping Analysis," Ph.D. Dissertation, University of Michigan, 2001.
- [4] Sixbey, D., Swanlund, M., Gagarin, N., and Mekemson, J. R., "Measurement and Analysis of Slab Curvature in JPC Pavements Using Profiling Technology," *Proceedings of the 7th International Conference on Concrete Pavements*, Orlando, FL, 2001.
- [5] Rasmussen, O., Karamihas, S., Chang, G., Merritt, D., and Swanlund, M., "Profile Data Analysis to Quantify Concrete Pavement Slab Curvature and Other Behavior," *5th Symposium on Pavement Surface Characteristics*, SURF2004, June 6–10, 2004, Toronto, Canada.
- [6] Gagarin, N., and Mekemson, J. R., "Warp and Curl Project," SEQS Reports for Task Orders 10, 15, 16, 17, 18, 19, and 20, Turner-Fairbank Highway Research Center, Federal Highway Administration, McLean, VA, 1999–2001.

Jian-Shiuh Chen¹ and Chien-Chung Huang²

Development of Pavement Smoothness Index Relationship

ABSTRACT: In its pursuit for providing smooth pavements, the Directorate General of Highways in Taiwan is developing and implementing ride quality specification as part of the construction assurance program. The straightedge and the profiler were used to measure pavement smoothness on 561 test sections. Probability distribution analysis showed that measurements of pavement smoothness of both devices follow the normal distribution. Smoothness specifications for construction quality control were developed for straightedge and profiler, respectively. The full-pay range is 1.36 to 2.45 mm and 2.16 to 3.65 m/km for straightedge and profiler, respectively. The smoothness relationship between straightedge and profiler was developed.

KEYWORDS: straightedge, profiler, smoothness specification

Introduction

Pavement smoothness is an important consideration for highway engineers [1–4]. Smoothness experienced by a roadway user is a function of pavement profile, vehicle speed, and various vehicle parameters including tire and suspension characteristics. A variation in any of these factors can make a road profile appear either smooth or rough. A general definition of smoothness describes the surface characteristics of a pavement that affect vehicle operation cost and the riding quality of that pavement as perceived by highway users.

Many engineers believe that pavement smoothness is an indicator of overall quality of workmanship by the contractor. It is generally believed that if the contractor provides very smooth pavement, there is greater likelihood that good-quality workmanship has been provided throughout the steps of highway construction that span from subgrade preparation to rolling of the final surface layer. There is also a growing belief among pavement engineers that smooth pavements not only provide a higher level of service but also last longer than otherwise equivalent but initially rougher pavements. Because of these considerations, specifications have been adopted by highway agencies to achieve smoother pavements. In some instances, incentives and disincentives are provided, depending on the initial level of smoothness achieved during construction.

Highway agencies conventionally use a 3-m straightedge for quality control and assurance of smooth surface on paving projects. A straightedge is relatively inexpensive, is simple to operate and maintain, and provides a trace of the surface that users can easily understand. However, this type of testing is time-consuming and insensitive to the ride quality felt by the user. Inertial profilers that offer greater accuracy in profile measurement relative to those of the straightedge presently used in construction projects have been employed recently [5–7]. Profilers are used to quickly monitor the profile of a pavement from which the widely accepted International Roughness Index (IRI) can be computed. Since their introduction, highway agencies have begun using these devices as an alternative to the straightedge for surface smoothness on new construction or resurfacing projects.

However, contractors and highway engineers have raised their concerns. They usually do not understand the relationship between straightedge's and profiler's smoothness measurements very well. Con-

Manuscript received October 9, 2004; accepted for publication May 23, 2006; published online June 2006. Presented at ASTM Symposium on Pavement Surface Condition/Performance Assessment: Procedures and Technologies on 7 December 2004 in Washington, DC; B. Choubane, Guest Editor.

¹ Professor, National Cheng Kung University, Department of Civil Engineering, Sustainable Environment Research Center, Tainan 70101, Taiwan. Corresponding author; e-mail: jishchen@mail.ncku.edu.tw

² Graduate Student, National Cheng Kung University, Department of Civil Engineering, Sustainable Environment Research Center, Tainan 70101, Taiwan.

tors and engineers are accustomed to measuring surface smoothness based on a straightedge. A key question needs to be answered: how do agencies make the switch from their current specifications to IRI specifications? It is important to analyze the smoothness relationship between a straightedge-based specification and a profiler-based specification. This research effort is to develop a relationship that can assist highway engineers in selecting appropriate IRI specification for modifying current specifications to the more reproducible and portable smoothness index.

At present time, smoothness specifications vary among highway agencies. The Directorate General of Highways in Taiwan initiates research to compare smoothness specifications to assist in the transition. Probability models need to be established for analysis and interpretation of pavement smoothness data. These statistical assessments follow the nature of pavement surfaces with their complicated profiles and variability characteristics. An accepted probability model has significant influence on the results of calculating confidence intervals and establishing specifications. The objectives of this study are as follows:

- to investigate the probability distribution of smoothness measurements on flexible pavements;
- to compare smoothness measurements collected by straightedge and profiler;
- to establish a protocol to convert the smoothness measurements; and
- to develop the incentive/disincentive policy based on statistical considerations.

Test Sections and Methods

Input from division field personnel for examples of both smooth and rough-riding pavements was solicited to determine the nature of flexible pavement smoothness. Thirty roadways were submitted for considerations. From these 30 locations, three types of representative roadways were selected for testing as follows: excellent riding quality, fair riding quality, and relatively poor riding quality.

The 3-m straightedge and the ICC Surface Profiler were used for measuring pavement smoothness. Reference marks were established every 200 m and station numbers were painted on the shoulder every 20 m. A total of 561 test sections were identified for evaluation. Smoothness or roughness is defined to be a statistic that summarizes the variations in the surface characteristics of the pavements. The measurement unit for straightedge and profiler is expressed by standard deviation (SD) and the International Roughness Index (IRI), respectively. Level surveys in addition to straightedge and profiler tests were conducted on these three roadways for validation.

Statistical Approach

Determination of Probability Distribution for Pavement Smoothness

The probability distribution of measurements collected by straightedge and profiler is essential to estimate the statistical parameters for pavement smoothness. In practice, the underlying distribution can be established by (1) drawing a frequency diagram, (2) plotting data on a probability paper, and (3) conducting goodness-of-fit tests for distribution [8–10]. When sufficient data are available, a histogram or frequency diagram can be used to describe the underlying distribution. Using a probability paper could be cumbersome because a judgment needs to be made as to whether the relationship between the smoothness data and the corresponding cumulative properties is close to linear. A more definitive and less cumbersome method is the goodness-of-fit test. The chi-squared (χ^2) test serves this purpose. The chi-squared test is based on the error between the observed and assumed probability of the distribution. In the χ^2 goodness-of-fit test, the range of the n observed data is divided into k intervals. The number of times (n_i) of the random variable observed in the i th interval is counted ($i=1$ to k). Measured frequencies M_1, M_2, \dots, M_m of m intervals of smoothness data are then compared with corresponding theoretical frequencies T_1, T_2, \dots, T_m of an assumed distribution. The test statistic, $\sum_{i=1}^k (M_i - T_i)^2 / T_i$, approaches the χ^2 distribution with $f=k-1-m$ degrees of freedom as the total sample points n tends to be ∞ . Here, k is the number of intervals and m is the number of distribution parameters estimated from the data. The number of degrees of freedom f is a parameter of the χ^2 distribution. $\chi_{k-1-m, \alpha}^2$ is denoted as the value of the χ^2 distribution with f degrees of freedom at a significance level α . If the calculated value is less than the tabulated value, the assumed distribution is acceptable at the significance level α .

TABLE 1—Summary of smoothness measurements.

	SD, mm	IRI, m/km
Test sections	561	561
Minimum value	0.62	1.06
Maximum value	4.32	5.90
Average	1.91	2.90
Standard deviation	0.64	0.88
Coefficient of variation	34%	30 %

Both k and the T_i should be greater than or equal to 5 to obtain satisfactory results. However, this may not always be possible. The following equation is proposed to remedy this problem

$$\sum_{i=1}^k \frac{\left[|M_i - T_i| - \frac{1}{2} \right]^2}{T_i} \quad (1)$$

Hypothesis Tests for Comparing Two Devices

The inferences concern a difference between the means of pavement smoothness measured by two different devices, i.e., profiler (\bar{X}_{IRI}) and straightedge (\bar{X}_{SD}). The parameter of interest is identified as $\mu_{\text{IRI}} - \mu_{\text{SD}}$. The test statistic can be stated as follows:

$$Z = \frac{(\bar{X}_{\text{IRI}} - \bar{X}_{\text{SD}}) - (\mu_{\text{IRI}} - \mu_{\text{SD}})}{s_{\bar{X}_{\text{IRI}} - \bar{X}_{\text{SD}}}}$$

in which $s_{\bar{X}_{\text{IRI}} - \bar{X}_{\text{SD}}} = \sqrt{\left(\frac{s_{\text{IRI}}^2}{n_{\text{IRI}}}\right) + \left(\frac{s_{\text{SD}}^2}{n_{\text{SD}}}\right)}$, where s_{IRI}^2 and s_{SD}^2 are the variances for profiler and straightedge, respectively; n_{IRI} and n_{SD} are the sample sizes for profiler and straightedge, respectively.

Development of Smoothness Relationship

Model development begins with the selection of the most suitable functional form that best describes the smoothness relationship between straightedge and profiler. As indicated by a preliminary scatter plot, the straightedge-profiler relationship could be estimated by the regression analysis. For a significance level (α), the confidence interval can be expressed as follows:

$$P \left\{ \frac{(\bar{X}_{\text{IRI}} - \bar{X}_{\text{SD}}) - (\mu_{\text{IRI}} - \mu_{\text{SD}})}{s_{\bar{X}_{\text{IRI}} - \bar{X}_{\text{SD}}}} \geq Z_{\alpha} \right\} = 1 - \alpha$$

where Z_{α} is the critical value at a significance level α .

Discussion of Test Results

Smoothness Measurements

The smoothness data are summarized in Table 1. A total of 561 test sections on newly constructed and resurfaced highways were selected to measure pavement smoothness using a straightedge and a profiler. The average values for straightedge and profiler are 1.91 mm and 2.90 m/km, respectively with standard deviations of 0.64 mm and 0.88 m/km, respectively. The average value of straightedge meets the current specification of 4 mm. Note the coefficients of variation of both devices are about the same, indicating that data collected by straightedge and profiler appear to exhibit similar variation.

Constructing a histogram for smoothness data entails subdividing measurements into class intervals as shown in Figs. 1 and 2 for straightedge and profiler, respectively. These two figures resemble a normal distribution in that the frequency is centered on the sample mean and is symmetrical about this point. It is

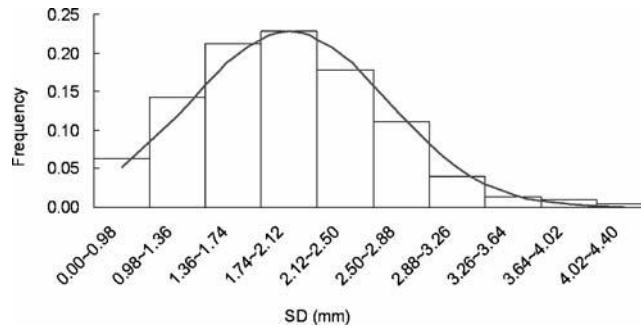


FIG. 1—Smoothness data based on standard deviation.

necessary to test whether pavement smoothness is normally distributed. The chi-squared goodness-of-fit test is employed for this purpose. An overall comparison was made for observed and normally distributed frequencies that fall into specified intervals as illustrated in Figs. 1 and 2.

The steps of chi-squared goodness-of-fit test are summarized in Tables 2 and 3 at the 5 F significance level for straightedge and profiler, respectively. All 561 measurements on pavement smoothness are divided into nine intervals according to the principle of constructing a histogram. The number of measurements in each interval is counted and tabulated under *M*. The theoretical frequency for each interval for normal distribution is calculated under *T*.

The theoretical frequencies for other intervals can similarly be calculated. The theoretical frequencies for all intervals are shown to add up to the total number of observations. Similar calculation procedures are also listed in Table 2 for straightedge. After readjustment, the goodness-of-fit test leads to calculate χ^2 values that equal to 8.35 and 8.54 for straightedge and profiler, respectively. For the normal distribution, its two parameters, i.e., mean and variance, are estimated from the sample mean and variance. Thus, the degrees of freedom are $f=8-1-2=5$. For the 5 % significance level, the corresponding χ^2 value is found

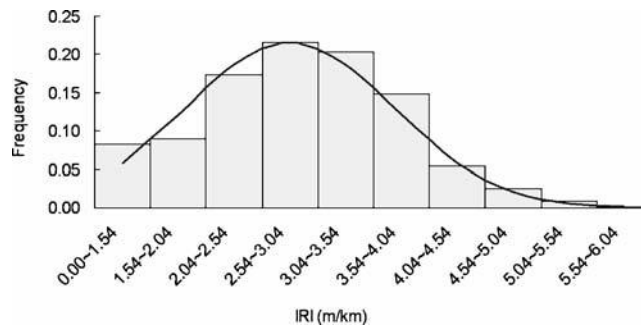


FIG. 2—Smoothness data based on IRI.

TABLE 2—Goodness-of-fit test on SD data.

Bottom Interval Limit (L)	Upper Interval Limit (U)	Measured Frequency (M)	Z _L	Z _U	Probability Value	Theoretical Frequency (T)	(M-T) ²	(M-T) ² /T
0.00	0.98	35	0.00	0.07	0.07	39.44	19.74	0.50
0.98	1.36	80	0.07	0.19	0.12	68.10	141.54	2.08
1.36	1.74	119	0.19	0.39	0.20	112.52	42.05	0.37
1.74	2.12	128	0.39	0.63	0.23	131.55	12.62	0.10
2.12	2.50	100	0.63	0.82	0.19	108.86	78.42	0.72
2.50	2.88	62	0.82	0.94	0.114	63.74	3.04	0.05
2.88	3.26	22	0.94	0.98	0.0471	26.41	19.46	0.74
3.26	3.64	8	0.98	1.00	0.0138	7.74		
3.64	4.02	5	1.00	1.00	0.0029	1.60	29.39	3.80
4.02	4.40	2	1.00	1.00	0.0004	0.23		
		561			1.00			8.35

TABLE 3—Goodness-of-fit test on IRI data.

Bottom Interval Limit (<i>L</i>)	Upper Interval Limit (<i>U</i>)	Measured Frequency (<i>M</i>)	Z_L	Z_U	Probability Value	Theoretical Frequency (<i>T</i>)	$(M-T)^2$	$(M-T)^2/T$
0.00	1.54	46	0.00	0.06	0.06	33.21	163.68	4.93
1.54	2.04	50	0.06	0.16	0.10	57.29	53.18	0.93
2.04	2.54	97	0.16	0.34	0.18	99.12	4.48	0.05
2.54	3.04	121	0.34	0.56	0.22	124.91	15.32	0.12
3.04	3.54	114	0.56	0.77	0.20	114.69	0.48	0.00
3.54	4.04	83	0.77	0.90	0.137	76.71	39.54	0.52
4.04	4.54	30	0.90	0.97	0.0666	37.38	54.40	1.46
4.54	5.04	14	0.97	0.99	0.0236	13.26		
5.04	5.54	5	0.99	1.00	0.0061	3.43	7.11	0.54
5.54	6.04	1	1.00	1.00	0.0011	0.64		
		561			1.00			8.54

to be 11.07, which is larger than the calculated values. Thus, the results of the test support the practical distribution of using the normal distribution for pavement smoothness. In a usual form, the mean and variance are used as parameters of the normal distribution. The pavement smoothness can be expressed by the normal distribution $N_{SD} (1.91, 0.64^2)$ and $N_{IRI} (2.90, 0.88^2)$ for straightedge and profiler, respectively.

Significance of Smoothness Data

The hypothesis test is to determine whether or not the smoothness data are significantly different between straightedge and profiler. The test statistic is calculated as follows:

$$Z = \frac{(\bar{X}_{IRI} - \bar{X}_{SD}) - (\mu_{IRI} - \mu_{SD})}{s_{\bar{X}_{IRI} - \bar{X}_{SD}}} = \frac{(2.90 - 1.91) - (0)}{\sqrt{\frac{0.88^2}{561} + \frac{0.64^2}{561}}} = 21.55 > Z_{0.05} = 1.64$$

The calculated value (21.55) is larger than the tabulated one (1.64) at the 5 % significance level. Significant differences are declared to exist among smoothness data collected by these two devices. The conversion of straightedge and profiler measurements is essential to develop a guide for smoothness specification.

Relationship of Smoothness Index

As shown in Fig. 3, measured smoothness for standard deviation and IRI as explanatory and response variables, respectively, demonstrates a significant relationship that allows construction of a corresponding equation. The coefficient of determination, the R^2 value, equals to 0.72, and consequently, the explained

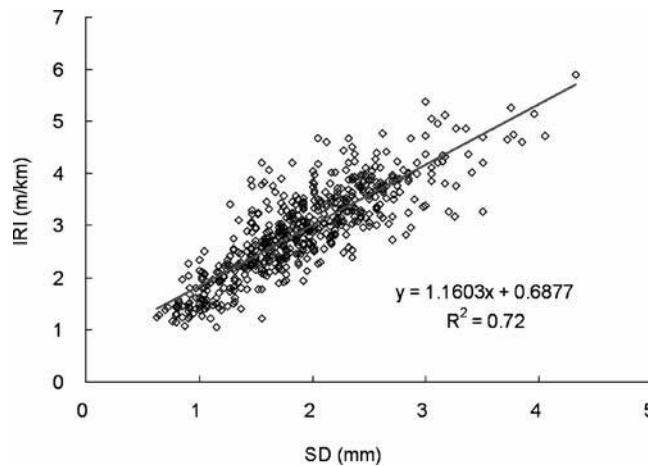


FIG. 3—Relationship of pavement smoothness index.

TABLE 4—Acceptance smoothness level.

Tolerance, mm or m/km	Cumulative Relative Frequency	
	SD, %	IRI, %
0.50	1.4	0.3
1.00	7.7	1.5
1.37	20.0	4.0
1.50	26.1	5.5
2.00	55.8	15.2
2.17	66.0	20.2
2.45	80.3	30.4
2.50	82.4	32.4
2.96	95.1	52.7
3.00	95.7	54.5
3.50	99.4	75.3
3.65	99.7	80.4
4.00	99.9	89.5
4.35	100.0	95.1
4.50	100.0	96.6
5.00	100.0	99.2
5.50	100.0	99.8
6.00	100.0	100.0

variation is greater than 0.5 of the total variation. With the R^2 value equal to 0.72, it means that 72 % of profiler variation can be explained by the linear relationship between profiler and straightedge. Corresponding estimation for the root mean square error equals 0.485. The IRI versus SD presented in Fig. 3 shows that both measurements are in good agreement.

Smoothness Specifications

After the χ^2 goodness-of-fit test provides the validity of the normal distribution, it is possible to calculate the acceptable smoothness level (ASL) for straightedge and profiler, as listed in Table 4. ASL is that level of percent of within limit at or below which the tolerance value is considered acceptable. Distinct differences are observed between straightedge's and profiler's ASLs in Table 4. A current smoothness specification in Taiwan calls for 4 mm for straightedge, in which 99.9 % of collected data pass the specification. However, in some instances the riding quality of the new pavements turns out to be poor even though the construction smoothness requirement has been met. The high percentage of passing the 4-mm specification implies that the current specification cannot properly discriminate between smooth and uneven highways. Another set of smoothness specification will be required to reflect the feelings of road users.

Smoothness specifications should provide an effective means of improving the initial smoothness of pavements. When coupled with appropriate incentive/disincentive provisions, contractors are encouraged to purchase new equipment, train personnel, improve paving operations, and so on. These revisions are required for achieving a smooth pavement surface. To assist highway agencies in revising their existing straightedge specification and transitioning to a profiler specification, the statistical distribution and model developed in the previous sections are applied to the specification limits shown in Figs. 4 and 5. The determination of the bonus and the full-pay ranges is based on the cumulative distribution curves. For flexible pavements the full-pay range is selected between 20th and 80th percentile of the cumulative smoothness probability distribution. This relatively conservative selection reflects the fact that highway agencies in Taiwan have not yet had experience of a new specification. Therefore, the conservative selection will give contractors enough time to adjust for the new specification.

The 20th percentile gives 1.35 mm and 2.15 m/km for straightedge and profiler, respectively. Smoothness values lower than the 20th percentile are determined as the bonus range. The final 20 % of the accumulative distribution is selected as the penalty and the correction ranges. Some 15 % will be subject to a penalty, and the other 5 % need to work on smoothness correction, i.e., contractors have to grind the identified irregularities to meet the criteria. The conversion equation as well as the 95 % confidence interval is considered in the development of the smoothness specification, which is summarized in Table 4.

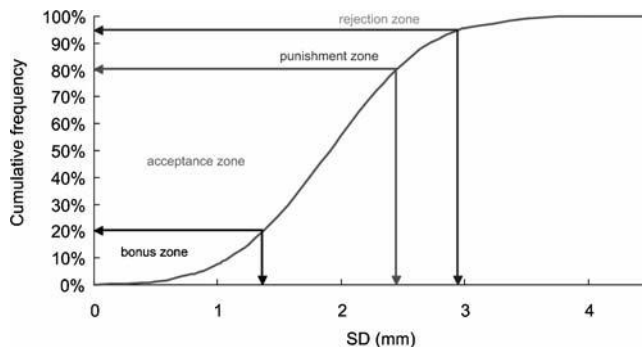


FIG. 4—Cumulative frequency distribution of standard deviation.

While the profiler and the 3-m straightedge are used on a surface course, in addition to the requirements listed in Table 5, all areas having a high point deviation in excess of 10 and 8 mm, respectively, need to be corrected.

The allowable tolerances specified in Table 4 are generally higher than those adopted by highway agencies in the U.S. The differences result from the fact that manholes and other utilities boxes are commonly observed on Taiwan highways, thus contributing to the dramatic decrease in the smoothness of pavements. Also the speed limit on these highways is relatively lower compared with one set in the U.S. While physical highway-smoothness measurements such as SD and IRI could provide an indication of pavement roughness, other factors such as the type of vehicle used, vehicle speed and users' characteristics might be significant. In comparison with the current pay scale, the pay adjustment curves developed in this study provide much greater incentive amounts and much more punitive disincentive amounts. From the observations of the smoothness measurement overtime, it will take a few years for contractors and highway engineers to become acquainted with smoothness specifications. With incentives and disincentives placed in the specifications, contractors are encouraged to pave smooth surfaces, and discouraged from any possibility of constructing rough-riding pavements.

Conclusions

- Test results obtained from straightedge are found to be significantly different from those from profiler. Smoothness specifications applied for straightedge cannot be directly used to those for

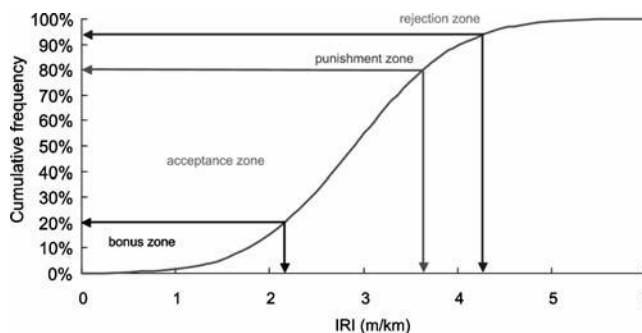


FIG. 5—Cumulative frequency distribution of International Roughness Index.

TABLE 5—Smoothness specification for asphalt pavements.

Zones	Percentile	Tolerance Value	
		Straightedge (mm)	Profiler (m/km)
Bonus	0–20th	≤1.35	≤2.15
Acceptance	20th–80th	1.36–2.45	2.16–3.65
Punishment	80th–95th	2.46–2.96	3.66–4.35
Rejection	95th–100th	>2.96	>4.36

profiler. A conversion equation is developed to assist agencies and contractors in converting smoothness measurements between these two devices based on the same acceptance level.

- Four following ranges are proposed for the smoothness specification according to qualification probability: bonus, acceptance, penalty, and rejection. As the qualification probability sets at 20 %, the bonus threshold value should be less than 1.35 mm and 2.15 m/km for straightedge and profiler, respectively.
- The tolerance value for an acceptance level is found to be below 2.45 mm and 3.65 m/km for straightedge and profiler, respectively. The demarcation line between penalty and correction is drawn at 95 % of the qualification probability with corresponding values of 2.96 mm and 4.36 m/km for straightedge and profiler, respectively.

Acknowledgments

The authors are very grateful to the Directorate General of Highways of Taiwan for providing financial support.

References

- [1] Janoff, M. S., "Pavement Roughness and Rideability: A State-of-the-Art Review." *J. Transp. Eng.*, Vol. 108, 1982, pp. 662–675.
- [2] Hegmon, R. R., "Some Results From Ongoing Research on Road Roughness," ASTM STP 1164, pp.14–31, ASTM, Philadelphia, 1992.
- [3] Smith, K. L., Smith, K. D., Evans, L. D., Hoerner, T. E., and Darter, M. I., "Smoothness Specifications for Pavements," NCHRP Web Document 1, National Research Council, Washington, DC, 1997.
- [4] Perera, R. W. and Kohn, S. D., Issues in Pavement Smoothness: A Summary Report, NCHRP Web Document 42, National Research Council, Washington, DC, 2002.
- [5] Sayers, M. W., "Profiles of Roughness," *Transp. Res. Rec.*, Vol. 1260, 1990, pp. 106–111.
- [6] Fernando, E. G., "Development of a Profile-Based Smoothness Specification for Asphalt Concrete Overlay," Project Summary Report No. 1378-S, Texas Transportation Institute, Texas A&M University, College Station, Texas, 1998.
- [7] El-Korchi, T., Bacon, J., Turo, M., and Ecmecian, M. "Ride Quality Assessment With Pavement Profiling Devices," *Transp. Res. Rec.* Vol. 1806, 2002, pp. 140–148.
- [8] Walpole, R. E., Myers, R. H., and Myers, S. L., *Probability and Statistics for Engineers and Scientists*, 6th ed., Prentice Hall, Inc., NJ, 1998.
- [9] Johnson, R. A., *Probability and Statistics for Engineer*, 6th ed., Prentice Hall, Inc., NJ, 2000.
- [10] Devore, J. L., *Probability and Statistics for Engineering and Science*, 6th ed., Thomson Books, New York, 2003.

Gerardo W. Flintsch,¹ ManQuan Huang,¹ and Kevin McGhee²

Harmonization of Macrotexture Measuring Devices

ABSTRACT: This paper compares pavement macrotexture measurements obtained using the volumetric method and three laser-based devices. The study used data from a controlled experiment conducted at the Virginia Smart Road, as well as samples of in-service highway and airport surfaces. The data collected at the Virginia Smart Road, a controlled-access two-lane road that includes various hot mix asphalt (HMA) and concrete surfaces, were used for the main analysis. The other two sets of data were used for verification and validation of the model developed. The analysis of the data collected at the Virginia Smart Road showed that the Circular Texture Meter (CTMeter) mean profile depth (MPD) had the highest correlation with the volumetric (Sand Patch) mean texture depth (MTD). Models for converting the laser-based texture measurements to an estimated MTD were developed. The developed model was tested using measurements collected on several other highway and airport surfaces and with positive results.

KEYWORDS: pavement, surface characteristics, macrotexture, Circular Texture Meter, mean profile depth (MPD), mean texture depth (MTD)

Introduction

Surface texture is a very important feature of the pavement surface, affecting friction, tire wear, exterior vehicle noise emission, interior vehicle noise emission, light reflection, and rolling resistance [1]. Tire pavement friction is affected by the presence of water on the pavement surface; thereby reducing the interaction area, which induces hydroplaning, reduces skid resistance, and adversely affects vehicle control. Pavement texture should supply not only enough tire-pavement interaction, but also quick drainage during precipitation.

According to the wavelength of surface irregularities, pavement surface texture can be divided into four categories: microtexture, macrotexture, megatexture, and roughness [2]. Microtexture plays an important role in maintaining satisfactory pavement friction level [3]. Macrotexture is also necessary for providing quick water drainage, which is required to maintain an appropriate pavement friction, especially at medium and high speeds.

The technology for direct macrotexture measurement is well developed; today's laser-based macrotexture measuring devices can measure the surface profile at traffic speeds. However, available macrotexture measuring devices do not necessarily measure the same surface properties and thus produce different measurements [4]. Hence, it is important to determine the most appropriate method for measuring macrotexture. In addition, it is necessary to investigate whether it is possible to harmonize the various macrotexture measurements obtained with different devices to a standard macrotexture measurement.

Manuscript received 12 November 2004; accepted for publication 22 April 2005; published October 2005. Presented at ASTM Symposium on Pavement Surface Condition/Performance Assessment: Reliability and Relevancy of Procedures and Technologies on 7 December 2004 in Washington, DC.

¹ Virginia Tech, Blacksburg, VA, USA.

² Virginia Transportation Research Council, Charlottesville, VA, USA.

The objective of this paper is to compare pavement macrotexture measurements obtained using three laser-based devices available in Virginia and to correlate the results with the traditional volumetric method. The study used data from a controlled experiment conducted at the Virginia Smart Road, as well as samples of in-service highway and airport surfaces. The data collected at the Virginia Smart Road were used for the main analysis. The other two sets of data were used for verification and validation of the model developed. Details of the study are presented in the following sections.

Macrotexture Measuring Techniques

The volumetric method is usually considered as a ground truth method for macrotexture measurement. In the volumetric technique (ASTM E 965 [5]), the average depth of pavement surface macrotexture is determined by careful application of a known volume of material on the surface and subsequent measurement of the total area covered. Dividing the volume by the area covered provides the MTD. According to the material used, the method can be classified as Sand Patch or Grease Patch, among others.

Several laser-based systems that measure macrotexture at traffic speeds are available. These systems measure the pavement profile and then use this profile to compute various surface macrotexture parameters, such as MPD and the overall Root Mean Square (RMS) of the profile height [6].

The two profilers evaluated in this paper (MGPS and ICC) share similar operation principle for measuring macrotexture. They both use a short-range laser range finder, an accelerometer, and a distance measuring transducer to measure and compute the pavement profile. However, the ICC profiler uses lower-frequency lasers and a bigger imprint [7]. The MGPS system uses the profile to compute the standard MPD specified in ASTM E 1845 [8]. The ICC profiler uses an RMS-based proprietary algorithm to calculate MPD, which is not fully consistent with ASTM E 1845 [8].

The CTMeter uses a laser to measure the profile of a circle, 284 mm (11.2 in.) in diameter or 892 mm (35 in.) in circumference. It can be used both in the laboratory and the field. The profile is divided into eight segments of 111.5 mm (4.4 in.) for analysis, with two segments (A&E) parallel to travel direction and two (C&G) perpendicular to travel direction. The CTMeter reports both MPD and RMS measurements for all eight segments [9].

Data Collection

The data collected for this study were obtained from three different sources: a two-phase controlled experiment conducted at the Virginia Smart Road; measurements of a sample of in-service highway pavement surfaces used in the Commonwealth; and measurements conducted on runway pavement surface at the Wallops Flight facility.

The Virginia Smart Road contains a 3.2 km fully instrumented pavement test facility located in Montgomery County, Virginia. Once completed, the Virginia Smart Road will be a connector road between U.S. 460 and Interstate 81. At present, the Virginia Smart Road is a two-lane controlled-access road, composed of 14 pavement sections. Measurements on seven of these sections (Table 1) were conducted for this investigation. Only one lane (East Bound, EB) was measured for most sections. However, both lanes were measured for Sections J and Section K (Open-Graded Friction Course, OGFC).

TABLE 1—Test surfaces at the Virginia Smart Road.

Section ID	Width (m)	Length (m)	Surface Description (VDOT Designation)
Loop	4.9	173.7	Stone Matrix Asphalt (SMA 19)
A	7.3	96.6	Dense-graded HMA (SM 12.5D)
G	7.3	83.5	Dense-graded HMA (SM 9.5D)
J	7.3	85.3	Dense-graded HMA (SM 9.5D)
K	7.3	79.9	Open-Graded Friction Course (OGFC 12.5)
L	7.3	96.6	Stone Mastic Asphalt (SMA 12.5)
Concrete	7.3	76.2	Continuously Reinforced Portland Cement Concrete (Transversely Tined)

The macrotexture measurements obtained with these four devices for each section are compared in Fig. 1. The ICC macrotexture values are, in general, larger than others: on average 89 % larger than the sand patch MTD, 96 % larger than the CTMeter MPD, and 65 % larger than the MGPS MPD. The large difference between the ICC measurements and the other measurements may be due to the specific method used by the ICC profiler to calculate the MPD. While the ICC MPD is estimated using a proprietary algorithm, not consistent with ASTM E 1845, the other devices calculate the MPD using the ASTM method. Hence, the ICC macrotexture measurements are referred as ICC Texture (ICCTEX), rather than MPD, in this paper.

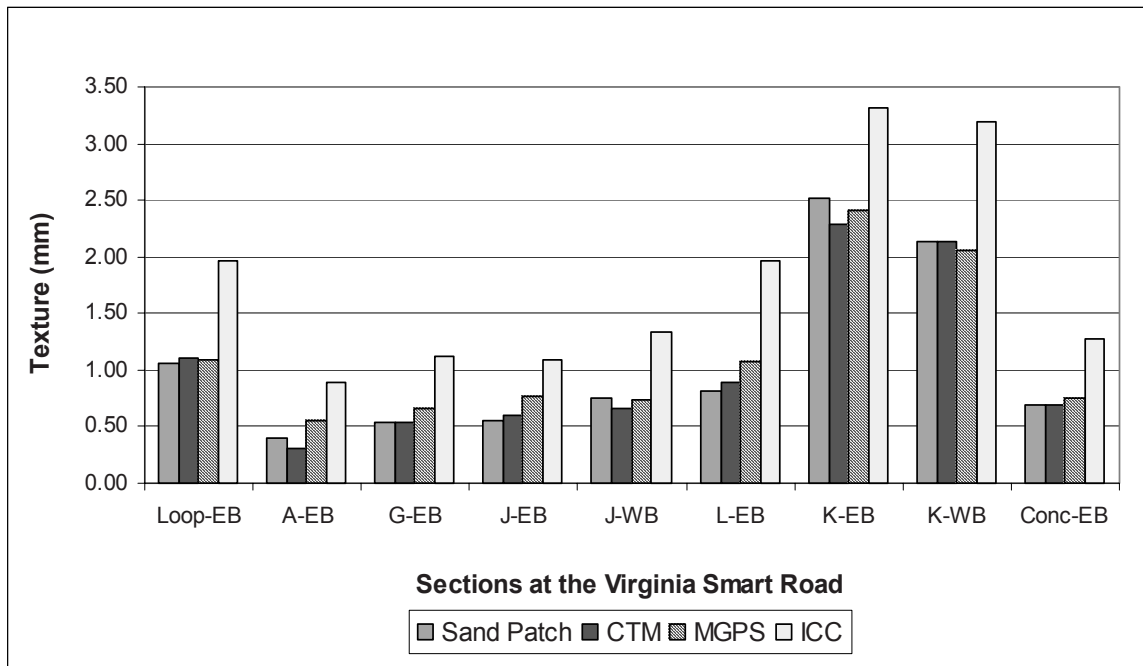


FIG. 1—Comparisons of laser-based macrotexture measurements.

Model Development

The model development was based mainly on the data collected at the Smart Road under controlled conditions. Extreme care was taken in this experiment to ensure that the data were collected in the same physical locations among the various pavement sections investigated.

Repeatability

Before comparison among devices could be conducted, it was necessary to determine the repeatability of the various measurement methods on the same surfaces. The two statistics commonly used to evaluate the repeatability of measures from an instrument, standard deviation (SD) and coefficient of variation (CV), were used in this study. The standard deviations are shown in Fig. 2. For the surfaces investigated, the CTMeter appears to be the most repeatable system, followed by the MGPS system, and then the ICC profiler. However, all three devices have relatively low standard deviation (lower than 0.17 mm) and coefficient of variation (lower than 10 %).

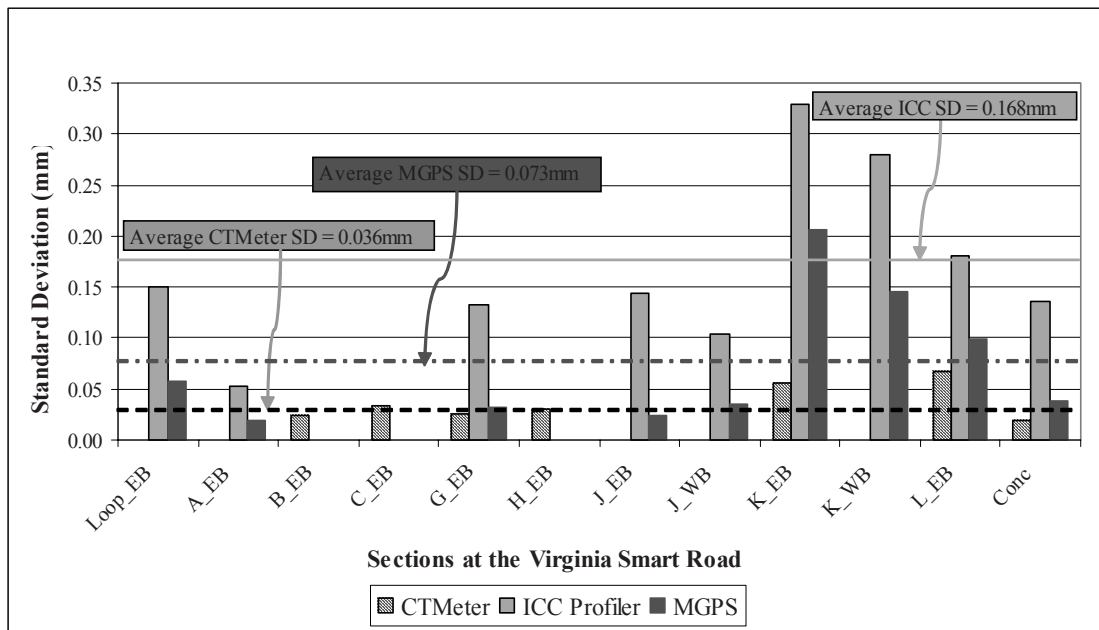


FIG. 2—Standard deviation of laser-based macrotexture measurements.

Correlation Between Laser-Based and Sand Patch Measurements

The correlation between the three laser-based measurements with the volumetric method was first evaluated to determine the suitability of these technologies to replace the widely used but time consuming and operator dependent Sand Patch test.

Previous research suggests that the macrotexture measurements experienced more variation on the OGFC surface. Furthermore, there are some physical limitations associated with performing Sand Patch measurements on very porous surfaces. Therefore, in order to investigate the effect of the OGFC surface on the correlation between the laser-based devices and Sand Patch, correlation analyses on all surfaces including and excluding the OGFC surface were conducted.

Furthermore, in order to evaluate the effects of the various outputs from the CTMeter and the correlation with Sand Patch, the correlation analyses included RMS, Longitudinal MPD, and Transversal MPD. Linear regression analyses are summarized in Table 2. The correlations are higher with the OGFC because this surface adds data at a very high range, thus significantly extending the regression range. Of the three laser-based devices, the CTMeter has the highest correlation (and smallest standard error) with the Sand Patch, followed by the MGPS system.

TABLE 2—Correlation between laser-based and Sand Patch measurements.

Device	Type of Measure	All Surfaces Included			OGFC Excluded		
		R ²	StdErr	No. of obsv	R ²	StdErr	No. of obsv
CTMeter	MPD	0.943	0.176	38	0.833	0.111	29
	RMS	0.923	0.198	38	0.752	0.135	29
	Long. MPD	0.940	0.180	38	0.735	0.140	29
	Tran. MPD	0.868	0.268	38	0.859	0.102	29
ICC Profiler	ICCTEX	0.884	0.251	38	0.792	0.124	29
MGPS	MPD	0.927	0.199	38	0.796	0.123	29

Conversion Model

Since different devices usually give different results, even measuring the same texture, it is important and useful to harmonize the measurements obtained with different texture measuring devices. Since the Sand Patch test is generally considered a ground truth method for macrotexture measurement, and this test correlates well with other methods, it was used as a reference to convert all the measurements obtained with the laser-based devices. Because of previously reported difficulties measuring texture on the OGFC, the harmonizing process has been conducted excluding the OGFC.

The conversion coefficients were determined using linear regression. Only the CTM_MPD outputs were considered because the average MPD outputs of all eight segments have the highest correlation coefficient among the various CTMeter outputs with Sand Patch, also with the smallest standard error. The following model was used for all the devices:

$$MTD_{SP} = y_0 + a * MPD_{Laser-Based} + \epsilon \tag{1}$$

where,

- y_0 = the intercept parameter,
- a = the slope parameter of the first order polynomial, and
- ϵ = error.

Table 3 summarizes the conversion coefficients obtained with the data collected at the Virginia Smart Road. Since the volumetric patch test cannot be used to measure texture depths lower than 0.25 mm and it is difficult to be performed on very porous surfaces, certain limits for application of these conversion equations should be set. Consequently, the following ranges of application were determined for the conversion equations:

- CTMeter: 0.15 mm ≤ MPD ≤ 1.55 mm,
- ICC profiler: 0.47 mm ≤ ICCTEX ≤ 2.92 mm, and
- MGPS: 0.39 mm ≤ MPD ≤ 1.52 mm.

TABLE 3—Conversion coefficients based on the Virginia Smart Road measurements.

Model	Device	Type of Measure	y ₀	a	R ²	StdErr
OGFC Excluded	CTMeter	MPD	0.130	0.815	0.833	0.111
	ICC Profiler	ICCTEX	0.034	0.465	0.792	0.124
	MGPS	MPD	-0.138	1.007	0.797	0.123

Surface Mix Effect

The macrotexture measurements analyzed were collected on four significantly different types of surface mixes, including:

- Stone Mastic Asphalt (SMA): Loop and Section L,
- Dense Asphalt: Section A, G, and J,
- Open-Graded Friction Course (OGFC): Section K, and
- Concrete Section.

In this step, the macrotexture measurements obtained with the laser-based devices on each type of surface were correlated to each other separately. The various linear regression analyses are summarized in Table 4.

TABLE 4—*Correlation between laser-based measurements separated by surface mix types.*

Surface Mix Type	X/Y	ICC			MGPS		
		R ²	StdErr	No. of Obsv	R ²	StdErr	No. of Obsv
SMA	CTM_MPD	0.6202	0.215	12	0.522	0.111	12
	CTM_RMS	0.6876	0.195	12	0.5368	0.110	12
	ICC	/	/	/	0.8417	0.064	12
	MGPS	0.8417	0.139	12	/	/	/
Dense-Asphalt	CTM_MPD	0.7292	0.101	24	0.7142	0.058	24
	CTM_RMS	0.6286	0.119	24	0.375	0.086	24
	ICC	/	/	/	0.3674	0.086	24
	MGPS	0.3674	0.155	24	/	/	/
OGFC	CTM_MPD	0.4728	0.352	12	0.8934	0.213	12
	CTM_RMS	0.2233	0.428	12	0.6939	0.362	12
	ICC	/	/	/	0.5426	0.442	12
	MGPS	0.5426	0.328		/	/	/
Concrete	CTM_MPD	0.6982	0.174	6	0.7295	0.045	6
	CTM_Tran	0.604	0.200	6	0.655	0.051	6
	CTM_Long	0.1056	0.300	6	0.2096	0.077	6
	CTM_RMS	0.7537	0.158	6	0.6426	0.052	6
	ICC	/	/	/	0.8833	0.030	6
	MGPS	0.8833	0.109	6	/	/	/

As expected, the R² for the various comparisons is lower than those in the previous cases because the range of texture for each mix is significantly narrower than for all mixes combined. From the table, the following conclusions were drawn:

- The MPD output from the CTMeter generally correlates better with the MGPS system than the RMS output.
- On the OGFC section, the correlation coefficient between the CTMeter and the MGPS system is much higher than that between either of them and the ICC profiler.

- On the Concrete section, the CTMeter longitudinal MPD outputs have very low correlation coefficient with the measurements from the other two devices. This was unexpected, and further research is recommended to verify this finding.

Models Validation

Three additional data sets were used to test the model developed, including a second data set collected at the Virginia Smart Road, measurements on several newly constructed highway pavements throughout Virginia, and data collected on airport pavements at the Wallops flight facility, also in Virginia.

Second Set of Virginia Smart Road Data

This data set was collected on some extra sections at the Virginia Smart Road. This set included data from the CTMeter and the ICC profiler only. For each section, average MPD on the LWP and BWP were used for MTD prediction, as shown in Fig. 3. As expected, the model in general predicts the same MTD based on ICCTEX and CTM_{MPD} . Paired t-test indicates that for a 95 % level of significance the MTD predicted based on the MPD_{CTM} , and the ICCTEX measurements are not significantly different (Table 5).

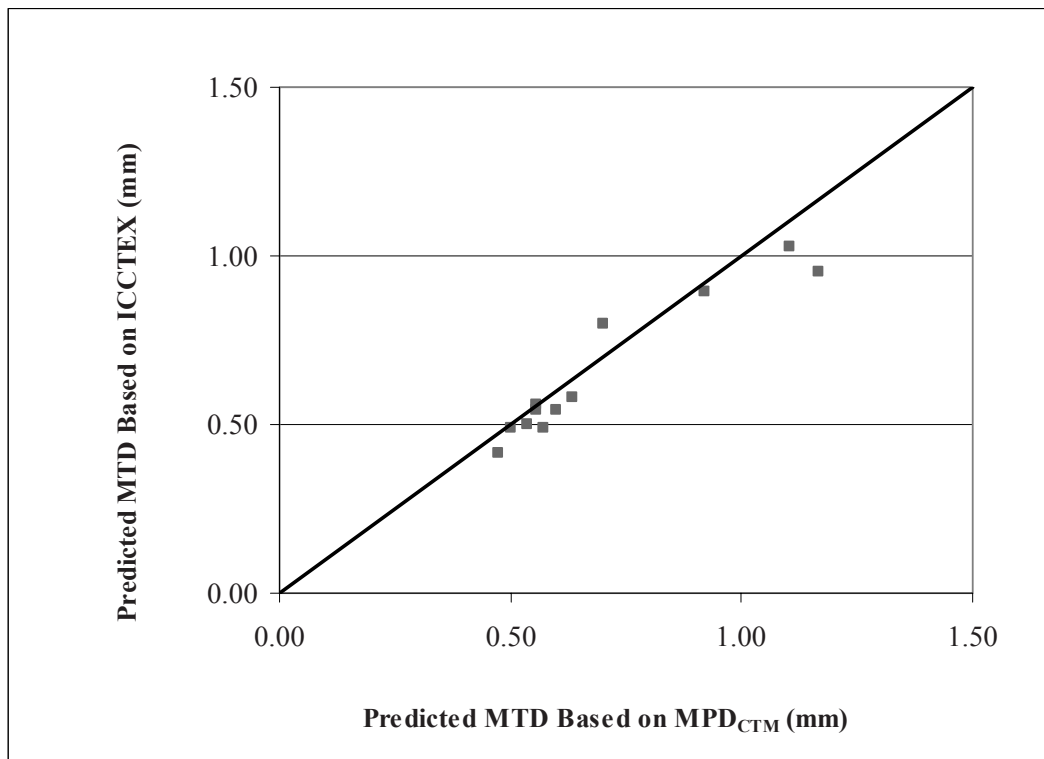


FIG. 3—Comparison of MTD predictions based measurements at the Virginia Smart Road.

TABLE 5—Comparison of measured and predicted MTD based on average macrotexture measurements at Virginia Smart Road.

Statistics Parameter	OGFC Excluded Model	
	CTM Prediction	ICC Prediction
Mean	0.693	0.649
Variance	0.056	0.044
Observations	12	12
Pearson Correlation	0.957	
Hypothesized Mean Difference	0	
df	11	
t Stat	2.153	
P(T<=t) two-tail	0.054	
t Critical two-tail	2.201	

Highway Pavements

The models were also tested with data obtained from a selected sample of typical VDOT highway mixes, which were measured during the summer 2003. The ICC and CTMeter macrotexture data were collected on eight highway projects (summarized in Table 6), as part of a study to detect and quantify HMA segregation [10]. For each project, average MPD on the LWP and BWP were used for MTD prediction, as shown in Fig. 4. As expected, the model predicts rather close MTD values based on the MPD_{CTM} and ICCTEX, except at points A, B, and C. However, these locations have some special features that may explain this discrepancy. Point A had a localized area with particularly low CTMeter measurements. Points B and C correspond to measurements taken on heavily segregated areas. Paired t-test indicates that for a 95 % level of significance the MTD predicted based on the MPD_{CTM} , and the ICCTEX measurements are not significantly different (Table 7).

TABLE 6—Test site locations.

Project	Location	County	District	Mix
02-1026	I-81 Southbound from Woodstock	Shenandoah	Staunton	BM-25
02-1039	Rt. 7 West of Leesburg	Loudon	NOVA	SM-9.5 D
02-1041	Rt. 7 East of Berrysville	Frderick	Staunton	SM-12.5
02-1043	Rt. 15 East of Gordansville	Orange	Culpeper	SM-9.5
02-1050	Rt. 522 West of Rt 3 in Culpeper	Culpeper	Culpeper	BM-25
02-1056	Rt. 29 North of Danville	Pittsylvania	Lynchburg	IM-19.0
02-1068	Rt. 33 West of Elkton	Rockingham	Staunton	SM-12.5 A
02-1079	Rt. 460 East of Cedar Bluff	Tazewell	Bristol	SM-19.0

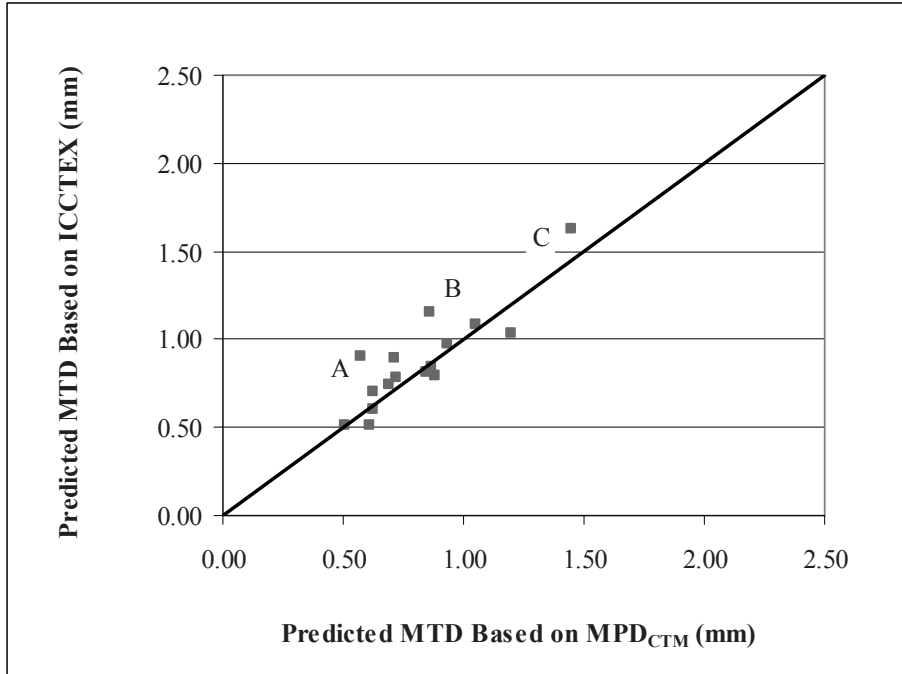


FIG. 4—MTD predictions based on average ICCTEX and CTM_{MPD} measurements on newly constructed highway pavements.

TABLE 7—Comparison of measured and prediction MTD based on average ICCTEX and CTM_{MPD} measurements on highway surfaces.

Statistics Parameter	OGFC Excluded Model	
	CTM Prediction	ICC Prediction
Mean	0.822	0.873
Variance	0.062	0.074
Observations	16	16
Pearson Correlation	0.870	
Hypothesized Mean Difference	0	
df	15	
t Stat	-1.501	
P(T<=t) two-tail	0.154	
t Critical two-tail	2.131	

Airport Pavements

The Wallops flight facility is an operational airport owned and run by the National Aeronautics and Space Administration (NASA). Table 8 lists the subsets of the surfaces available at Wallops that were used for this study [11]. Three randomly selected locations were used for the CTMeter and volumetric measurements on each section. Figure 5 compares the MTD predicted based on the average CTMeter measurements to the average measured PSU MTD. This figure suggests that the model predicts MTD values based on the CTMeter measurements that are very close to the measured MTD. The largest difference between the

predicted and measured MTD is found at point A, which corresponds to a special Surface S-4 (non-grooved PCC w/Skidabrader® with very high texture). Paired t-test indicates that for a 95 % level of significance the MTD predicted based on the MPD_{CTM} and the ICCTEX measurements are not significantly different (Table 9).

TABLE 8—*Evaluated test surfaces at Wallops.*

Surface Code	Width (m)	Length (m)	Surface Description
A	4.6	32.6	Non-grooved canvas belt-finished PCC
B	4.6	32.6	Grooved 1x1/4x1/4-inch canvas belt-finished PCC
C	4.6	32.6	Grooved 1x1/4x1/4-inch burlap drag-finished PCC
D	4.6	32.6	Non-grooved burlap drag-finished PCC
E	4.6	93.0	Non-grooved small-aggregate HMA
F	4.6	32.6	Grooved 2x1/4x1/4-inch small aggregate HMA
K	0.9	25.9	Driveway sealer without sand on K0
K0	0.9	25.9	Non-grooved float-finished PCC
S-0	1.2	18.6	Untreated area adjacent to skidabrader sites
S-1	1.2	18.6	Non-grooved PCC w/Skidabrader® light texture (1994)
S-2	1.2	18.6	Non-grooved PCC w/Skidabrader® medium texture (1994)
S-3	1.2	18.6	Non-grooved PCC w/Skidabrader® high texture (1994)
S-4	1.2	18.6	Non-grooved PCC w/Skidabrader® very high texture (1994)
S-5	1.2	83.5	Non-grooved PCC w/Skidabrader® medium texture (1995)
S-6	1.2	55.8	Non-grooved PCC w/Skidabrader® medium texture (1997)
MS/1	0.9	27.7	MS/0 with slurry seal overlay (1995)
MS/2	0.9	27.7	MS/0 with microsurface, single overlay (1995)
MS/3	0.9	27.7	MS/0 with microsurface, double oberlay (1995)
MS/4	0.9	27.7	MS/0 with anti-skid overlay (1999)

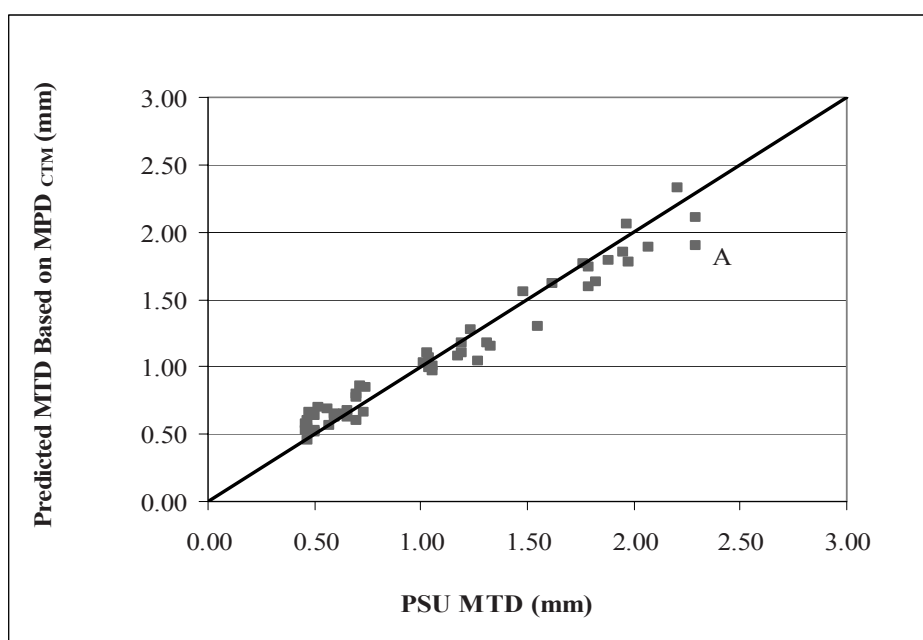


FIG. 5—*MTD predictions based on CTMeter measurements on airport surfaces.*

TABLE 9—Comparison of measured and predicted MTD based on CTMeter measurements on airport surfaces.

Statistics Parameter	OGFC Excluded Model	
	PSU MTD	CTM Prediction
Mean	1.114	1.093
Variance	0.339	0.266
Observations	51	51
Pearson Correlation	0.982	
Hypothesized Mean Difference	0	
df	50	
t Stat	1.192	
P(T<=t) two-tail	0.239	
t Critical two-tail	2.009	

Findings

The following findings were obtained from the correlation analyses:

- The three laser devices were found to have relatively low standard deviation (lower than 0.17 mm) and coefficient of variation (lower than 10 %). Hence, their repeatability was considered acceptable. The CTMeter appears to be the most repeatable of the three devices, followed by the MGPS System, and then the ICC profiler.
- The output of the devices appears to be different. This is probably due to the different analytical approach used by the devices. However, they are all highly correlated with the Sand Patch MTD ($R^2 \geq 0.88$). The CTMeter MPD has the highest correlation with the Sand Patch MTD, followed by the MGPS system, and then the ICC profiler.
- The CTMeter MPD outputs correlate better with the other devices’ macrotexture measurements than its RMS output. Furthermore, among the various CTMeter MPD outputs, the average MPD of all eight segments correlates better with the other devices’ macrotexture measurements than the average MPD of Longitudinal or Transversal segments.

Conclusions

The very high coefficients of determination (R^2) between the laser-based macrotexture measurements and the Sand Patch MTD confirm the potential of using the laser-based macrotexture measurements in light of the traditional volumetric method for measuring surface macrotexture. The following models were developed to convert laser-based measurements to the volumetric MTD on non-porous surfaces.

CTMeter	$MTD_{Predicted} = 0.8147 * MPD_{CTM} + 0.1303$ $[0.15mm \leq MPD_{CTM} \leq 1.55mm]$
ICC Profiler	$MTD_{Predicted} = 0.4646 * ICCTEX + 0.0342$ $[0.47mm \leq ICCTEX \leq 2.92mm]$
MGPS System	$MTD_{Predicted} = 1.0073 * MPD_{MGPS} - 0.1383$ $[0.39mm \leq MPD_{MGPS} \leq 1.52mm]$

The models developed were based on measurements on a limited number of surface types. Testing on a wider range of surfaces is recommended for further calibration and validation of the conversion models.

References

- [1] Nordic, "Influence of Road Surface Texture on Traffic Characteristics," Road & Transport Research, No. 2, 1999 ([Http://www.vti.se/nordic/2-99mapp/299sw.html](http://www.vti.se/nordic/2-99mapp/299sw.html), 8/25/2003).
- [2] Henry, J. J., "NCHRP Synthesis 291 Evaluation of Pavement Friction Characteristics: A Synthesis of Highway Practice," Transportation Research Board, Washington, D.C., 2000.
- [3] Dupont, P. and Ganga, Y. "Skid Resistance and Texture of Road Surfaces on Difficult Sites," Permanent International Association of Road Congresses (PIARC), Individual Papers Committees and Working Groups, Montreal, 1995, pp. 35–39.
- [4] Wambold, J. C., Antle, C. E., Henry, J. J., and Rado, Z. "International PIARC Experiment to Compare and Harmonize Texture and Skid Resistance Measurements," Final Report, May 1995.
- [5] ASTM Standard E 965-96, "Standard Test Method for Measuring Pavement Macrotexture Depth Using a Volumetric Technique," *Annual Books of ASTM Standards*, Vol. 4.03. ASTM International, West Conshohocken, PA.
- [6] Abe, H., Tamai, A., Henry, J. J., and Wambold, J. "Measurement of Pavement Macrotexture with Circular Texture Meter," Transportation Research Record 1764, Transportation Research Board, Washington, D.C., 2000, pp. 201–209.
- [7] McGhee, K. K. and Flintsch, G. W., "High-Speed Texture Measurement of Pavements," Virginia Transportation Research Council Report VTRC 03-R9, VTRC, Charlottesville, VA, 2003.
- [8] ASTM Standard E 1845, "Calculating Pavement Macrotexture Profile Depth," *Annual Book of ASTM Standards*, Vol. 4.03, ASTM International, West Conshohocken, PA.
- [9] ASTM Standard E 2157-01, "Standard Test Method for Measuring Pavement Macrotexture Properties Using the Circular Track Meter," *Annual Book of ASTM Standards*, Vol. 4.03. ASTM International, West Conshohocken, PA.
- [10] Flintsch, G. W., McGhee, K. K., and de Leon, E. "Use of Surface Macrotexture Measurement to Detect Segregation," Virginia Transportation Research Council Report VTRC 03-R12, VTRC, Charlottesville, VA, 2003.
- [11] Yager, T. J. "Seventh Annual Tire/Runway Friction Workshop: Summary and Proceedings Document," NASA Langley Research Center, Hampton, VA, 2000.

N. Mike Jackson,¹ Bouzid Choubane,² Charles Holzschuher,² and Salil Gokhale³

Measuring Pavement Friction Characteristics at Variable Speeds for Added Safety

ABSTRACT: Pavement friction testing is frequently conducted in accordance with the provisions outlined in ASTM E 274, “Standard Test Method for Skid Resistance of Paved Surfaces Using a Full-Scale Tire.” The standard speed of testing in Florida is 40 mph (64.4 km/h). However, due to safety concerns related to testing on high-speed facilities, considerable attention has been focused in recent years on height-sensor based (non-contact) technology. It is potentially well suited for surveying the surface texture characteristics of pavement sections while operating at highway speed.

Although the height-sensor based technology has been available since the 1960s, it continues to mature. A considerable amount of research has been conducted to gain further understanding on the factors affecting high-speed pavement surface surveying from both the analytical and experimental points of view. Still some problems have not fully been resolved, particularly in the interpretation of the measured data and selection of adequate sensing technology (or sensor designs).

The Florida Department of Transportation (FDOT) initiated the present study to assess the feasibility of using high-speed, laser-based sensors to quantify the texture and friction characteristics of asphalt pavements. The main objective of this study is to provide for a safer, faster and more appropriate method of estimating pavement friction characteristics on high-speed facilities, ramps, and at other potentially hazardous sites. Further, it is also intended to provide for a means to obtain a measure of International Friction Index (IFI) in accordance with ASTM E 1960.

This paper presents a description of the FDOT testing program, the data collection effort, as well as the subsequent analyses and findings.

KEYWORDS: pavement texture, friction testing, International Friction Index, skid resistance

Introduction

The Florida Department of Transportation (FDOT) has conducted standard friction tests on state roadways since 1958. The first Pavement Friction Testing Unit, meeting the requirements of ASTM Committee E17 on Vehicle-Pavement Systems, was fabricated for the Department in 1966. FDOT currently owns and operates four modern Pavement Friction Testing Units. Each of these Units consists of a tow vehicle, water tank, friction trailer, and mobile data processor. Friction measurements are obtained from the force induced on a locked test wheel as it is dragged over a wetted pavement surface. The mean Friction Number (FN) of the pavement surface is obtained from this test. All pavement friction testing currently performed by FDOT is conducted in accordance with the provisions outlined in ASTM E 274, “Standard Test Method for Skid Resistance of Paved Surfaces Using a Full-Scale Tire [1].” Testing is typically

Manuscript received 15 October 2004; accepted for publication 3 June 2005; published November 2005. Presented at ASTM Symposium on Pavement Surface Condition/Performance Assessment: Reliability and Relevancy of Procedures and Technologies on 7 December 2004 in Washington, DC.

¹ University of North Florida, Division of Engineering 4567, St. Johns Bluff Rd., South, Jacksonville, FL 32224-2645.

² Florida Department of Transportation, Materials Research Park, 5007 N.E. 39th Avenue, Gainesville, FL 32609.

³ Applied Research Associates, Inc., ERES Consultants Division, 5007 N.E. 39th Avenue, Gainesville, FL 32609.

performed at the specified speed of 40 mph (64.4 km/h), using the standard “Ribbed Tire” as specified by ASTM E 501, “Specification for Standard Rib Tire for Pavement Skid-Resistance Tests [2].”

Although the current FDOT friction testing program is fully implemented, there are several areas that need to be addressed, most importantly safety while conducting the test. The current specified test speed of 40 mph (64.4 km/h) is used on all state roadways including primary, secondary, interstates, and toll roads. To maximize safety and minimize traffic disruption, friction testing is typically conducted on weekdays and sometimes at night. Nevertheless, there are still safety concerns related to potential conflicts with the motoring public on high-speed facilities, ramps, and at other potentially hazardous sites. In order to properly address these safety concerns, FDOT is currently evaluating the use of height-sensor based (non-contact) technology to accommodate variable testing speeds, comparable to the speed limit of the facility being tested.

Background

FDOT Friction Testing Program

Friction testing is conducted by FDOT on all newly constructed pavement surfaces; all overlays; spot hazard locations identified as having an unusual number of wet weather accidents; re-test locations; and special requests, including research test sections, milled surfaces, or bridge decks. Testing is performed in the center of the left wheel path of the traffic lane and in both directions for four-lane and multi-lane roadways. For two-lane roadways, only one lane is tested, unless otherwise requested. As previously noted, FDOT uses the standard ribbed tire to obtain a measure of friction, FN_{40R} , in accordance with ASTM E 501, unless otherwise noted.

Equipment and Calibration

FDOT currently maintains four skid trailers meeting the ASTM specifications, as previously described. A photograph of a typical unit is presented in Fig. 1. These units are equipped with International Cybernetics Corporation (ICC) Mobile Data Recorders (MDR 4040) for automated data acquisition purposes. The units are calibrated biennially at the Central/Western Field Test and Evaluation Center, Texas Transportation Institute, Texas A&M University System, College Station, Texas. FDOT personnel verify the calibration of these units using a force plate every thirty to forty-five days. Water flow verifications are also performed every six months to ensure proper water flow and distribution. The units are also checked for repeatability on five test sections located in the vicinity of the State Materials Research Park in Gainesville, Florida after each calibration check.

Friction Testing at Variable Speeds

Due to safety concerns associated with friction testing on both high and low-speed facilities, testing at variable speeds has been proposed by some FDOT personnel. As previously noted, the ASTM and FDOT standard test speed is 40 mph (64.4 km/h). It is envisioned that appropriate correlations may be developed for test data obtained at the standard speed and data obtained at other speeds. ASTM has already promoted this concept with the introduction of International Friction Index (IFI) in ASTM E 1960 [3].



FIG. 1—Typical FDOT pavement friction testing unit performing a test.

Smooth-Tire Testing

In 1984, FDOT began collecting “Smooth-Tire” skid data at wet-weather accident sites in accordance with ASTM E 524, “Specification for Standard Smooth Tire for Pavement Skid Resistance Tests,” in addition to ribbed tire data [4]. It has been documented that the ribbed tire test is predominantly influenced by micro-texture, whereas the smooth tire test is influenced to a greater extent by macro-texture [5]. Historical analysis of smooth-tire friction test data collected by FDOT at wet-weather accident sites is reproduced here in Fig. 2 [6]. As presented by the horizontal line in Fig. 2, corresponding to a mean smooth-tire Friction Number (FN_{40S}) of 25, the smooth tire data have been documented to correlate better with wet-weather accidents. As a result, additional smooth tire testing has been included in this study.

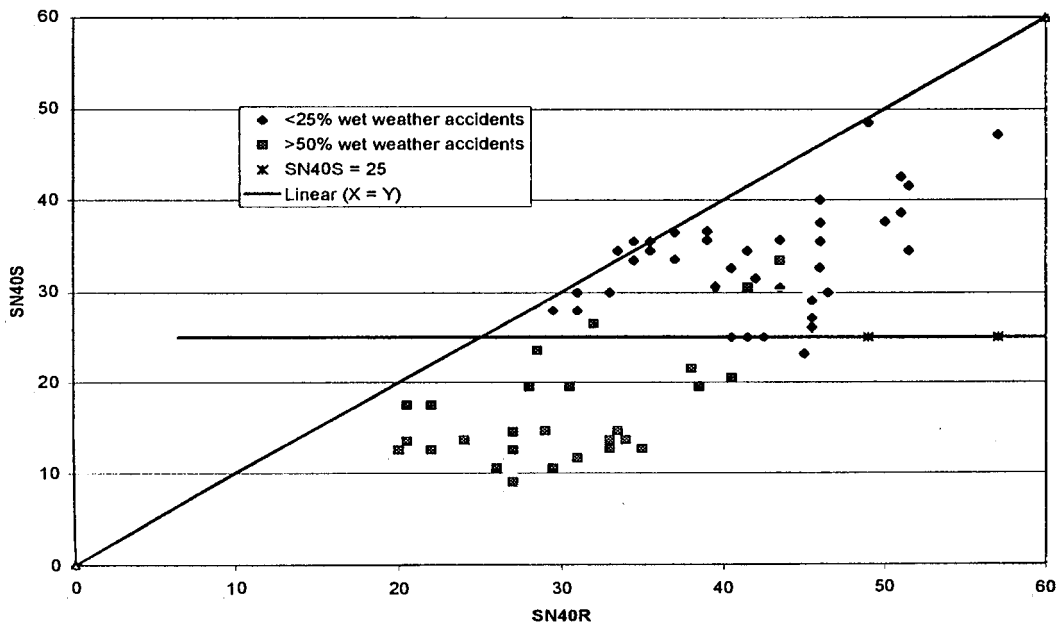
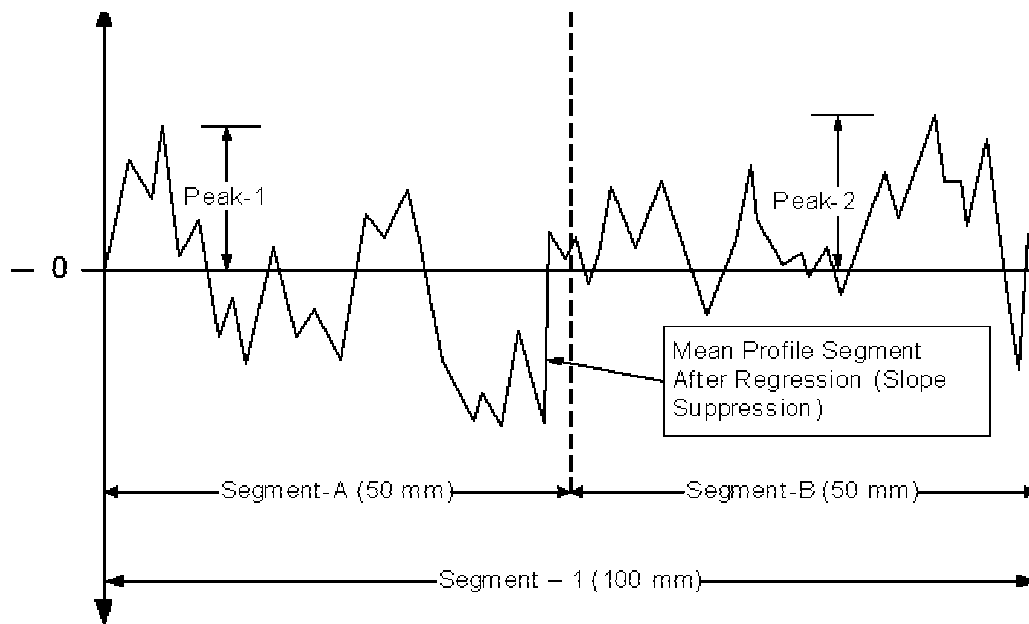


FIG. 2—Ribbed-tire versus smooth-tire friction numbers for Florida pavements [6].

Recent Technological Advances

In recent years, technological advances in microprocessors and personal computers have made it possible to consider the use of high-speed lasers in the evaluation of pavement surface characteristics, such as profile, distress, and even texture. Research by others [7] has demonstrated that laser-based sensors have evolved to the point where they are now durable enough to be used in the field to measure pavement surface texture (macro-texture). The Texas Department of Transportation (TXDOT) currently employs 78 kHz lasers in the collection of texture data [8]. TXDOT and others have demonstrated that this technology has progressed to the point where it is possible to collect both surface texture measurements and friction data, simultaneously.

The measurement of pavement texture using high-speed laser technology has now been standardized in ASTM E 1845, “Standard Practice for Calculating Pavement Macrotexture Mean Profile Depth [9].” In accordance with ASTM E 1845, such laser texture data are processed as shown in Fig. 3, to estimate the mean segment depth for a given 100 mm segment of pavement. Mean segment depths are averaged over the length of pavement section being tested to obtain the Mean Profile Depth (MPD).



ASTM E 1845-01: Standard Practice for Calculating Pavement Macrotexture Mean Profile Depth

Mean Segment Depth $_{segment1} = (Peak-1 + Peak-2)/2$

$$Mean\ profile\ depth_{Section} = \frac{\sum_{i=1}^n Mean\ Segment\ Depth_{Segment(i)}}{n}$$

FIG. 3—Standard method used for calculating mean profile depth [9].

Conversations with equipment manufacturer representatives (Selcom and ICC) have raised questions regarding the functional durability of lasers beyond about 78 kHz in speed [10,11]. In addition, it is expected that the number of invalid data points collected at such high speeds would increase significantly in Florida, where open-graded surfaces are common. For these reasons, it was recommended that FDOT explore the use of a 64 kHz laser for texture measurement in this initial study.

International Friction Index

With measures of both macrotexture and friction, it is possible to estimate the International Friction Index (IFI) for a given pavement section in general accordance with ASTM E 1960, “Standard Practice for Calculating International Friction Index of a Pavement Surface [3].” The IFI was developed as a common reference scale for quantifying pavement surface frictional properties [12]. IFI is currently being adopted worldwide as the standard skid resistance measure. The IFI consists of two parameters: (1) one that represents the wet friction of a pavement at 60 km/h (F60) and (2) a speed constant of wet pavement friction (S_p).

Measurement of the pavement macrotexture is used to estimate the pavement speed constant (S_p). The speed constant (S_p) in km/h is determined from MPD in mm as follows:

$$S_p = 14.2 + 89.7 * MPD \quad (1)$$

The calibrated wet friction parameter (F60) can be estimated from the results of friction testing in accordance with ASTM E 274, using either the standard ribbed tire, as described in ASTM E 501, or the smooth tire, as described in ASTM E 524. The International PIARC Experiment to Compare and Harmonize Texture and Skid Resistance Measurements resulted in a set of regression-based relationships that can be used to transform ASTM E 274 data (FN_{40R} or FN_{40S}) to the IFI, F60 parameter [12]. This relationship, as published in ASTM E 1960 is:

$$F60 = A + B * FRS * \exp[-(60-S)/S_p] + C * MPD \quad (2)$$

Where A, B, and C are calibration constants, and FRS is the measured friction at some slip speed, S.

If we use FN_{40R} as an estimate of FRS, the calibration constants are: A = -0.023, B = 0.607, and C = 0.098; and if we use FN_{40S} as our estimate of FRS, the calibration constants are: A = 0.045, B = 0.925, and C = 0. The resulting F60 and S_p parameters are reported as IFI (F60, S_p).

As noted in Note 3 of ASTM E 1911, “Standard Test Method for Measuring Paved Surface Frictional Properties Using the Dynamic Friction Tester,” results from the International PIARC Experiment to Compare and Harmonize Texture and Skid Resistance Measurements indicated a correlation with the Friction Numbers from ASTM E 274 produced a correlation coefficient (R) of 0.86 [13]. Thus, for demonstration purposes in this paper, it is reasonable to estimate the wet friction of the pavement (F60) from FN_{40} values obtained from the FDOT Pavement Friction Testing Unit, in accordance with ASTM E 274. It is anticipated that calibration of the FDOT friction test data collected in this study, as described in ASTM E 1960, will be performed at a future date as part of a follow-up study. The results of this additional effort will be used to further promote the use of IFI within the FDOT.

Test Program

The present study was initiated in September of 2003 to evaluate the feasibility of enhancing the existing FDOT friction-testing program through the use of non-contact, laser-based sensors.

Under a contract with the University of North Florida (UNF) and ICC, a LMI Technologies, Selcom, Optiocator 64 kHz laser system was installed on a selected FDOT Pavement Friction Testing Unit, as shown in Fig. 4. Five FDOT calibration sections, located in the vicinity of the State Materials Research Park in Gainesville, Florida were tested as part of this initial study. These five calibration sections represent a wide range of surface textures, including both dense-graded and open-graded friction courses common to Florida state roadways. Each of these calibration sections is further divided into five sub-sections.

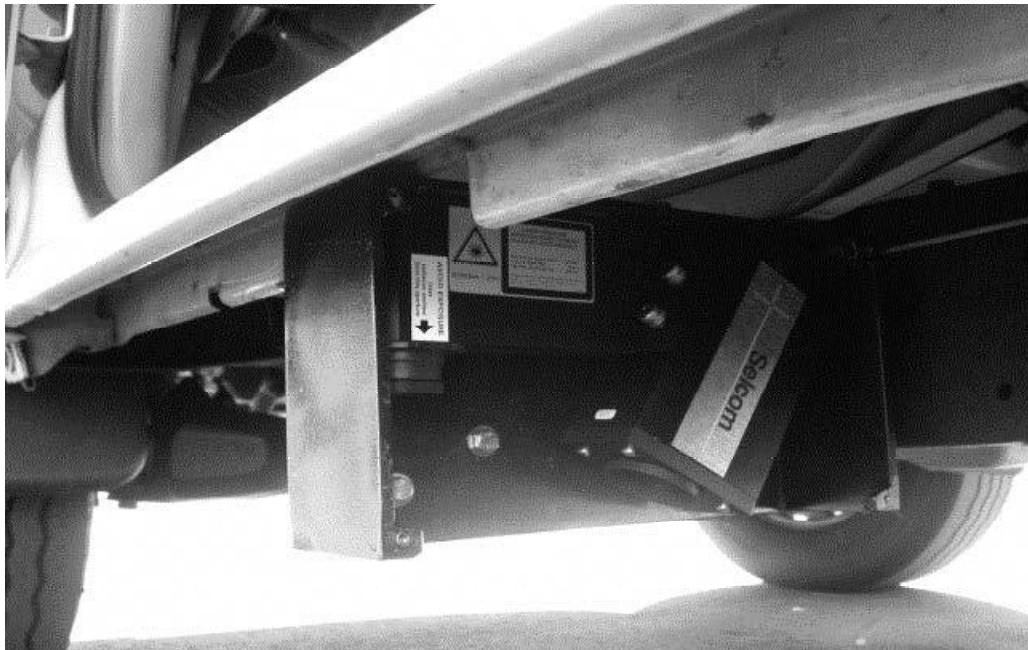


FIG. 4—FDOT skid test unit instrumented with LMI Technologies, Selcom, Optiocator 64 kHz, high-speed laser system.

The tests conducted on each sub-section of each calibration section included: (1) friction testing in accordance with ASTM E 274, using both the standard ribbed tire, as described in ASTM E 501, and the smooth tire, as described in ASTM E 524; (2) non-contact, macrotexture measurement, using the 64 kHz laser system installed on the FDOT Pavement Friction Testing Unit, in accordance with ASTM E 1845; and (3) volumetric macrotexture measurement in accordance with ASTM E 965, “Standard Test Method for Measuring Pavement Macrotexture Depth Using a Volumetric Technique,” more commonly referred to in practice as the “Sand Patch” test [14].

All field-testing was conducted within a two-day period to minimize temporal variations in the test data. Care was also taken to ensure that all data were collected in the test wheel path and within the wheel lock-up zone of each calibration sub-section to control spatial variations in the data. Testing was also performed by the same individuals (FDOT personnel) in order to limit unnecessary operator variability in the resulting data. Each calibration sub-section was tested for Friction Number (FN) at 40 mph (64.4 km/h), once with the ribbed tire (FN_{40R}) and once with the smooth tire (FN_{40S}). Laser macrotexture data were collected at three different speeds of 20, 40, and 60 mph (32.2, 64.4, and 96.6 km/h) and were collected at least twice for each calibration sub-section. It should be noted that laser macrotexture data were not collected at 60 mph (96.6 km/h) on the dense-graded surfaces due to safety concerns. Sand Patch tests were also conducted

in accordance with ASTM E 965 within each calibration sub-section, at a frequency of four tests within the wheel lock-up zone of each friction test. Sand Patch testing on a typical section is exhibited in Fig. 5.

This test program strategy was selected in order to provide sufficient data to assess the feasibility of using high-speed, laser-based sensors to quantify the texture and friction characteristics of asphalt pavements. The following results and analyses document the level of accuracy and repeatability of the 64 kHz non-contact, macrotexture measurement, as well as the effects of testing speed gradients. As previously noted, it is anticipated that this technology will lead to a safer, faster, and more appropriate method of estimating pavement friction characteristics on high-speed facilities, ramps, and other potentially hazardous sites.



FIG. 5—Sand patch testing (ASTM E 965) within the wheel lock-up zone of a typical FDOT calibration test section.

Test Results

The results of this study are summarized in Table 1 in the form of mean and standard deviation values for the different calibration sections tested. Table 2 provides an example of how typical ASTM E 274 results are transformed to the IFI parameters of F_{60} and S_p using the relationships and calibration constants developed in the International PIARC Experiment to Compare and Harmonize Texture and Skid Resistance Measurements [12]. The data provided in Table 1 are plotted in Figs. 6–9 for discussion purposes. The test results are discussed in greater detail in the following paragraphs.

TABLE 1—Summary of test results.

Test Section	Friction Number				Sand Patch (in.)		Non-Contact 64 kHz Laser Macrotexture (in.)											
	Mean FN _{40R}	Std. Dev.	Mean FN _{40S}	Std. Dev.	MTD	Std. Dev.	20 mph			40 mph			60 mph					
							MPD	Std. Dev.	ETD	MPD	Std. Dev.	ETD	MPD	Std. Dev.	ETD			
FC-2	35.5	1.08	32.5	1.06	0.064	0.0062	0.098	0.0057	0.087	0.101	0.0047	0.089	0.103	0.0019	0.090			
FC-3	36.6	0.51	27.4	0.81	0.021	0.0021	0.021	0.0028	0.025	0.025	0.0025	0.028	N/A	N/A	N/A			
FC-4	51.3	2.06	41.4	0.97	0.062	0.0078	0.035	0.0018	0.036	0.037	0.0023	0.038	N/A	N/A	N/A			
FC-5-Oolite	35.3	1.66	33.4	1.16	0.086	0.0047	0.114	0.0051	0.099	0.117	0.0039	0.101	0.116	0.0034	0.101			
FC-5-Granite	43.3	0.18	37.8	1.12	0.117	0.0094	0.148	0.0051	0.126	0.149	0.0047	0.127	0.145	0.0041	0.124			

TABLE 2—International Friction Index (IFI), F₆₀, S_p.

Calibration Test Section	Transformed From FN _{40S} and MPD		Transformed From FN _{40R} and MPD	
	Wet Friction, F ₆₀ *	Speed Constant, S _p (km/h)	Wet Friction, F ₆₀ *	Speed Constant, S _p (km/h)
FC-2	30.6	244.77	22.2	244.77
FC-3	27.0	70.80	23.7	70.80
FC-4	40.1	98.43	32.6	98.43
FC-5-Oolite	31.4	280.05	22.1	280.05
FC-5-Granite	35.5	353.38	27.0	353.38

* Note that the Wet Friction (F₆₀) values reported herein are estimated from Eq 2 using the calibration coefficients of the International PIARC Experiment to Compare and Harmonize Texture and Skid Resistance Measurements [12].

International Friction Index

As noted above, Table 2 provides an example of IFI output for the calibration sections tested in this study. The speed constant (S_p) values reported in Table 2 were transformed from the test-section MPD values using Eq 1. The calibrated wet friction (F60) values were transformed from the ASTM E 274 (FN_{40}) values using Eq 2. As shown in Table 2, the F60 values, as estimated from the standard ribbed tire, as described in ASTM E 501, are not in close agreement with the F60 values estimated from the smooth tire, as described in ASTM E 524. Presumably, if the calibration constants used in the transformation, Eq 2, were correct, the F60 values would be in agreement. Thus, it is confirmed that FDOT will have to develop in-house calibration/harmonization constants as described in ASTM 1960 in order to fully implement IFI as a standardized measure of pavement friction. It is anticipated that such calibration/harmonization will be performed at a future date, as part of a follow-up study. The results of this additional effort will be used to implement the use of IFI within FDOT.

It should be noted that the speed constant estimate is the same, regardless of test method, as it is calculated from texture, MPD.

Mean Profile Depth (MPD)

Figure 6 exhibits MPD, as obtained from the 64 kHz laser, plotted alongside the Mean Texture Depth (MTD), as obtained from the Sand Patch test. The respective 95 % Confidence Intervals associated with the mean values are provided to illustrate the relative repeatability of MPD at the variable speeds tested. Note that the overlapping Confidence Interval bars for the MPD obtained at different speeds is a good indication that test speed does not significantly affect the 64 kHz measure of texture between 20 and 60 mph (32.2 and 96.6 km/h). In other words, at a 95 % level of confidence, the MPD measured for a given calibration section is statistically the same at 20, 40, and 60 mph (32.2, 64.4, and 96.6 km/h). The MPD, as measured with the 64 kHz laser, is highly repeatable at variable speeds.

If we take the results of the Sand Patch test (MTD) as being the correct measure of texture, it is clear from Fig. 6 that the 64 kHz laser does not provide an accurate measure of this parameter in all cases except for the FC-3 calibration section. This discrepancy is recognized in ASTM E 1845 by way of the following transformation equation:

$$ETD = 0.008 + 0.8*MPD \quad (3)$$

where ETD is the Estimated Texture Depth in inches, and MPD is also expressed in inches. As noted in ASTM E 1845, the use of Eq 3 should yield ETD values which are close to the MTD values of the volumetric technique according to Test method E 965 [11]. Thus, it should not be surprising that we see a difference in Sand Patch data and laser texture data in Fig. 6.

The correlation between MTD and MPD for the calibration sections tested in this study is presented in Fig. 7. As noted, the Coefficient of Determination (R^2) for all pavement surfaces tested in this study is relatively strong at 0.78. It is also interesting to note that the resulting linear regression relationship between MTD and MPD is remarkably close to the ASTM E 1845 transformation equation, Eq 3 above, that is:

$$MTD = 0.77*MPD \quad (4)$$

The 64 kHz laser appears to provide a relatively accurate estimate of MTD.

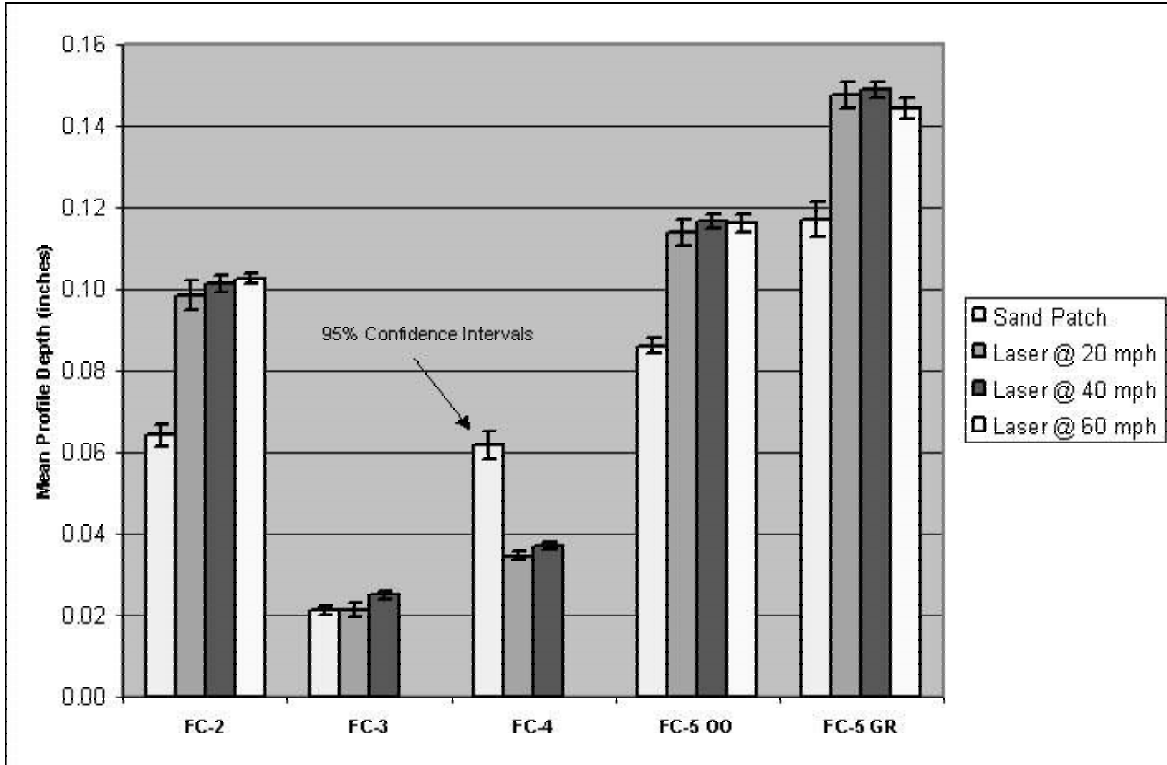


FIG. 6—Mean Profile Depth (MPD) at 20, 40, and 60 mph.

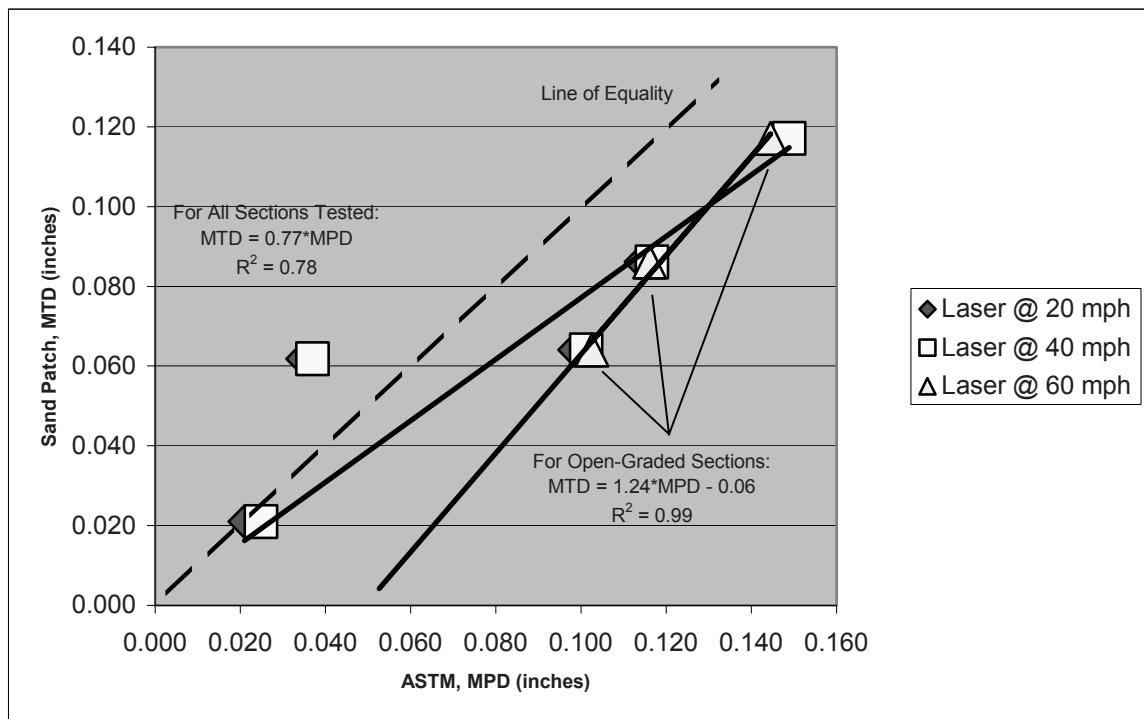


FIG. 7—Mean Profile Depth (MPD) versus Mean Texture Depth (MTD).

A final observation from Fig. 7 is that there appears to be a much stronger relationship available for open-graded surfaces, when these sections are considered separately as identified in the figure. The R^2 value obtained for the three open-graded sections tested in this study was found to be 0.99. The resulting linear regression relationship between MPD and MTD for open-graded surfaces is:

$$\text{MTD} = 1.24 * \text{MPD} - 0.06 \quad (5)$$

again, where MTD and MPD are expressed in inches. This observation suggests that it may be advantageous for FDOT to develop separate relationships for open-graded surfaces and dense-graded surfaces, as the texture of these surfaces is so different. It is envisioned that further testing and analyses related to this hypothesis will be performed at a future date as part of a follow-up effort.

Friction Number

Figures 8 and 9 present correlations between Friction Number ($\text{FN}_{40\text{R}}$ and $\text{FN}_{40\text{S}}$, respectively) and MPD for the calibration sections tested in this study. As noted, the R^2 values for both the standard ribbed tire, as described in ASTM E 501, and the smooth tire, as described in ASTM E 524 are extremely weak (0.03 and 0.08, respectively) when including all five of the pavement surfaces tested in this study. This result is not surprising when recognizing that pavement texture is only one component of friction. This multi-component concept is inherent in IFI, which makes use of standardized measures of both texture and friction.

Although it is tempting to seek a simple empirical method to estimate pavement friction, the data presented in Figs. 8 and 9 clearly demonstrate that macro-texture is a poor predictor of overall pavement friction. There is evidence that this limitation may be overcome, again by developing separate relationships for open-graded surfaces and dense-graded surfaces, as was described in the previous section. Figure 9 exhibits a much stronger relationship for open-graded surfaces, if these sections are considered separately. As noted, the R^2 value obtained for the three open-graded sections tested in this study was found to be 0.98. The resulting linear regression relationship between MPD and $\text{FN}_{40\text{S}}$ for the open-graded surfaces is:

$$\text{FN}_{40\text{S}} = 132 * \text{MPD} + 19 \quad (6)$$

where MPD is expressed in inches. It should be noted, however, that this relationship is provided for illustration purposes only. Further testing and analyses will be required to refine and validate this preliminary relationship.

Conclusions

The goal of this study was to assess the feasibility of using high-speed, laser-based sensors to estimate the texture and friction characteristics of asphalt pavements. The results of this study demonstrate that the 64 kHz non-contact, macrotexture measurement system described herein provides a repeatable and accurate measure of MPD. Further, the linear regression relationship between MTD and MPD, as developed from the data obtained in this study (Eq 4) is remarkably close to the transformation equation provided in ASTM E 1845 (Eq 3). This confirms that the 64 kHz laser provides a relatively accurate estimate of MTD. Even stronger correlations were found when separate relationships were developed for open-graded and dense-graded surfaces, as the texture of these surfaces is so different.

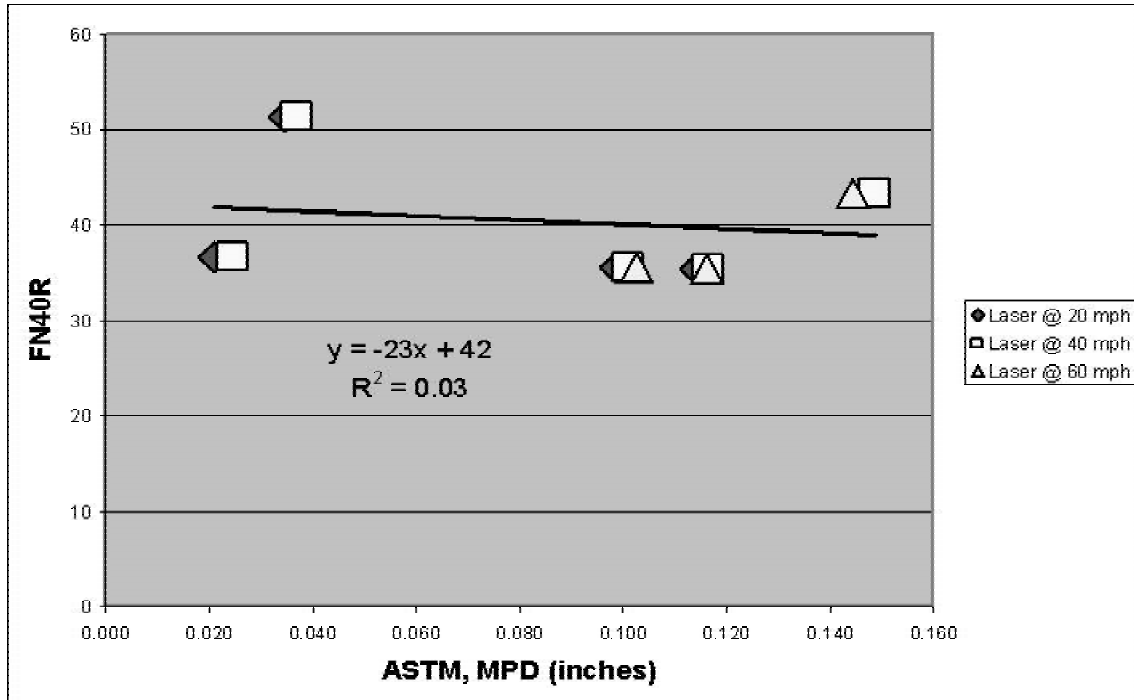


FIG. 8—Mean Profile Depth (MPD) versus Mean Friction Number (FN_{40R}).

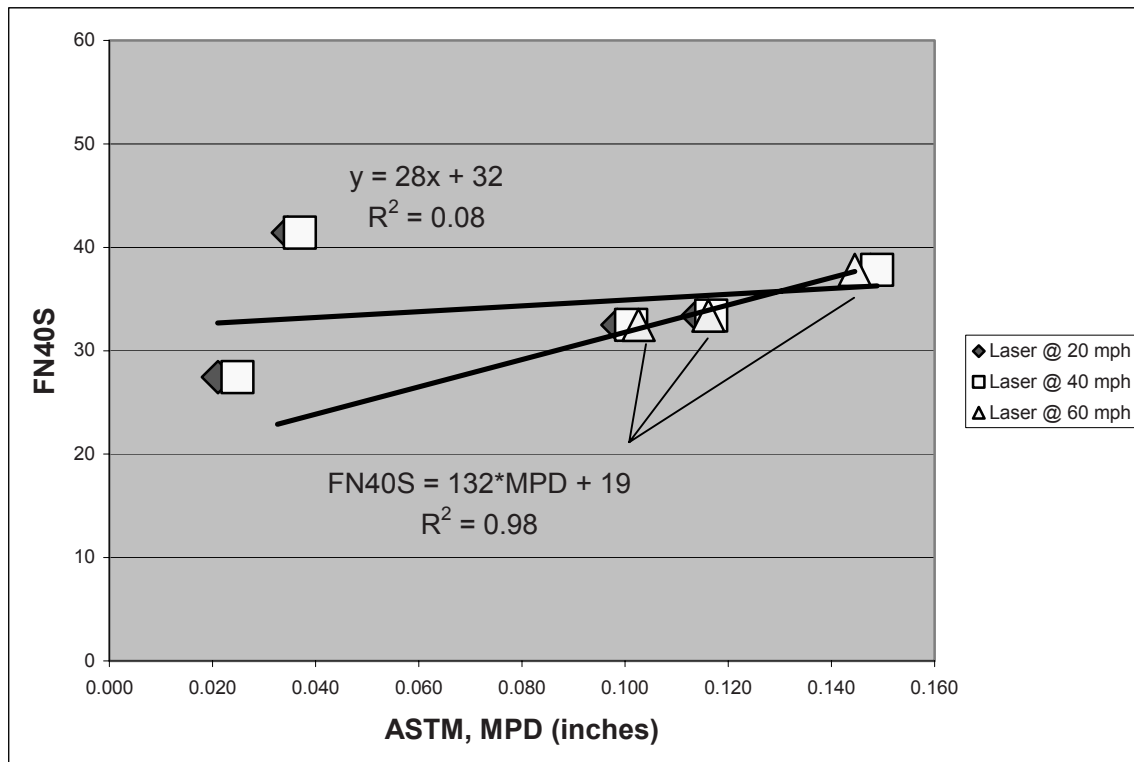


FIG. 9—Mean Profile Depth (MPD) versus Mean Friction Number (FN_{40S}).

With a repeatable measure of MPD and wet friction, IFI can be reported in accordance with ASTM E 1960. An example is provided of how FN_{40} data, as obtained from ASTM E 274, and MPD, as obtained from the 64 kHz non-contact, macrotexture measurement system described herein, can be transformed for IFI reporting. It is anticipated that a follow-up study will be conducted at a future date for calibration/harmonization of FDOT friction test data for IFI reporting. This follow-up effort would further promote the implementation of IFI within FDOT.

In general, macro-texture was found to be a poor predictor of overall pavement friction. However, evidence is provided that suggests this limitation may also be overcome by developing separate relationships for open-graded surfaces and dense-graded surfaces (Eq 6). Verification of this hypothesis will require an expanded test program.

In summary, the results of this study, when fully implemented, will yield a safer, faster, and more appropriate method of estimating pavement friction characteristics on high-speed facilities, ramps, and other potentially hazardous sites in Florida.

References

- [1] ASTM Standard Test Method E 274-97, "Skid Resistance of Pavements Using a Full-Scale Tire," *Annual Book of ASTM Standards*, Vol. 4.03, ASTM International, West Conshohocken, PA, 2004.
- [2] ASTM Standard Specification E 501-94, "Standard Rib Tire for Pavement Skid-Resistance Tests," (Reapproved 2000), *Annual Book of ASTM Standards*, Vol. 4.03, ASTM International, West Conshohocken, PA, 2004.
- [3] ASTM Standard Practice E 1960-03, "Standard Practice for Calculating International Friction Index of a Pavement Surface," *Annual Book of ASTM Standards*, Vol. 4.03, ASTM International, West Conshohocken, PA, 2004.
- [4] ASTM Standard Specification E 524-88, "Standard Smooth Tire for Pavement Skid-Resistance Tests," (Reapproved 2000), *Annual Book of ASTM Standards*, Vol. 4.03, ASTM International, West Conshohocken, PA, 2004.
- [5] Henry, J. J., *NCHRP Synthesis of Highway Practice 291: Evaluation of Pavement Friction Characteristics*, Transportation Research Board, National Research Council, Washington, D.C., 2000.
- [6] Hewett, D. L. and Miley, W. G., "Use of the Smooth Tire in Evaluation of Friction Characteristics of Surface Courses in Florida," *Presented at the meeting of TRB Committee A2B07 on Surface Properties-Vehicle Interaction*, Transportation Research Board, National Research Council, Washington, D.C., 1992.
- [7] Walker, R. S., "Development of a Laser Based Texture Measuring System," Research Project #2981, The University of Texas at Arlington, Transportation Instrumentation Laboratory, 2001.
- [8] Bertrand, C., TXDOT, Personal Communication, July 20, 2004.
- [9] ASTM Standard Practice E 1845-01, "Standard Practice for Calculating Pavement Macrotexture Mean Profile Depth," *Annual Book of ASTM Standards*, Vol. 4.03, ASTM International, West Conshohocken, PA, 2004.
- [10] Howe, D., Selcom, Personal Communication, July 15, 2004.
- [11] Olenoski, R. F., ICC, Personal Communication, July 15, 2004.
- [12] Wambold, J. C., Antle, C. E., Henry, J. J., and Rado, Z., "International PIARC Experiment to Compare and Harmonize Texture and Skid Resistance Measurements, Final Report," *Permanent International Association of Road Congresses (PIARC)*, Paris, 1995.

- [13] ASTM Standard Test Method E 1911-98, "Standard Test Method for Measuring Paved Surface Frictional Properties Using the Dynamic Friction Tester," (Reapproved 2002), *Annual Book of ASTM Standards*, Vol. 4.03, ASTM International, West Conshohocken, PA, 2004.
- [14] ASTM Standard Practice E 965-96, "Standard Test Method for Measuring Pavement Macrottexture Depth Using a Volumetric Technique," (Reapproved 2001), *Annual Book of ASTM Standards*, Vol. 4.03, ASTM International, West Conshohocken, PA, 2004.

Shuo Li,¹ Samy Noureldin,¹ and Karen Zhu¹

Realistic Approach for Enhancing Reliability of Pavement Surface Friction Testing

ABSTRACT: This paper presents the state-of-the-practice by the Indiana Department of Transportation (INDOT) in enhancing the reliability of pavement friction testing with the ASTM Standard E 274-97 [1] locked wheel tester. In order to detect the potential changes in system performance, INDOT conducts weekly and monthly system verification on a special friction test track. A multiparameter method has been used in assessing the performance of the locked wheel tester. This method cross examines the sample mean, the standard deviation, and the coefficient of variations of the friction measurements saved in a dynamic friction database that is upgraded after each verification testing. It was found that the system performance of the locked wheel tester varies with the type of test tire and pavement surface characteristics. The smooth tire produces greater friction variations than the ribbed tire. As pavement surface becomes rougher, friction variations decrease. A realistic approach has been established for verifying system performance.

KEYWORDS: pavement friction, locked wheel tester, system performance, reliability, friction test track

Introduction

It has been widely accepted that pavement surface friction is relevant and varies with testing methods. As a result, an important issue, i.e., how pavement engineers can justify the friction test results whose actual values are unknown in nature, may arise associated with the reliability of friction testing. Pavement friction is one of the important factors included in pavement management system (PMS) by many state highway agencies. However, the information on pavement friction is produced by network pavement inventory friction testing which is usually conducted with a spacing of 0.5 or 1.0 mile. It is of significance to provide reliable pavement friction data so as for PMS engineers to make effective and informed decisions.

Currently, many state highway agencies uses the ASTM Standard E 274 locked wheel tester [1] in network pavement inventory friction testing. Great effort has been made by many researchers so as to enhance the performance of the whole tester [2,3]. Many state highway agencies have established procedures for calibrating the tester's components such as force transducers. It should be pointed out, however, even after all components are properly calibrated, there is no guarantee for a locked wheel tester to produce reliable results. This is because the locked wheel tester is subject to variations due to not only the effects of its individual components but the effect of the system integrity, i.e., the performance of the system as a whole. Therefore, it is essential that the performance of the whole testing system be properly verified.

An effort has been made by the Florida Department of Transportation to investigate the precision of the locked wheel tester in terms of the repeatability and reproducibility [4]. Repeatability is the variation in measurements due to the testing system, and reproducibility refers to the variation in measurements due to factors other than the testing system. To the authors' knowledge, reliability and precision are to some extent related and it is difficult to distinguish between the two variations in friction measurements. However, though the true friction value is not available, it is possible to assess the reliability of friction testing by conducting friction testing on a pavement with constant friction value. The objective of this paper is to present the effort made by the Indiana Department of Transportation (INDOT) to enhance the reliability of

Manuscript received September 13, 2004; accepted for publication July 17, 2006; published online October 2006. Presented at ASTM Symposium on Pavement Surface Condition/Performance Assessment: Procedures and Technologies on 7 December 2004 in Washington, D.C.; B. Choubane, Guest Editor.

¹ Indiana Department of Transportation, Division of Research, 1205 Montgomery Street, West Lafayette, IN 47906.

friction testing. The focus is on the state-of-the-practice used by INDOT in verifying the performance of the locked wheel tester with both the standard smooth and ribbed tires.

The INDOT Friction Test Track

The Role of Friction Test Track

INDOT has been long utilizing the locked wheel tester in pavement friction testing. The calibrations of the tester's components are conducted by following the standard procedures [5]. The pavement wetting system is calibrated annually, which is usually conducted by two operators because the procedure is exhausting and may be hazardous. The calibration of the speed-measuring transducer is also conducted annually on a selected straight highway section. INDOT has established an in-house platform to calibrate the friction force measurement. The calibration of the force transducers is conducted monthly and at anytime when significant changes have been identified with the system. However, a locked wheel tester may fail to function properly even after its components are properly calibrated. For example, water may enter into transducers during testing, resulting in low friction numbers. Moreover, network pavement inventory friction testing usually lasts for several months. The testing system performance may change over time. In order to provide meaningful and comparable friction data, it is necessary to ensure consistent performance of the system.

A distinct feature of the INDOT friction testing system calibration is the use of a special friction test track. Pavement friction measurements may involve great variations due to those factors other than the possible system anomalies. For example, pavement friction experiences both lateral and longitudinal variations. In addition, pavement surface characteristics may change because of the repeated traffic applications, resulting in different pavement friction values over time. Therefore, it is difficult to quantify the variations due to the possible system anomalies. With the use of the INDOT friction test track, it has become possible for the authors to address the above issues. The surface characteristics in the test track may remain unchanged because the test track is not open to traffic. Also, the verification testing can be conducted at the same location so as to minimize the lateral and longitudinal friction variations. Another advantage with the friction test track is that its surface was finished to provide the desired surface characteristics so as to cover the range of possible friction measurements on highway pavements.

Surface Characteristics of Friction Test Track

The INDOT friction test track consists of three sections of different surface characteristics: slick concrete, asphalt, and tined concrete. As mentioned earlier, the surfaces in the three sections were finished so as to roughly cover the range of possible friction values on the real-life highway pavements. The selection of the surface characteristics is solely based on engineering judgment and resources available. Nevertheless, it requires at least three different sections so as to provide three typical pavement surfaces with low, medium, and high friction values. For example, asphalt pavements with severe rutting usually have very low friction in the wheel path. Tined concrete pavements have very high friction at early time. The friction values for most pavements are in between.

The surface of the slick concrete section was finished with very fine surface texture. The asphalt section was constructed with 9.5-mm hot mix asphalt (HMA) mixture. The coarse aggregates consist of blast-furnace slag and dolomite which, respectively, account for 27 % of the total aggregates. The asphalt binder of PG 76-22 was used in producing the mixture. The surface of the tined concrete section was finished with transverse grooves of 3-mm wide, 3-mm deep, and a spacing of 18–20 mm. All these three sections are long enough to provide a distance for the tester to skid over a 1.0-s period at the anticipated test speed. The test track has an approaching section and an exiting section to allow the operator to adjust the test speed so as to maintain a safe operation. Table 1 shows the detailed information on the surface characteristics and typical friction values measured with two different methods, i.e., the locked wheel tester and the dynamic friction tester.

TABLE 1—INDOT friction test track surface characteristics.

Section	MPD ^a (mm)	DFT20 ^b	F60 ^c	FN ^d (40 mph, smooth tire)
Slick concrete	0.04	0.58	0.08	<10.0
Asphalt	0.45	0.75	0.33	35.0 ~50.0
Tined concrete	1.35	0.86	0.56	>60.0

^aMPD=surface texture depth from circular texture meter.

^bDFT20=friction value from dynamic friction tester at 20 km/h.

^cF60=friction value at 60 km/h computed from MPD and DFT20.

^dFN=friction number from locked wheel tester.

System Performance Verification Testing

Minimum Sample Size Requirements

The system verification testing is conducted weekly in the friction test track during test seasons and monthly after the force transducers have been calibrated. The verification of the system performance is to determine the sample mean and the variations of friction measurements so as to examine the performance of the locked wheel tester as a whole and maintain consistent system performance. It is well known that the sample mean and standard deviation are random variables. They depend not only on the magnitude and variability of the friction measurements but also on the sample size. Statistically, the estimated sample mean and standard deviation, respectively, converge to the population mean and standard deviation as the sample size (the number of test runs) increases. Significant errors may arise when the sample size is small (usually less than 3).

In order to establish a minimum sample size requirement, friction measurements were made in the INDOT friction test track. In each of the three sections, eight tests were conducted consecutively at the same location. Figure 1 shows the standard deviations with respect to the sample sizes for the smooth tire and the ribbed tire, respectively. Careful inspection of Fig. 1 resulted in three observations. First, the greatest standard deviation occurred when the sample size equals two. The standard deviation became stable as sample size increased. This indicates that a minimum sample size of three test runs should be employed. Second, the standard deviation varied with the surface characteristics. The greatest standard deviation occurred in the asphalt section regardless of the type of the test tire. Third, the smooth and ribbed tires produced different deviations. In the asphalt and slick concrete sections, the ribbed tire produced greater standard deviations than the smooth tire. In the tined concrete section, however, the ribbed tire generated lower standard deviations than the smooth tire.

In general, the minimum sample size at a confidence level of 95 % can be estimated by using the following equation:

$$N = \left(\frac{1.96\sigma}{\varepsilon} \right)^2 + 3 \quad (1)$$

where N is the minimum sample size, σ is the population standard deviation of the friction test results, and ε is the allowable error for the verification testing. The estimation of the population standard deviation and the allowable error will be discussed later.

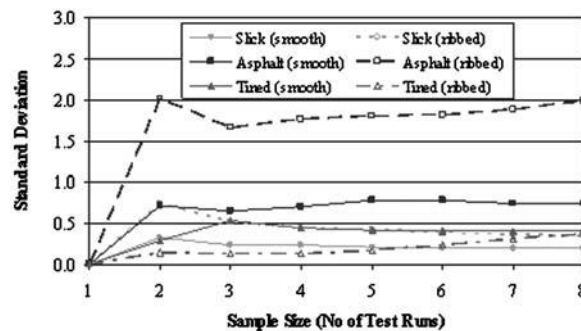


FIG. 1—Standard deviation versus sample size.

TABLE 2—Friction test results and 95 % confidence intervals in INDOT friction test track.

Tester	Test section	Test runs	Smooth Tire				Ribbed Tire				
			Mean	S.D. ^a	Lower bound	Upper bound	Test runs	Mean	S.D. ^a	Lower bound	Upper bound
300-4	Slick	34	8.3	1.4	7.8	8.8	34	33.3	2.7	32.4	34.2
	Asphalt	36	51.8	6.1	49.8	53.8	39	60.2	4.0	59.0	61.4
	Tined	35	71.6	3.4	70.5	72.7	30	73.4	2.5	72.5	74.3
379-6	Slick	34	8.3	1.2	7.9	8.7	32	31.6	1.9	31.0	32.2
	Asphalt	35	54.2	6.1	52.1	56.3	34	66.8	4.2	65.4	68.2
	Tined	36	71.3	2.2	70.6	72.0	35	73.1	2.4	72.3	73.9

^aS.D.=standard deviation.

Estimation of True Friction Values

As mentioned earlier, the true friction value for a certain pavement is unknown. This creates a dilemma for verifying system performance, i.e., what friction values should be used as the true friction values. A rational approach is to utilize the valid and comparable historical data to estimate the true friction values. It is doubtless that with more data available, engineers are able to gain more confidence in estimating the possible true friction values. In the past years, friction testing has been conducted routinely in the friction test track during each test season. The INDOT friction test season starts in April and ends in November each year. Summarized in Table 2 are the results of weekly and monthly system calibration tests conducted during the test season in 2003 with the two testers that are currently used in the INDOT friction testing. The potential seasonal variations are negligible over the test reason [6] and no temperature correction was considered. The friction values in the tined concrete are greater than those in the asphalt section and much greater than those in the slick concrete section. The friction values also vary with the test tire. The friction values measured with the ribbed tire are usually greater than those with the smooth tire. As the surface texture increases the friction values with the two tires become very close. Discrepancies can be observed between the friction values with the testers, especially in the asphalt section. The friction measurements in the asphalt section experienced greater variations than the slick and tined concrete sections.

Statistically, it is very common to establish the confidence bounds on the true mean instead of estimating the true mean directly. As an illustration, Table 2 also presents the 95 % confidence bounds for true friction values, i.e., the lower and upper bounds establish an interval in which the true mean lies. The number of test trials is 30 or more for each case. It is shown that all intervals are less than five units in terms of the friction number. The largest interval occurred in the asphalt section regardless of the test tire. Notice that the mean and standard deviation are themselves random variables. During the verification testing, only four to five test runs are usually conducted. The resulting mean and standard deviations may be different from the historical data. Therefore, the verification of friction testing system performance also requires sound engineering judgment.

Verification of System Performance

Friction Variations Due to Testing System Anomalies

As described in the preceding paragraphs, the system verification testing is conducted, respectively, in each of the three test sections in the friction test track. In each test section, four to five test runs are conducted at the same location so as to minimize the friction variations due to the factors rather than system anomalies. Consequently, the variations in friction measurements can be attributed solely to the system anomalies. Presented in Figs. 2 and 3 are the standard deviations from the verification testing with the two friction testers in 2002 and 2003, respectively. The friction measurements in each month as shown in these two figures were made within a short time period so as to allow the authors to identify the differences between the two tires. With the smooth tire, the greatest variations occurred in the asphalt section and the lowest variations in the slick concrete section. With the ribbed tire, the greatest variations occurred in the asphalt section and the lowest variations in the tined concrete section. Again, the smooth tire created greater variations than the ribbed tire.

Presented in Figs. 4 and 5 are the coefficients of variations in the friction measurements. The coeffi-

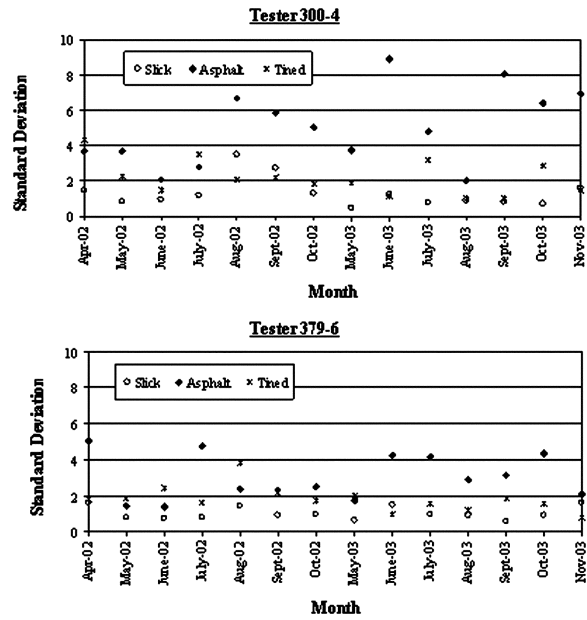


FIG. 2—Standard deviations with smooth tire.

cient of variations refers to as the ratio of the standard deviation to the mean and is also a statistical parameter for measuring the dispersion of random measurements. The coefficient of variations is usually used as a comparison in assessing relative variability by engineers. It is shown that with the smooth tire, the greatest variations occurred in the slick concrete section and lowest variations in the tined concrete section. The coefficient of variations decreased as the surface texture became rougher. Similar observations were made with the ribbed tire. The coefficient of variations tends to produce more consistent results than the standard deviation.

Multiparameter Assessment of System Performance

A greater standard deviation does not necessarily imply a worse system performance because the standard deviation depends not only on the variability but on the scale of the variable. In general, the standard deviation can provide valid conclusions. However, the standard deviation may provide unclear information

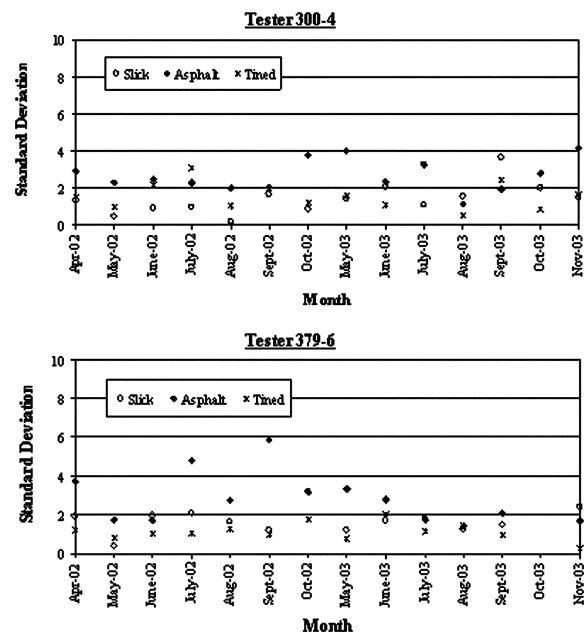


FIG. 3—Standard deviations with ribbed tire.

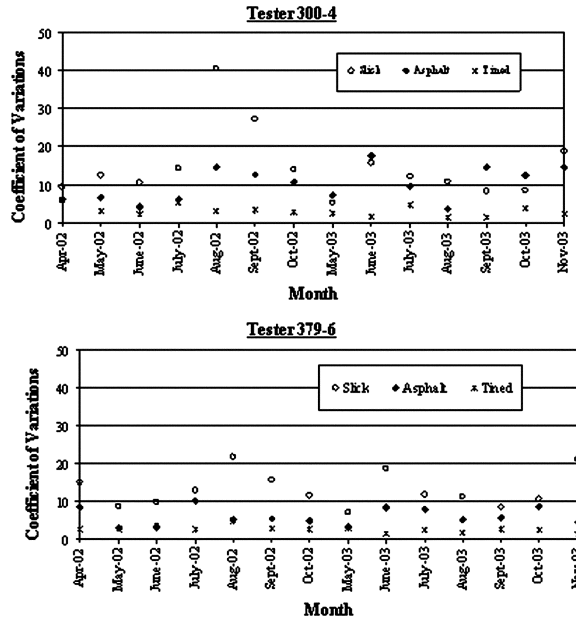


FIG. 4—Coefficients of variations with smooth tire.

in some cases. As an illustration, the average friction numbers for Tester 300-4 with the smooth tire are approximately 8.3, 51.8, and 71.6 for the slick concrete, asphalt, and tined concrete sections, respectively (see Table 2). A standard deviation of 2.0 accounts for a coefficient of variations of 24 %, 4 %, and 3 %, respectively, for each of the three sections. Apparently, the tester provides the best performance in the tined concrete section. In order to detect the potential system anomalies reliably, the authors have employed a multi-parameter method to verify the system performance.

The multiparameter method consists of two steps. The first step is to cross examine the mean friction values. The discrepancies between the mean friction values from the current verification testing and those from previous verification testing should not exceed the allowable errors. The second step is to examine the standard deviations and the coefficients of variations. Table 3 presents all requirements employed for the verification testing. The allowable errors for the friction values were established in terms of the historical friction data made in the friction test track in the past years. While the variations with the ribbed tire may be less than those with the smooth tire, the requirements apply to both the smooth and ribbed

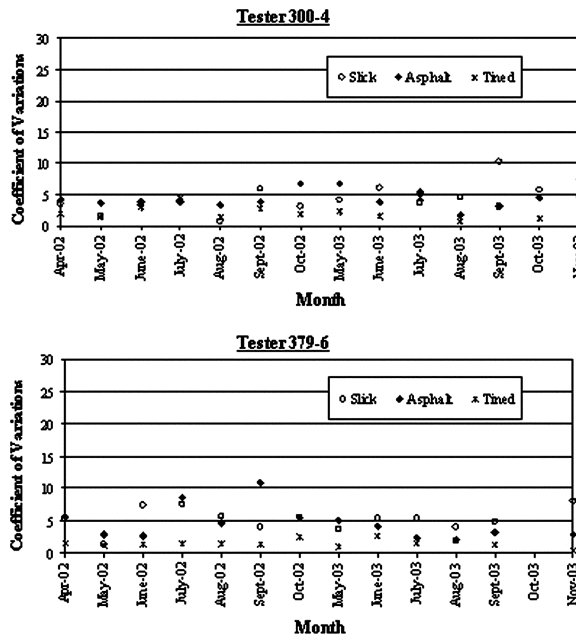


FIG. 5—Coefficients of variations with ribbed tire.

TABLE 3—Requirements for system verification testing.

Test section	Min.no.of testruns	Test speed (mph)	Allowable errors for friction values		
			Mean	S.D. ^a	COV ^b (%)
Slick concrete	4	±1	±3	2	20
Asphalt	4	±1	±5	4	12
Tined concrete	4	±1	±4	3	5

^aS.D.=standard deviation.

^bCOV=coefficient of variations.

tires. The allowable error for the coefficient of variations is 20 % for the slick concrete section, which is much higher than those for the asphalt and tined concrete sections. This is because the scale of the friction value in the slick concrete section is very small and any insignificant variations may result in great variations. Also, the allowable errors are used to estimate the sample size using Eq 1.

Conclusions

The reliability of friction testing with the locked wheel tester depends ultimately on the performance of the testing system as a whole. INDOT has employed a realistic approach to ensure consistent system performance over the test season. This approach consists of two core parts: weekly/monthly system verification testing and assessment of system performance. INDOT has built a special friction test track for system verification testing. The test track includes three sections of different surface characteristics so as to cover the range of possible friction values in highway pavements. The use of the friction test track enables the authors to quantify the friction variations due to the possible system anomalies and minimize the effect of the other factors. The assessment of system performance is conducted with a multiparameter method that cross examines the sample means, standard deviations, and coefficients of variations of the friction measurements in the friction test track.

The system performance of the locked wheel tester varies with the type of test tire and the pavement surface characteristics. The smooth tire usually produces greater friction variations than the ribbed tire. As the pavement surface texture becomes rougher the friction variations decrease. While the standard deviation has been widely used in measuring the friction variations, the coefficient of variations may be a better measurement of the friction variations. It was found that the coefficient of variations could provide more consistent results. Based on the data from the system verification testing conducted in the INDOT friction test track in the past years, a minimum of four test runs can produce a good assessment of the system performance. The friction variations in terms of the coefficient of variations due to the system performance are 20 %, 12 %, and 5 % on the slick concrete, asphalt, and tined concrete pavements, respectively.

References

- [1] ASTM Standard E 274-97, "Standard Test Method for Skid Resistance of Paved Surfaces Using a Full-Scale Tire," *Annual Book of ASTM Standards*, Vol. 04. 03, 1997, ASTM International, West Conshohocken, PA.
- [2] Wambold, J. C., Henry, J. J., Antle, C. E., Kulakowski, B. T., Meyer, W. E., Stocker, A. J., Button, J. W., and Anderson, D. A., "Pavement Friction Measurements Normalized for Operational, Seasonal, and Weather Effects," FHWA-RD-88-069, 1989.
- [3] Jayawickrama, P. W. and Thomas, B., "Correction for Field Skid Measurements for Seasonal Variations in Texas," *TRR 1639*, Transportation Research Board, National Research Council, Washington D. C., 1998, pp. 147–154.
- [4] Choubane, Bouzid, and Holzschuher, C. R., "Precision of Locked-Wheel Testers for Measurement of Roadway Surface Friction Characteristics," *Presented at 2004 TRB Annual Meeting*, January 11–15, 2004, Washington D.C.
- [5] ASTM Standard F 377-94a, "Standard Test Method for Calibration of Braking Force for Testing of

Pneumatic Tires,” *Annual Book of ASTM Standards*, Vol. 09. 02, 1999, ASTM International, West Conshohocken, PA.

- [6] Li, Shuo, Zhu, Karen, Noureldin, Samy, and Kim, Daeheon, “Pavement Friction Testing Using the Standard Smooth Tire: The Indiana Experience,” *Presented at 2004 TRB Annual Meeting*, January 10–15, 2004, Washington D.C.